의학박사 학위논문

Molecular mechanisms for polarized distribution of NCKX2 in rat hippocampal neurons

해마 신경 세포에서 NCKX2 의 세포막 불균등 발현을 조절하는 분자 기전

2013년 2월

서울대학교 대학원

의학과 생리학 전공

이 규 희

A thesis of the Degree of Doctor of Philosophy

해마 신경 세포에서 NCKX2 의 세포막 불균등 발현을 조절하는 분자 기전

Molecular mechanisms for polarized distribution of NCKX2 in rat hippocampal neurons

February 2013

The Department of Physiology,

Seoul National University

College of Medicine

Kyu-Hee Lee

해마 신경 세포에서 NCKX2 의 세포막 불균등 발현을 조절하는 분자 기전

지도 교수 이 석 호

이 논문을 의학박사 학위논문으로 제출함

2013년 2월

서울대학교 대학원

의학과 생리학 전공

이 규 희

이규희의 의학박사 학위논문을 인준함

2013년 2월

위 원 장 _____ (인)

부위원장 _____ (인)

위 원 _____ (인)

위 원 _____ (인)

위 원 _____ (인)

Molecular mechanisms for polarized distribution of NCKX2 in rat hippocampal neurons

by

Kyu-Hee Lee

A thesis submitted to the Department of Physiology

in partial fulfillment of the requirement

of the Degree of Doctor of Philosophy in Physiology

at Seoul National University College of Medicine

February 2013

Approved by Thesis Committee:

Professor _____Chairman

Professor _____Vice chairman

Professor _____

Professor _____

Professor _____

ABSTRACT

K^+-dependent Na^+/Ca^{2+} exchanger (NCKX) is a major calcium clearance mechanism at the large axon terminals of central neurons, whereas their somata display little NCKX activity. I investigated mechanisms underlying the axonal polarization of NCKX2 in rat hippocampal neurons. I identified NCKX2 as the first neuron-specific cargo molecule of kinesin family member 21A (KIF21A). The intracellular loop of NCKX2 (NCKX2-loop) specifically interacted with the WD-40 repeats, a putative cargo-binding domain, of KIF21A. Dominant negative mutant or depletion of KIF21A inhibited the transport of NCKX2-GFP to axon fibers. Knockdown of KIF21A caused calcium dysregulation at axonal boutons but not at somatodendritic regions. Despite the axonal polarization of the NCKX activity, both somatodendritic and axonal regions were immunoreactive to NCKX2. The surface expression of NCKX2 revealed by live-cell immunocytochemistry, however, displayed highly polarized distribution to the axon. In cultured hippocampal neurons, surface expression of NCKX2 on the somatodendritic compartment was significantly increased when endocytosis was suppressed by treating a dynamin inhibitor, dynasore, or overexpression of dynamin-1 mutant (DYN1-K44A). Moreover, dynasore increased NCKX activity at proximal dendrites of hippocampal dentate granule cells (GCs). It is well known that the μ2 subunit of AP-2 interacts with the canonical tyrosine motif (YxxΦ) and initiates the clathrin-mediated endocytosis. NCKX2 has two putative tyrosine motifs (^{365}YGKL and ^{371}YDTM) in its cytoplasmic loop region. First, I investigated whether NCKX2 interacts with the μ2 subunit in a heterologous expression system. NCKX2-loop was coimmunoprecipitated with the μ2, but the Y365A mutant of NCKX2-loop was not. In contrast, the interaction between μ2 and NCKX2-loop was little affected by the mutation of Y371A, suggesting that the

^{365}YGKL motif is essential for interacting with the μ2 subunit. Next, I investigated whether the ^{365}YGKL motif is essential for the endocytosis of NCKX2. Although the surface expression of NCKX2 was polarized to axon, the immunoreactivity of internalized NCKX2 was stronger in the somatodendritic region than the axon. Exogenous NCKX2-Y365A was little internalized and exhibited no axonal polarization of its surface expression. Furthermore, knock-down of the μ2 subunit blocked the endocytosis of wild-type NCKX2 and significantly reduced the axonal polarization of its surface expression. I hypothesized that interaction between ^{365}YGKL motif of NCKX2 and μ2 subunit is regulated by phosphorylation. Tyr-365 of NCKX2 was phosphorylated by carbachol which is known to activate Src family kinase (SFK) through PYK2. Furthermore, applying SFK-activating peptide increased NCKX activity at proximal dendrites of hippocampal dentate GCs. These results indicate that KIF21A-mediated axonal transport and selective somatodendritic endocytosis underlie the axonal polarized surface expression of NCKX2 and the endocytosis of NCKX2 in the somatodendritic region is mediated by SFK signaling pathway and AP-2.

Keywords : NCKX2, KIF21A, AP-2, axonal transport, clathrin-mediated endocytosis, calcium imaging

Student number: 2005-22402

CONTENTS

LIST OF FIGURES AND TABLE

Figures

Table

LIST OF ABBREVIATIONS

A/SD ratio, axon-to-somatodendrite ratio

aa, amino acid

ACSF, artificial cerebrospinal fluid

ADR, Aon-to-dendrite ratio

AIS, axon initial segment

AP, action potential;

AP-2, adaptor-binding protein 2

AP-CaT, AP-induced Ca^{2+} transient

Caspr2, contactin-associated protein 2

CaT, Ca^{2+} transient

CCh, carbachol

CCM, calcium clearance mechanism

CFEOM1, congenital fibrosis of extraocular muscle type 1

ctrl, control

DIC, differential interference contrast

DIV, day(s) in vitro

dn-, dominant negative

DPBS, Dulbecco's phosphate buffered saline

dpi, day(s) post-infection

DSR, dendrite-to-soma ratio

DYN1, dynamin-1

E, embryonic day(s)

FBS, fetal bovine serum

GC, granule cell

HBS, HEPES-buffered saline

HFS, high-frequency stimulation

HS, horse serum

i-, internalized

ICQ, intensity correlation quotient

IP, immonoprecipitation

KIF, kinesin superfamily protein

MAP2, microtubule-associated protein 2

MEM, minimum essential medium

MFB, mossy fiber bouton

MOI, Multiplicity of infection

mRFP1, monomeric red fluorescent protein1

MWCO, Molecular weight cut-off

NaCaX, Na^{+}/Ca^{2+} exchanger

NCKX, K^{+}-dependent Na^{+}/Ca^{2+} exchanger

NCKX2-loop, cytoplasmic region of NCKX2

NCX, K^{+}-independent Na^{+}/Ca^{2+} exchanger

NF-H, neurofilament heavy chain

nKHC, neuronal kinesin heavy chain

NT control, non-targeting shRNA

OGB-1, Oregon Green 488 BAPTA-1

OGB-5N, Oregon Green 488 BAPTA-5N

P, postnatal day(s)

PBS, phosphate-buffered saline

PBST, phosphate-buffered saline plus Triton X-100

PDM, product of difference from the mean

PFA, paraformaldehyde

PKC, protein kinase C

pLL, pLentiLox3.7 plasmids

PMCA, Plasma membrane Ca^{2+}-ATPase

PS, penicillin-streptomycin

pTyr, phosphotyrosine

PYK2, proline-rich tyrosine kinase2

ROI, region of interest

RT, room temperature

r_w, weighted average of rate constants

s-, surface

SD, Sprague-Dawley

SD-, somatodendritic

SDS-PAGE, sodium dodecyl sulfate polyacrylamide gel electrophoresis

SEM, standard error of mean

SERCA, sarco-endoplasmic reticulum Ca^{2+}-ATPase

SFK, Src family kinase

SH2, Src homology-2

shKIF21A, KIF21A-targeting shRNA

shNCKX2, NCKX2-targeting shRNA

shRNA, short-hairpin RNA

shμ2, μ2-targeting shRNA

siRNA, short-interfering RNA

SON, supraoptic nucleus

Syp, synaptophysin

tdTomato, tendom dimer Tomato

TF, transfection

TMD, transmembrane domain

VAMP2, vesicle associated membrane protein 2

WB, western blot

WT, wild type

INTRODUCTION

Calcium is the most versatile second messenger in cell signal transduction of a neuron. The calcium signaling at axon terminals is not only a direct trigger of neurotransmitter release but also a crucial mediator of synaptic plasticity (Neher and Sakaba, 2008). On the other hand, dendrite calcium signaling can modulate a wide range of dendritic functions such as surface expression of ion channels (Kim et al., 2007), reorganization of cytoskeleton (Liu et al., 2008), and gene expression (Lee et al., 2011), which lead to synaptic plasticity too. Spatial and temporal extents of calcium signaling are highly regulated by calcium influx, cytosolic calcium buffers and calcium clearance mechanisms (CCMs). These strict regulations of calcium signaling render it not promiscuous despite its versatile nature. Such regulation mechanisms may play an essential role in specifying the downstream coupling of a calcium signal. There is accumulating evidence for crucial roles of calcium clearance mechanisms in synaptic plasticity and Ca^{2+} homeostasis (Jeon et al., 2003; Lee et al., 2007a; Li et al., 2006).

The somatodendritic and axonal regions in a neuron display distinct spectra of membrane proteins which serve specialized functions in each compartment. Although there are many studies about polarized expression of ion channels and receptors for neurotransmitters (Arnold, 2007; Hirokawa et al., 2010), little is known about polarization of calcium clearance mechanisms. Previously, it has been reported that NCKX (K^+-dependent Na^+/Ca^{2+} exchanger) is the most important calcium clearance mechanism at the axon terminals of central neurons, whereas the Na^+/Ca^{2+} exchanger (NaCaX) activity in the somata was independent of intracellular K^+ (Kim et al., 2005; Kim et al., 2003; Lee et al., 2009; Lee et al., 2002; Lee et al., 2007c). Despite evidence

for the role of NCKX in large axon terminals, it is still obscure whether NCKX plays a role in calcium clearance at a small axon terminal. Furthermore, molecular mechanisms underlying axonal restriction of NCKX activity has not been investigated. Among members of the NCKX family, only NCKX2 is brain-specific (Tsoi et al., 1998), and the knockout of NCKX2 has profound effects on motor learning and ischemic brain damage (Cuomo et al., 2008; Li et al., 2006). Several lines of evidence support the notion that NCKX2 is a major isoform responsible for the NCKX activity at axon terminals (see Discussion). Therefore, I investigated mechanisms underlying polarized action of NCKX2 in hippocampal neurons.

There are two prevailing hypotheses for the mechanism underlying polarization of axonal proteins: 1) axonal transport by a motor protein that differentiates axonal microtubules from somatodendritic ones (selective trafficking) (Hirokawa and Takemura, 2005); 2) preferential endocytosis from the somatodendritic surface (selective retention) (Sampo et al., 2003). In any case, selective entry of a kinesin superfamily (KIF)-cargo complex into the axonal compartment through the axon initial segment (AIS) filter seems to be essential for axonal targeting (Song et al., 2009). I identified KIF21A as a putative binding partner of the intracellular loop of NCKX2. I present here the compelling evidence that KIF21A is essential for the axonal transport of NCKX2. The expression level of KIF21A is high in axon-rich tissues similar to KIF3A and nKHC, molecules known to participate in axonal transport (Hirokawa et al., 2010; Marszalek et al., 1999; Silverman et al., 2010). Point mutations in KIF21A were found in patients of congenital cranial dysinnervation disorders (Heidary et al., 2008; Yamada et al., 2003). Although the genetic disorder implies that KIF21A is involved in axonal transport, no neuron-specific cargo of KIF21A has been identified. I report here NCKX2 as the first neuron-specific cargo molecule transported to the axon by KIF21A.

The plasma membrane Ca^{2+}-ATPase (PMCA) and Na^{+}/Ca^{2+} exchanger (NCX) have been known to be major CCMs in dendrites. PMCA has higher affinity for calcium but is easily saturated at high [Ca^{2+}] (Kim et al., 2003; Lee et al., 2009). Because NCX shows higher turnover rate and capacity than PMCA, NCX has been considered a major CCM at high [Ca^{2+}] in dendrites. Dendritic NCX is a key player in the modulation of the spatial extent of calcium signals induced by excitatory synaptic inputs (Goldberg et al., 2003; Lőrincz et al., 2007). Accordingly, deletion of genes encoding different forms of NCX causes alterations in synaptic plasticity and cognitive functions (Jeon et al., 2003; Molinaro et al., 2011). In contrast to NCX, dendritic function of the K^{+}-dependent Na^{+}/Ca^{2+} exchanger (NCKX) is controversial. Previously, based on studies of the decay phase of calcium transients, it has been reported that NCKX activity is the major CCM at axon terminals but is not detectable in somatodendritic regions of central neurons (Kim et al., 2005; Kim et al., 2003; Lee et al., 2009). This view is in disagreement with other studies, which showed the direct recording of NCKX current or Ca^{2+}-influx via the reverse mode of NCKX in the somata of cortical neurons (Cuomo et al., 2008; Kiedrowski, 2004). These discrepancies on the dendritic NCKX activity have not been reconciled. Because these two kinds of studies with opposite views probed the dendritic NCKX activity using different methods, the resolving the discrepancy needs detection of surface NCKX2 in dendritic and axonal compartments of a neuron using antibody that detects extracellular epitopes of NCKX2 in a live cell condition.

In this thesis, I present evidence that the surface expression of NCKX2 is polarized to the axonal compartment in cultured hippocampal neurons. Nevertheless, when total NCKX2 was detected, I found that not only axon terminals but also somatodendritic regions are immunoreactive for NCKX2 in cultured hippocampal neurons, implying the selective retention hypothesis as the mechanism for polarized axonal surface expression

of NCKX2. Consistently, I found that suppression of endocytosis allowed the dendritic surface expression of NCKX2. These findings prompted me to further study the molecular mechanism regulating the surface expression of NCKX2 in dendrites of central neurons.

Clathrin-mediated endocytosis, the most ubiquitous form of endocytosis, is initiated by recruitment of the adaptor protein complex, AP-2, to the target molecule. The AP-2 complex is composed of four subunits: large α, β2 and small μ2 and σ2 (Kirchhausen, 1999). AP-2 interacts with one of two well-known canonical endocytosis motifs. One is a dileucine motif ([D/E]xxxL[L/I]; x = any amino acid) recognized by the β2 subunit of AP-2 (Rapoport et al., 1998), and the other is a tyrosine motif (YxxΦ; Φ = hydrophobic amino acid) recognized by the μ2 subunit of AP-2 (Ohno et al., 1995). NCKX2 has two tyrosine motifs (^{365}YGKL and ^{371}YDTM) in its intracellular loop region (Tsoi et al., 1998). Activities of many ion channels and neurotransmitter receptors are regulated by phosphorylation of tyrosine motifs (Ohnishi et al., 2011).

I tested whether the tyrosine motifs of NCKX2 are involved in the endocytic regulation of its dendritic surface expression. In this thesis, I report that the first tyrosine motif interacts with the μ2 subunit of AP-2 and that the interaction is required for endocytosis of NCKX2 from the dendritic surface. Furthermore, I show that a Src family tyrosine kinase (SFK) modulates the endocytosis of NCKX2 by tyrosine-phosphorylation of the AP-2 recognition motif in NCKX2.

MATERIALS AND METHODS

1. DNA constructs

The full length rat NCKX2 (NM_031743.2; O54701) was cloned into pcDNA3.1(+) plasmid (Invitrogen). The cytoplasmic loop region of NCKX2 [NCKX2-loop, amino acids (aa) 288-478] was isolated from full length NCKX2 and subcloned into the yeast expression vector pGBKT7 (Clontech) and the mammalian expression vector pcDNA3.1(+) with N-terminal c-myc tag (myc-NCKX2-loop). NCKX2-GFP was constructed by inserting the EGFP coding sequence into the N-terminal *BstEII* restriction site of NCKX2 in the pcDNA3.1(+) vector. The NCKX2-FLAG construct was created by replacing the N-terminal 8 amino acids (aa 90-97; DLNDKIRD) by the FLAG tag (DYKDDDDK). Mouse KIF4 (NM_008446.2), KIF5B (NM_008448.3), KIF21A (NM_001109042.1) and KIF21B (NM_001039472.1) cDNAs were obtained by RT-PCR from total mouse brain RNA and ligated into the mammalian expression vector pFLAG-CMV2 (Sigma). The dominant negative kinesin (dnKIF) constructs were generated by deleting motor domains and placing the resulting constructs into the pFLAG-CMV2 and yeast expression vector pGADT7 (Clontech). For dnKIF21A, aa 1-1231 were deleted; for dnKIF21B, aa 1-1301 were deleted; for dnKIF4, aa 1-350 were deleted; and for dnKIF5B, aa 1-330 were deleted. C-terminal EGFP-tagged synaptophysin (Syp-GFP) was cloned into pcDNA3.1(+). The wild-type and mutant (K44A) dynamin-1 cloned into pEGFP-C1 (Clontech) were gifts from Dr. Chang (Seoul Nat'l Univ., South Korea). Y365A or Y371A mutants of NCKX2 were obtained by using QuickChange Site-directed Mutagenesis kit (Agilent Thechnologies). The HA tagged μ2 (NM_053837.1; P84092) cloned into pcDNA3 (HA-μ2) and non-targeting or μ2-targeting shRNA cloned into pSuper (OligoEngine) were gifts from Dr. Kim (Weill

Cornell Medical College) (Kim and Ryan, 2009). The luciferase-targeting siRNA sequence (5'-TAAGGCTATGAAGAGATAC-3') was used as a non-targeting siRNA control (Dharmacon). pDsRed2-N1 (Clontech) and tdTomato were used for visualizing the entire morphology of a cultured hippocampal neuron.

2. Yeast two-hybrid screening

Yeast two-hybrid screening for proteins interacting with the NCKX2-loop was carried out with the MATCHMAKER System (Clontech) according to the user manual. The yeast strain AH109 containing the pGBKT7-NCKX2-loop as bait plasmid was mated with the yeast strain Y187 pretransformed with a cDNA library (~10^6 clones) from mouse brain cloned into the vector pGADT7. Selection of positively interacting clones was based on their abilities to express HIS3 and ADE2 genes, which enabled the yeast to grow in the absence of histidine or both histidine and adenine at 30°C. Positive clones were identified by sequencing. Positive interactions were confirmed by the growth of AH109 co-transformed with both pGBKT7-NCKX2-loop (bait) and pGADT7-dnKIF21A (prey) on the selective plates of synthetic dropout media. The combination of the p53-bait and SV40 large T antigen-prey was used as a control for positive interaction.

3. Cell culture

Hippocampal neurons were cultured on coverslips suspended above an astrocyte feeder layer. The protocol for low-density neuron-glia co-culture is described in ref. (Kaech and Banker, 2006). All work with animals was conducted in accordance with the animal welfare guidelines of the Seoul National University. In brief, 2 weeks before

neuronal culture, astrocytes were obtained by passing a cortical cell suspension from postnatal day (P) 1 Sprague-Dawley (SD) rat through a cell strainer (40 μm mesh, BD Falcon), and then cultured in glial medium [minimum essential medium (MEM; Invitrogen) supplemented with 0.6% glucose, 1 mM pyruvate, 2 mM GlutaMAX-I (Invitrogen), 10% horse serum (HS; Invitrogen) and 1% penicillin-streptomycin (PS; Invitrogen)]. Hippocampi from embryonic day (E) 18 SD fetal rats were dissected in Hank's balanced salt solution (Invitrogen), digested with papain (Worthington), and then triturated with a polished half-bore Pasteur pipette. The neurons in plating medium [the same composition with glial medium except for 10% fetal bovine serum (FBS; Invitrogen) instead of HS] were plated on poly-D-lysine (Sigma)-coated glass coverslips (Marienfeld, Germany) in a 60-mm culture dish at a density of 0.7-1.4 × 10^4 cells per cm^2. Paraffin dots ('feet' to suspend the coverslips above the glial feeder layer) were applied to the coverslips before neuron plating. The next day coverslips were transferred above the glial culture preincubated in Neurobasal A medium (Invitrogen) supplemented with 0.5 mM GlutaMAX-I and 2% B-27 supplement (invitrogen) for 1 day. To prevent proliferation of glial cells, 5 μM of 1-β-D-cytosine-arabinofuranoside (Sigma) was added at the 4th day in vitro (DIV4).

HEK293 cells (ATCC) were plated at a density of 5 × 10^4 cells per 100-mm culture dishes and maintained in Dulbecco's modified Eagle's medium (Invitrogen) supplemented with 10% FBS and 1% PS. PC-12 cells (Korean Cell Line Bank) were plated at a density of 5 × 10^4 cells per 0.01% poly-L-lysine (Sigma) coated 100-mm culture dishes and maintained RPMI-1640 medium (WelGENE, South Korea) supplemented with 10% HS, 5% FBS and 1% PS.

4. Transfection

Primary hippocampal neurons (DIV3-8) were transfected using calcium phosphate (Ryan et al., 2005). Before transfection, the conditioned culture medium was saved and neurons were incubated with 2 ml of Neurobasal A containing 25 mM HEPES (pH 7.3, adjusted with NaOH). The DNA/calcium phosphate precipitate was prepared by mixing one volume of DNA (up to 15 μg) in 250 mM $CaCl_2$ with an equal volume of 2X HBS (280 mM NaCl, 50 mM HEPES, 1.5 mM Na_2HPO_4, pH 7.1) using a vortex mixer. Then 200 μl DNA/calcium phosphate mixture was added dropwise to the cultured neurons, and neurons were incubated at 37°C for 15 min. After the incubation, DNA/calcium phosphate precipitates were washed out three times with fresh Neurobasal A for 5 min and the cells were returned to the saved original medium. For **Figs. 7 and 8**, NCKX2-GFP and DsRed with or without either of KIF21A, dnKIF21A or dnKIF21B were transfected to hippocampal neurons. NCKX2-GFP and each of the three kinesin constructs were co-transfected in a ratio of 1:4. NCKX2-FLAG and wild-type or mutant dynamin-1 constructs were co-transfected in a ratio of 1:1. For **Fig. 18**, wild-type (WT) or Y365A mutant of NCKX2-FLAG and tsTomato were transfected to hippocampal neurons. For **Fig. 19**, WT of NCKX2-FLAG and NT control or shμ2 were co-transfected in a ratio of 1:1. HEK293 cells were also transfected using calcium phosphate. The procedures were essentially the same except the medium was not changed before and after adding of DNA/calcium phosphate mixture to the culture. PC-12 cells were transfected with WT or Y365A mutant of NCKX2-FLAG using Lipofectamine 2000 (Invitrogen) according to the manufacturer's instructions.

5. Antibodies for NCKX2 and KIF21A

For NCKX2, I used two different kinds of antibodies denoted by anti-$NCKX2_{ext}$ and anti-$NCKX2_{loop}$. The former is a polyclonal antibody raised against the extracellular epitope (aa 90-102) of the rat NCKX2 (Thermo/Affinity BioReagents). I raised the latter antibody (anti-$NCKX2_{loop}$) against purified His6-tagged cytoplasmic region of NCKX2 (His6-NCKX2-loop; aa 288-478). The expression of His6-NCKX2-loop was induced by 0.1 mM isopropyl thio-β-D-galactopyranoside (Fluka, Switzerland) in *Escherichia coli* strain, BL21 (DE3) and purified by affinity column (QIAGEN). Immunizing and sampling of rabbit anti-sera were performed by a commercial facility (AbFrontier, Seoul, Korea). The anti-KIF21A antibody was a gift from Dr. Seog (Inje Univ., South Korea) which raised against glutathione S-transferase fused KIF21A (aa 1101-1213). Two different anti-KIF21A antibodies were obtained from two different rabbits which were immunized with the same immunogen.

6. Co-immunoprecipitation and peptide elution

Hippocampal neurons from E18 SD rats were plated at a density of 4.5 x 10^4 cells per cm^2 on 100-mm culture plates coated with 100 μg/ml poly-D-lysine and cultured for 2 weeks. The neurons at DIV14 were washed once with Dulbecco's phosphate-buffered saline (DPBS; Invitrogen) and lysed for 30 min on ice in lysis buffer containing 25 mM Tris (pH 7.4), 10 mM NaCl, 1% sodium cholate hydrate, 1% Triton X-100 (v/v), 1 mM phenylmethyl sulfonyl fluoride (Sigma) and 0.2% protease inhibitor mixture (Sigma) (Hong et al., 2009; Oh et al., 2006). Cell lysates were then centrifuged at 8,200 x g for 15 min at 4°C and the protein concentrations were determined by Bradford protein assay (Bio-Rad). The supernatants containing 500 μg total proteins were incubated with rabbit anti-KIF21A IgG or rabbit anti-$NCKX2_{loop}$ IgG immobilized on the amine-

reactive gel according to the manufacturer's instructions (ProFound co-immunoprecipitation kit; Thermo/Pierce). Non-immune rabbit IgG (Calbiochem) was used as control. The immunoprecipitated protein complexes were subjected to SDS-PAGE and western blot analysis with anti-$NCKX2_{ext}$ and anti-KIF21A antibodies.

HEK293 cells were seeded in 100-mm culture dishes at approximately 70% confluence and transfected with myc-NCKX2-loop and FLAG-tagged KIF variants, either KIF21A, KIF21B, dnKIF21A or dnKIF21B for **Fig. 1** and with HA-μ2 and the WT or mutant form (Y365A or Y371A) of myc-NCKX2-loop for **Fig. 17**, using calcium phosphate. After culture for 20-48 h, the cells were washed twice with DPBS, solubilized in ice-cold lysis buffer containing 20 mM Tris (pH 7.4), 140 mM NaCl, 10% sucrose, 1 mM EDTA, 1 mM Na_3VO_4, 1% NP-40 (v/v) and 0.2% protease inhibitor mixture for **Fig. 1** or 50 mM Tris-Cl (pH 7.4), 150 mM NaCl, 1 mM EDTA, 0.5% Triton X-100 (v/v) and 1% protease inhibitor mixture for **Fig. 17**. After the incubation on ice for 30 min cell lysates were clarified by centrifugation at 8,200 x g for 15 min at 4°C. The supernatants containing 500 μg total proteins were incubated with anti-c-myc antibody-conjugated agarose beads (Sigma) by gentle inverting for 1 h (for **Fig. 1**) or overnight (for **Fig. 17**) at 4°C. The beads were then washed three times with wash buffer containing 50 mM Tris-Cl (pH 7.4), 150 mM NaCl, 1 mM EDTA and 0.1% Triton X-100 (v/v) for 10 min. For **Fig. 1**, the immunoprecipitated protein complexes were denatured in 2X SDS sample buffer and for **Fig. 17**, the bound proteins were eluted from the agarose beads by incubation with 500 μg/ml c-myc peptide (Sigma) diluted in lysis buffer for 30 min on ice. Then the immunoprecipitated protein complexes in supernatants were denatured by boiling with 2X SDS sample buffer and subjected to SDS-PAGE and western blot analysis with mouse monoclonal anti-FLAG (Sigma), mouse monoclonal anti-HA.11 (Covance) and mouse monoclonal anti-c-myc

(9B11, Cell Signaling).

7. Western blotting

Cell lysates or immunoprecipitated proteins were separated by SDS-PAGE and transferred onto a polyvinylidene difluoride membrane (Millipore). The resulting blots were blocked for 1 h in phosphate-buffered saline (PBS) plus 0.1% Triton X-100 (0.1% PBST) containing 5% skim milk (Difco). The blots were incubated overnight at 4℃ with specific primary antibodies: rabbit polyclonal anti-$NCKX2_{ext}$ (1:100, Thermo/Affinity BioReagents), rabbit polyclonal anti-KIF21A (1:500), mouse monoclonal anti-FLAG M2 (1:5000), mouse monoclonal anti-c-myc (1:1000), mouse monoclonal anti-HA (1:1000), rabbit polyclonal anti-FLAG (1:2000, Sigma) or mouse monoclonal anti-β-actin (1:2500, Abcam, UK or 1:5000, Santa Cruz Biotechnology) as loading controls. After washing three times, the blots were incubated at room temperature (RT) for 1 h with the corresponding horseradish peroxidase-conjugated secondary antibodies: goat anti-rabbit IgG (1:2000, Abcam) or goat anti-mouse IgG (1:5000, Jackson ImmunoResearch). After washing three times with 0.1% PBST for 10 min, detection was performed using enhanced chemiluminescence reagent (Amersham Bioscience, UK). The membranes were then exposed to X-ray films (Agfa-Gevaert, Belgium). For **Fig. 9**, films were digitally scanned and signals were quantified using densitometric analysis software, Multi Gauge (Fujifilm, Japan). Immunoblots were washed in PBS containing either 0.1% Triton X-100 or 1% NP-40 and 0.1% SDS. For antibody pre-absorption test, prior to western blotting, each primary antibody (diluted in 0.1% PBST) was pre-incubated at RT for 2 h with 50 μg/ml of an appropriate antigen: affinity-purified protein or synthesized peptides. The antigen purification procedures for anti-$NCKX2_{loop}$ and anti-KIF21A are described above. The antigen peptide (aa 90-102;

DLNDKIRDYTPQP) for anti-$NCKX2_{ext}$ antibody was synthesized by a commercial facility (AnyGen, Gwangju, Korea). In order to enhance the antigenicity of the peptide, I used the synthesized peptides with cross-linked to polystyrene beads as an antigen, and thus bare polystyrene beads (BeadTech, Seoul, Korea) as control in **Fig. 3B**.

To detect phosphotyrosine (pTyr) residues of NCKX2, PC-12 cells were transfected with FLAG-tagged WT or Y365A mutant NCKX2. Two days later, we treated the transfected cells with 1 mM carbachol (CCh) or CCh plus 10 μM PP2 for 2 minutes (Calbiochem, San Diego, CA, USA). Immediately after the CCh treatment, we harvested the cell lysate using the same lysis buffer that we used for coimmunoprecipitation, with the addition of 1 mM Na_3VO_4. The cell lysates were pre-cleared by incubating with 25 μl of protein G-conjugated agarose beads (50% slurry, Santa Cruz Biotechnology, Santa Cruz, CA, USA). WT or Y365A mutant of NCKX2-FLAG was immunoprecipitated from pre-cleared cell lysates of PC-12 cells using anti-FLAG incubated protein G agarose beads and then, I performed immunoblotting assay with mouse monoclonal anti-phosphotyrosine antibody (1:1000, Millipore). The same blot probed for pTyr was stripped and then re-probed with anti-FLAG antibody to confirm that equal amounts of the immunoprecipitated protein were loaded between control and drug-treated groups.

8. Immunocytochemistry

For detecting total (both cytosolic and surface) protein, the cells were fixed with ice-cold 4% paraformaldehyde (PFA) or 3.8% formaldehyde in PBS for 20 min, washed with PBS, and then permeabilized with 0.1% PBST for 5 min at RT. The cells were further washed in PBS and blocked in blocking solution (5% donkey or goat serum in

0.1% PBST) for 1 h at RT. Primary antibodies were diluted in blocking solution, and incubated with samples for 1 h at RT or overnight at 4℃. Primary antibody dilutions were as follows: rabbit polyclonal anti-NCKX2$_{ext}$ (1:100), mouse monoclonal anti-FLAG M2 (1:2500), mouse monoclonal anti-synaptophysin (1:100, Sigma), mouse monoclonal anti-Tau-1 (1:500, Sigma), mouse monoclonal anti-microtuble-associated protein 2 (MAP2; 1:500, Millipore/Chemicon) and rat monoclonal anti-neurofilament H (NF-H; 1:500, Millipore). After three washes in PBS, cells were incubated with secondary antibodies diluted in blocking solution for 1 h at RT in the dark. Secondary antibodies were used as follows: Alexa Fluor 488-conjugated goat anti-rabbit IgG (1:400 dilution, Invitrogen/Molecular Probes) for immunostaining of endogenous NCKX2; Cy5-conjugated donkey anti-rabbit IgG (1:400, Millipore/Chemicon) for NCKX2-GFP; rhodamine-conjugated donkey anti-mouse IgG (1:200, Jackson ImmunoResearch) for NCKX2-FLAG, FLAG-KIF21A (**Fig. 5**) and MAP2 (**Figs. 14B and 15A**); Cy5-conjugated donkey anti-mouse IgG (1:200, Jackson ImmunoResearch) for NCKX2-FLAG (**Fig. 15B**), MAP2 (**Figs. 8, 10, 14A and 15E**), Tau-1 (**Figs. 8 and 14A**) and synaptophysin (**Fig. 14A**); For NF-H, Alexa Fluor 568-conjugated goat anti-rat IgG (1:400, Invitrogen/Molecular Probes; **Fig. 15**) and Cy5-conjugated goat anti-rat IgG (1:500, Jackson ImmunoResearch; **Fig. 5**) were used. Finally, the cells were washed three times in PBS and mounted with fluorescent mounting medium (DakoCytomation). In **Fig. 4A**, nuclear staining by DAPI was performed to visualize untransfected cells. Before mounting, cells were incubated with DAPI in PBS (1:5000, Sigma) for 5 min and washed with PBS then mounted.

For surface immunostaining of NCKX2, live cells were incubated with rabbit anti-NCKX2$_{ext}$ (1:100) or rabbit anti-GFP (1:100, Millipore/Chemicon) or rabbit anti-FLAG (1:2000) in serum-free Neurobasal A medium for 15 min at 36℃ or at 4℃, rinsed with

culture medium, fixed with ice-cold 4% PFA or 3.8% formaldehyde in PBS for 20 min and washed with PBS. For double-immunostaining with MAP2, Tau-1, synaptophysin or NF-H, cells labeled with anti-NCKX2$_{ext}$ or anti-FLAG antibody and then fixed were subsequently permeabilized with 0.1% PBST for 5 min at RT. The fixed cells were incubated in blocking solution for 1 h at RT, and then with anti-MAP2, Tau-1, synaptophysin or NF-H antibodies diluted in blocking solution for 1h at RT (Bel et al., 2009). After three washes in PBS for 10 min, cells were incubated with Alexa Fluor 488-conjugated donkey anti-rabbit (1:100, Invitrogen/Molecular Probes) and Alexa Fluor 647-conjugated donkey anti-mouse (1:200, Jackson ImmunoResearch) diluted in blocking solution for 1 h at RT. Finally, the cells were washed three times in PBS and mounted with fluorescent mounting medium (DakoCytomation).

For immunostaining of the internalized NCKX2, live cells were incubated with rabbit anti-FLAG (1:2000) in serum-free culture medium for 30 min at 37˚C. After a brief wash with culture medium, cells were washed with acidic buffer (Neurobasal A medium, pH 2 with HCl) for 2 min to remove surface-bound antibody (Kurisu et al., 2010). Then cells were rinsed with PBS, fixed with ice-cold 4% PFA in PBS for 10 min and washed with PBS. Subsequent steps were the same as those for surface protein immunostaining but Alexa Fluor 488-conjugated anti-rabbit antibody was incubated with Alexa Fluor 647-conjugated anti-mouse after the incubation of anti-MAP2.

The immunostained cells were imaged with FV300 (Olympus) or TCS-SP2 (Leica) confocal laser scanning microscopes with 60x or 63x water-immersion objectives, and then processed using Fluoview or Leica Lite.

9. Quantitative analysis of co-localization

I quantified the co-localization of NCKX2 with FLAG-KIF21A by intensity correlation analysis on the NF-H-immunoreactive axonal neurite of a DIV12 cultured hippocampal neuron, which were triple-immunostained with anti-$NCKX2_{ext}$ (green), anti-FLAG (red) and anti-NF-H (blue). The region of interest (ROI) was defined as a binary mask covering the axonal neurite of a neuron expressing FLAG-KIF21A. It was made from the NF-H fluorescence image of the FLAG-positive neuron using the "ImageSeedFill" routine supplied by Igor Pro (version 4.1; WaveMetrics, Lake Oswego, OR). This routine makes a cell mask by taking a seed pixel and filling a region defined by all contiguous pixels whose pixel values are higher than a given threshold value. After subtraction of background fluorescence, I analyzed paired green (G_i) and red (R_i) fluorescence intensities of each pixel within the ROI. The value for the product of difference from the mean (PDM) at the i-th pixel was calculated according to the equation:

$$PDM_i = (G_i - g) / G_{max} \times (R_i - r) / R_{max}$$

, where g and r are the mean values of green and red fluorescence intensities in the ROI, respectively; G_{max} and R_{max} are the maximal green and red intensities in the ROI, respectively. If the paired green and red fluorescence intensities vary together in an image, the number of pixels having a positive PDM value will be larger than 50% of total pixels, because a pixel above (below) the average in the one channel will be above (below) the average in the other. The intensity correlation quotient (ICQ) was calculated as:

ICQ = (the number of positive PDM pixels / the total number of pixels in the ROI) – 0.5.

The ICQ value is expected to be zero for random staining, $0 < ICQ < 0.5$ for dependent

staining, and -0.5 < ICQ < 0 for segregated staining. I tested if a ICQ value is significantly different from zero using the normal approximation of the sign-test (Li et al., 2004).

10. Determination of dendritic and axonal fluorescence of NCKX2

To determine the fluorescence ratio of axonal to dendritic compartment (ADR) in a neuron, I made a binary mask image of a dendrite or an axon using the "ImageSeedFill" routine of Igor Pro. After a dendritic mask was made from a MAP2 image (**Figs. 8C and 10C**, middle for an exemplar mask image), an axon image was obtained by setting the dendritic pixels (defined by the MAP2 mask) on the NCKX2 image to a zero value (**Figs. 8C and 10C**, right). To eliminate the background fluorescence of cell-free regions, I subtracted the mean background gray value from the image, and removed salt-and-pepper type background noise by convoluting the image with a 3 × 3 median filter. Finally, I defined ROIs along a dendritic or an axonal compartment on the processed image, and determined ADR from the averaged fluorescence count of non-zero pixels in the axonal and dendritic ROIs.

A few seed pixels on the cell were enough for the mask covering a MAP2 fluorescence image (**Figs. 8 and 10**), and thus they were manually set in Igor Pro. To make a cell mask from the image of NCKX2-GFP or EGFP-tagged dynamin-1 which exhibits a speckled fluorescence pattern (**Fig. 15**), I took a set of seed pixels from the pixels on the traced line drawn on the neurites of the same image using NeuronJ, and fed the seed pixels into the "ImageSeedFill" routine of Igor Pro. The consequent cell mask made from an image of EGFP fluorescence covered the entire cellular region expressing NCKX2-GFP or NCKX2-FLAG. I determined the dendritic surface

expression level from the mean gray value of pixels on the mask of the MAP2-positive neurites. The axonal surface expression level was determined from the MAP2-negative neurite.

11. Determination of somatodendritic and axonal fluorescence of NCKX2

To determine the fluorescence ratio of axonal to somatodendritic compartment (A/SD ratio) in a neuron, I made a binary mask image of a dendrite or an axon using the "ImageThreshold" routine of Igor Pro. A Tomato mask and a MAP2 mask were made from a tdTomato image and a MAP2 image, respectively. I defined the overlapping area of the Tomato mask (ROI of a transfected cell) and the MAP2 mask (ROIs of all somatodendritic neurites) as the somatodendritic ROI (SD-ROI) (**Fig. 18B**). Then the axonal ROI was obtained by subtracting SD-ROI from the Tomato mask. Finally, the A/SD ratio was calculated by dividing the spatially-averaged immunofluorescence intensity of NCKX2 over the axonal ROI by that of NCKX2 over the SD-ROI.

To determine the axonal or somatodendritic polarization for the subcellular distribution of surface NCKX2, I defined "normalized A/SD ratio" as an A/SD ratio of a protein normalized to that of tdTomato, which is assumed to display non-polarized subcellular distribution, in the same cell. If the normalized A/SD ratio of a protein is unity, I regarded the distribution of the protein as non-polarized. A value greater or less than one was regarded as preferential localization to the axon or to the somatodendritic region, respectively.

12. Hippocampal organotypic slice culture

Slice cultures were prepared from P6-8 SD rat pups of either sex mostly according to the procedure described by De Simoni (De Simoni and My Yu, 2006) according to the animal welfare guidelines of Seoul National University. Briefly, hippocampal slices (thickness, 350 μm) were obtained with vibratome (DTK-1000 ZERO 1, Dosaka, Kyoto, Japan) and placed on a porous (0.4 μm) membrane (Millicell-CM, Millipore). The culture medium was a mixture of 50% MEM, 25% HS, 24% Eagle's buffered salt solution and 1% PS. Glucose was added to reach a final concentration of 36 mM. After 4 days in culture, the medium was changed to serum-free Neurobasal A medium with 2% B-27 supplement, 1% GlutaMAX-I, 1% PS and 5 mM glucose added. The medium was changed every 2 days.

13. Lentiviral transduction system and RNA interference

In **Figs. 3 and 9-13**, I used a lentiviral delivery system to knockdown NCKX2 or KIF21A. NCKX2-targeting short-interfering RNA (siRNA) sequences (5'-ACAACAGTCTCATGAGGAA-3' for shNCKX2-1; 5'-GCTTCAATTCTCCACAAGA-3' for shNCKX2-2) and KIF21A-targeting siRNA sequence (5'-CGAGATCATCAACT TAGAC-3') were designed using the siRNA software tool available at the Whitehead Institute for Biomedical Research (http://www.whitehead.mit.edu). The synthesized NCKX2, KIF21A-targeting or non-targeting short-hairpin RNA (shRNA) oligonucleotides (Cosmogenetech, Seoul, Korea) were ligated into the lentiviral vector pLentiLox3.7 (pLL3.7) (Rubinson et al., 2003), which could co-express GFP or monomeric RFP (mRFP). In **Fig. 19**, μ2-targeting shRNA cloned into pSuper (OligoEngine) were gifts from Dr. Kim (Weill Cornell Medical College) (Kim and Ryan,

2009). The luciferase-targeting siRNA sequence (5'-TAAGGCTATGAAGAGATAC-3') was used as a non-targeting siRNA control (Dharmacon). Lentivirus was produced by the commercial lentiviral packaging service (Macrogen, Seoul, Korea). Lentiviruses in culture medium were filtered through 0.45-μm filters (Satorius, Germany) and then concentrated with Amicon Ultra-4 centrifugal filter unit, MWCO 100 kDa (Millipore) and aliquots were stored at -80°C (Braam et al., 2008; Hioki et al., 2009). The efficiency of gene silencing was assessed in HEK293 cells and cultured hippocampal neurons by immunoblot analysis or immunocytochemistry. Lentiviral stocks in the presence of fresh 4 μg/ml polybrene (Davis et al., 2004) were delivered to DIV7-8 organotypic cultured hippocampal dentate gyrus by local injection using a 10-μm pore glass pipette (Davis et al., 2004). Primary cultured hippocampal neurons (DIV1-3) were infected with shRNA lentivirus at an MOI of about 1.

14. Recording of reverse-mode NCKX current

The NCKX activity of NCKX2-GFP was tested by recording Ca^{2+} and K^+-dependent reverse mode exchange current in the HEK293 cell perfused with high Na^+ internal pipette solution using whole-cell patch-clamp technique. NCKX2 activity was identified by dependence of outward current at the holding potential of 0 mV on extracellular Ca^{2+} plus K^+. The procedure for recording reverse-mode (outward) NCKX currents was previously described in detail in Lee et al. (Lee et al., 2006). In brief, whole-cell patch-clamp recordings were attained on the HEK293 cells expressing NCKX2-GFP with a pipette solution containing the following (in mM): 120 Na-gluconate, 10 KCl, 20 HEPES, 1 EGTA, 4 MgATP, 0.3 Na_2GTP at pH 7.2 (adjusted with NaOH). Current recordings in baseline conditions were obtained while the cells were superfused with Ca^{2+}- and K^+-free bath solution containing the following (in mM) :

140 LiCl, 0.5 EGTA, 1 $MgCl_2$, 10 HEPES, 10 glucose at pH 7.4 (adjusted with LiOH). Reverse-mode of NCKX currents were induced by bath application of test solution. Ca^{2+} plus K^+ (or Ca^{2+} plus Cs^+) test solution contained 140 mM KCl (or 140 mM CsCl) and 1 mM $CaCl_2$ instead of 140 mM LiCl and 0.5 mM EGTA. Ca^{2+} test solution contained 1 mM $CaCl_2$ instead of 0.5 mM EGTA.

15. Recording of Ca^{2+}-transient in axon terminals of hippocampal granule cells

Cultured hippocampal slices were placed in a submerged recording chamber and perfused with artificial cerebrospinal fluid (ACSF) composed of (in mM): 124 NaCl, 26 $NaHCO_3$, 3.2 KCl, 2.5 $CaCl_2$, 1.3 $MgCl_2$, 1.25 NaH_2PO_4 and 10 glucose with pH adjusted at 7.4 by saturating with carbogen (95% O_2, 5% CO_2). For calcium imaging, whole-cell patch-clamp was attained on the mRFP-expressing soma of a dentate granule cell (GC) under visual control using differential interference illumination in an upright microscope (BX51WI; Olympus, Tokyo, Japan). The expression of mRFP was detected using an HcRed1 filter set (part# 41043, Chroma). The whole-cell recordings were made using an EPC-10 amplifier (HEKA Elektronik, Lambrecht, Germany) with a pipette solution containing (in mM) 140 K-gluconate, 5 di-Tris-phosphocreatine, 5 NaCl, 4 MgATP, 0.4 Na_2GTP, 15 HEPES, 2.5 Na-pyruvate (pH 7.3, adjusted with KOH) together with 200 μM Oregon Green 488 BAPTA-5N (OGB-5N, K_D ~50 μM) or 50 μM Oregon Green 488 BAPTA-1 (OGB1, K_D ~200 nM) (Invitrogen/Molecular probes). Both Ca^{2+}-indicators were excited at 488 nm. Calcium imaging was performed using a confocal laser scanning system (FV300; Olympus) and a 60x water-immersion objective (numerical aperture, 0.9; LUMPlanFl/IR; Olympus). Ca^{2+}-transients (CaTs) at hippocampal mossy fiber en passant boutons, somata, dendritic spines and shafts of

dentate granule cells were evoked by applying high frequency stimulation, a train of short depolarizing pulses (2 ms in duration) from -80 mV to 0 mV at 33 Hz or 100 Hz for 5 s, via whole-cell patch pipette on the soma, and recorded in XY scan mode at 5 Hz for 20 s. A single action potential-induced CaT (AP-CaT) was recorded in line-scan mode at 540 Hz. Suprathreshold current pulse to evoke AP-CaT was typically 600~900 pA for 12 ms. The relative Ca^{2+} increment is presented as $\Delta F/F_0$, where F_0 is resting fluorescence intensity of OGB-5N or OGB-1 after subtraction of background fluorescence, and ΔF is the fluorescence increment from F_0.

16. Estimation of dendritic Ca^{2+} clearance in the hippocampal granule cells

Acute hippocampal slices (thickness, 300 μm) were prepared from P14-19 SD rats as described in Lee et al. (Lee et al., 2007a). The whole-cell recordings were made at the soma of a hippocampal GC at 31-35°C. The K^+-based pipette solution contained (in mM) 125 K-gluconate, 20 KCl, 20 HEPES, 5 Na-phosphocreatine, 4 MgATP, 0.3 Na_2GTP and 0.1 fura-4F (Invitrogen/Molecular probes) with pH adjusted at 7.3 using KOH. For a K^+-free pipette solution (denoted as TMA^+-based pipette solution), K-gluconate and KCl were replaced with equimolar tetramethylammonium (TMA)-gluconate and tetraethylammonium (TEA)-Cl, respectively. For low [Na^+] ACSF, 125 mM NaCl was replaced with equimolar choline-Cl. Serial images of fura-4F fluorescence were taken using a monochromator (Polychrome-IV, TILL Photonics, Germany) and an air-cooled slow-scan CCD camera (SensiCam; PCO, Germany). I used the built-in on-chip binning (8 × 16 pixels) function to accelerate the frame rate (40 Hz; exposure time, 5 ms). In the off-line analysis, an ROI including the proximal dendrite was drawn on the fluorescence image of a GC, and the ratio ($R = F_{iso}/F_{380}$) of averaged fluorescence over the ROI at

the isosbestic wavelength (360 nm; F_{iso}) to that at 380 nm (F_{380}) was converted to $[Ca^{2+}]_i$ according to the equation: $[Ca^{2+}]_i = K_{eff} \cdot (R - R_{min}) / (R_{max} - R)$, where K_{eff} was estimated as 8.12 μM. Calibration parameters were determined by "in-cell" calibration as described previously (Lee et al., 2008).

To quantify Ca^{2+} clearance, I analyzed the decay phase of a CaT evoked by a short depolarizing pulse under different conditions. Because Ca^{2+} clearance depends on the peak $\Delta[Ca^{2+}]$ level, the duration of depolarization was adjusted in the range between 50 and 100 ms, such that the peak $\Delta[Ca^{2+}]$ level of the evoked CaT is typically 1 μM. The decay phase was fitted with a biexponential function: $A_0 + A_1 \cdot \exp(-r_1 \cdot t) + A_2 \cdot \exp(-r_2 \cdot t)$. Assuming that intracellular Ca^{2+} buffers are alike among GCs, the weighted average of the rate constants (r_w), which is defined as $(A_1 \cdot r_1 + A_2 \cdot r_2) / (A_1 + A_2)$, can be regarded as a parameter representing Ca^{2+} clearance at the peak of the CaT, and exhibits little dependence on the peak $\Delta[Ca^{2+}]$ level when it is higher than 0.8 μM (Lee et al., 2009).

For activating Src family kinase (SFK), phosphotyrosine peptide, EPQ(pY)EEIPIA (Liu et al., 1993) was synthesized by a commercial facility (AnyGen, Gwangju, Korea).

17. Statistical analysis

Data were analyzed using Igor Pro (version 6.2, WaveMetrics, Lake Oswego, OR, USA), and are presented as mean ± SEM. The statistical significance of differences between two experimental conditions was evaluated using Student's *t*-test using a significance level (p) of 0.05 or 0.01. That between more than two groups was evaluated using one-way ANOVA. In Results, the first and the second statistical values in parentheses intervened by "vs." represent statistical data under control conditions and under test conditions, respectively.

RESULTS

1. NCKX2 interacts with KIF21A

NCKX2 has 11 proposed transmembrane segments (TMSs) and a large intracellular loop between the 5th and 6th TMSs (Cai et al., 2002; Kinjo et al., 2003) (**Fig. 1A**). I hypothesized that the cytosolic loop of NCKX2 interacts with a transporter molecule that mediates the axonal transport of NCKX2. To identify proteins interacting with NCKX2, I performed yeast two-hybrid screening of a mouse brain cDNA library (~10^6 clones) using the central cytoplasmic loop of NCKX2 [NCKX2-loop; amino acids (aa) 288-478] as bait. Sequence analysis revealed that two different positive clones (aa 1475-1573, 1513-1573) encoded the C-terminal segment of KIF21A which contains WD-40 repeats, a putative cargo-binding domain (Marszalek et al., 1999). To verify the specific interaction of NCKX2 with KIF21A, I compared the interaction of NCKX2-loop with KIF21A to that with other KIF members using the yeast two-hybrid system. I created constructs for cargo-binding domains of four different KIF members: KIF4 (same family as KIF21A), KIF5B (different family from KIF21A), KIF21A and KIF21B, which are free of 'motor' or 'motor and stalk' domains (referred to as 'dominant negative' variants; **Fig. 1B**). NCKX2-loop and dominant negative KIF21A (dnKIF21A) were co-transformed into a haploid yeast, AH109, resulting in growth of colonies on the triple dropout plate (-Trp, -Leu, -His). However, none of the other dominant negative variants of KIF (dnKIF4, dnKIF5B or dnKIF21B) allowed growth of colonies on the triple dropout plate when co-transformed together with NCKX2-loop (**Fig. 2A**). These data are indicative of high specificity in the interaction between NCKX2-loop and KIF21A.

To test whether KIF21A and NCKX2-loop interact in a mammalian cell environment, I transfected HEK293 cells with c-myc-tagged NCKX2-loop (myc-NCKX2-loop) plus one of FLAG-tagged KIFs (FLAG-KIFs), and performed co-immunoprecipitation. I found that myc-NCKX2-loop was co-immunoprecipitated with FLAG-KIF21A or FLAG-dnKIF21A, but little with FLAG-KIF21B or FLAG-dnKIF21B (**Fig. 2B**). These results indicate that the NCKX2-loop interacts specifically with the WD-40 repeats of KIF21A.

Next, I verified the association of the endogenous NCKX2 with KIF21A in neurons. The lysate of cultured hippocampal neurons was immunoprecipitated with two different kinds of anti-KIF21A antibody (see Materials and Methods for details). NCKX2 was detected by immunoblotting in the anti-KIF21A immunoprecipitate (**Fig. 2C**, upper). Conversely, KIF21A was detected in the immunoprecipitate brought down by anti-$NCKX2_{loop}$ (see Materials and Methods for its definition; **Fig. 2C**, lower), indicating that endogenous NCKX2 and KIF21A are parts of a complex in a neuron. The specificity of anti-KIF21A and anti-NCKX2 antibodies was verified by immunocytochemistry (**Fig. 3A**) and/or by the antibody pre-absorption tests (**Fig. 3B**).

To test further the hypothesis that NCKX2 is associated with KIF21A, I examined whether NCKX2 and KIF21A are co-localized in a neuron. I performed immunocytochemistry on cultured hippocampal neurons expressing FLAG-KIF21A. Triple-immunostaining with anti-FLAG, anti-$NCKX2_{ext}$ (see Materials and Methods for its definition; **Figs. 4A and 4B** for specificity test) and anti-NF-H revealed that endogenous NCKX2 was co-localized with FLAG-KIF21A at the axon (**Figs. 5A and 5B**). To quantify the co-localization between NCKX2 and FLAG-KIF21A, the correlation of fluorescence intensities was estimated by calculating the product of difference from the mean (PDM) in each pixel in the binary mask of the FLAG-positive

axonal neurite (**Fig. 5C**; see Materials and Methods for details). Calculated PDM values are shown as a scattered plot of green and red pixel intensities against their PDM value at each paired pixel (total number of pixel pairs = 2056; **Fig. 5D**). The plot clearly skewed toward the positive PDM value, and this analysis generated the intensity correlation quotient (ICQ) of +0.20 that was significantly different from zero ($P_{sign\text{-}test} < 0.001$). The distribution of NCKX2/FLAG-KIF21A complexes along the axon could be clearly represented by the PDM image, an image where each pixel is equal to the PDM value at that location (**Fig. 5Cb**). The line profiles of NCKX2 (green) and FLAG-KIF21A (red) fluorescence intensities as well as the PDM image demonstrate that the NCKX2/FLAG-KIF21A complexes are localized in puncta along the axon fiber and in the axon terminal (**Fig. 5E**).

2. Axonal transport of NCKX2 is mediated by KIF21A

I tested whether the interaction of NCKX2 with KIF21A is functionally relevant to the transport of NCKX2. In order to visualize NCKX2 in neurons, I created a NCKX2-GFP fusion protein by inserting EGFP into the extracellular domain of NCKX2, downstream of the N-terminal signal sequence (**Fig. 1A**). Its functional competence was confirmed following expression in HEK293 cells (**Fig. 6A**). When I expressed NCKX2-GFP in cultured rat hippocampal neurons, NCKX2-GFP was distributed throughout the cell including neurites (**Fig. 6B**, left). In contrast, when dnKIF21A was co-expressed together with NCKX2-GFP, little GFP signal was observed on the longest neurite, a putative axon fiber (Dotti et al., 1988) (**Fig. 6B**, right), implying that overexpressed dnKIF21A inhibits the axonal transport of NCKX2 by overriding endogenous KIF21A. I quantified the transport of NCKX2 by axon tracing. To this end, NCKX2-GFP was co-

transfected with DsRed, a red fluorescent protein into primary cultured hippocampal neurons. Cell morphology was visualized from the fluorescence of DsRed. After tracing the longest neurite using NeuronJ, a neurite tracing program (Meijering et al., 2004), I measured the GFP intensity values on the traced line (**Figs. 7A and 7B**). In this experiment, I presumed the longest neurites as axons. Overexpression of dnKIF21A affected neither the length of axon fibers (**Fig. 7D**) nor the expression level of NCKX2-GFP judged from the GFP fluorescence at the soma (**Figs. 7A, 7B and 7C**). Compared with the neurons expressing NCKX2-GFP alone or NCKX2-GFP plus KIF21A, those expressing dnKIF21A displayed significantly lower fluorescence intensity of NCKX2-GFP along the axon fiber, suggesting that the axonal transport of NCKX2-GFP is inhibited by dnKIF21A (**Fig. 7C**). In contrast, dnKIF21B did not inhibit the axonal transport of NCKX2-GFP (**Fig. 7C**).

In order to confirm the effects of dnKIF21A on the axonal transport of NCKX2, dendrites and axon fibers were identified by immunochemical labeling with MAP2 or Tau-1, respectively. When NCKX2-GFP was co-expressed with KIF21A, NCKX2-GFP was localized at both the MAP2-positive neurites (dendrites) and the MAP2-negative neurite (axon) (**Fig. 8A**). When NCKX2-GFP was co-expressed with dnKIF21A, however, NCKX2-GFP overlapped with MAP2 but not with Tau-1 (**Fig. 8B**). To quantify the effect of dnKIF21A on the axonal transport of NCKX2-GFP, I calculated the axon-to-dendrite ratio (ADR) of NCKX2-GFP fluorescence. The dendritic and axonal NCKX2-GFP fluorescence levels were measured from the ROI that covers the MAP2-positive or -negative neurite, respectively, after nullifying the background fluorescence (**Fig. 8C**, see Materials and Methods for details). The ADR of NCKX2-GFP was significantly reduced in the neurons co-expressing dnKIF21A compared to those co-expressing KIF21A (**Fig. 8D**; KIF21A, 0.914 ± 0.059, n = 12; dnKIF21A,

0.474 ± 0.078, n = 9, $p < 0.01$). In contrast, the fluorescence of NCKX2-GFP in the dendrites normalized to that in the soma (DSR) was not significantly different between KIF21A and dnKIF21A-expressed groups (**Fig. 8D**; KIF21A, 0.109 ± 0.017, n = 12; dnKIF21A, 0.156 ± 0.016, n = 9, $p > 0.05$). These results confirm that dnKIF21A inhibited the axonal transport of NCKX2.

To verify that the effects of dnKIF21A are specific for NCKX2, I examined transport of another presynaptic protein, synaptophysin. dnKIF21A did not inhibit the axonal transport of GFP-tagged synaptophysin (**Fig. 8E**), indicating that dnKIF21A does not cause nonspecific inhibition of axonal transport.

3. Knockdown of KIF21A abolishes the axonal transport of NCKX2

To test whether KIF21A mediates the axonal transport of endogenous NCKX2, I depleted KIF21A using short hairpin RNA (shRNA). Co-transfection in HEK293 cells of shRNA targeted to KIF21A (shKIF21A) together with FLAG-KIF21A completely knocked down the expression of KIF21A (**Fig. 9A**). I used a lentiviral delivery system to knockdown the endogenous KIF21A in hippocampal neurons. Immunoblot analyses at different time points after infection of virus encoding shKIF21A revealed that the expression level of KIF21A was decreased by 73% of non-infected control levels at 11~14 days post-infection (dpi), whereas it was not affected by non-targeting shRNA (NT) control (**Fig. 9B**). I transfected shKIF21A to hippocampal neurons on the 3rd day *in vitro* (DIV3), and then immunostained them with anti-$NCKX2_{ext}$ at 15th day after transfection to observe the subcellular distribution of endogenous NCKX2. The KIF21A-depleted cells could be distinguished from untransfected cells by the fluorescence of monomeric red fluorescent protein (mRFP) contained in the shRNA

constructs as an expression marker. Similar to exogenous NCKX2-GFP (**Fig. 8A**), endogenous NCKX2 was detected at both the axon and dendrites of the untransfected control (**Fig. 10A**). In the KIF21A-depleted neuron, however, immunoreactivity of endogenous NCKX2 was reduced in the axonal compartment, but not in the dendritic region (**Fig. 10B**).

To quantify the knockdown effect of KIF21A on the axonal transport of endogenous NCKX2, I calculated ADR of NCKX2 immunofluorescence in the similar manner as in **Fig 8C** (**Fig. 10C**). The ADR of endogenous NCKX2 was significantly reduced in the KIF21A-depleted neurons compared to the untransfected control (control, 0.832 ± 0.066, n = 8; shKIF21A, 0.287 ± 0.043, n = 6, $p < 0.01$). In contrast, the DSR of NCKX2 was not significantly different between control and KIF21A-depleted groups (control, 0.135 ± 0.010, n = 8; shKIF21A, 0.140 ± 0.014, n = 6, $p > 0.1$). These results confirm that KIF21A is essential for the axonal transport of NCKX2.

4. Knockdown of KIF21A alters calcium kinetics at the axon terminal

Previous studies revealed that NCKX is the major calcium extrusion machinery at axon terminals but not in the soma (Kim et al., 2003; Lee et al., 2009; Lee et al., 2002). I tested whether the depletion of endogenous KIF21A has differential effects on calcium signaling in the soma and axon terminals in hippocampal neurons.

I measured Ca^{2+} transients (CaTs) at mossy fiber boutons (MFBs), *en passant* boutons of dentate granule cells (GCs), in hippocampal organotypic slice cultures. On DIV7-8, the slices were infected with lentivirus encoding shKIF21A, shNCKX2 (**Fig. 11**) or non-targeting shRNA (as a control) by local injection. On 13-17 dpi, I identified lentivirus-infected cells by mRFP fluorescence (**Fig. 12A**), and loaded the infected GCs

with 200 μM Oregon Green 488 BAPTA-5N (OGB-5N), a low-affinity Ca^{2+} indicator dye (K_D ~ 50 μM), via whole-cell patch pipette (**Fig. 12B**). The CaTs were evoked by applying high-frequency stimulation [HFS, a 5 s train of action potential (AP)-like pulses, each comprising a 2 ms depolarization pulse to 0 mV] delivered at 33 Hz to the somata of GCs. Because calcium clearance mechanisms undergo developmental change, my analysis was restricted to mature GCs which exhibit low input resistance (< 300 MΩ) (Lee et al., 2009). I traced the mossy fiber under the confocal microscope, and identified MFBs by morphological characteristics (Lee et al., 2007a) (**Fig. 12B**, inset). The plateau $[Ca^{2+}]$ level attained by a train of AP-induced CaTs (AP-CaTs) depends on both calcium clearance and the amplitude of individual AP-CaTs (Regehr et al., 1994). Thus, I confirmed that the mean amplitude of AP-CaTs measured by line-scan imaging of Oregon Green 488 BAPTA-1 (OGB-1) fluorescence at the MFBs was not affected by shKIF21A or shNCKX2, ruling out any possible alteration in calcium influx (**Figs. 13A and 13B**).

The mean value for $[Ca^{2+}]_i$ increment ($\Delta[Ca^{2+}]_i$) of HFS-induced CaTs (presented as $\Delta F/F_0$) at the MFBs of KIF21A-depleted GCs was significantly higher than of control GCs, but was almost the same as that of NCKX2-depleted MFBs [**Fig. 13C**, peak $\Delta F/F_0$ of CaTs in MFBs, 1.302 ± 0.050 in the control (n = 64, 12 cells) *vs*. 2.161 ± 0.079 in shKIF21A (n = 46, 15 cells, $p < 0.01$) *vs*. 2.171 ± 0.148 in shNCKX2 (n = 26, 5 cells, $p < 0.01$)]. CaTs in the somata, dendritic shafts and spines of GCs, on the other hand, were not significantly different between control and KIF21A or NCKX2-depleted groups (**Fig. 13C and Table 1**).

Previously Kim et al. showed that effects of NCKX inhibition on Ca^{2+} clearance became evident when the $\Delta[Ca^{2+}]_i$ was higher than about 0.4 μM (Kim et al., 2005). The $[Ca^{2+}]_i$ level attained by HFS at 33 Hz in the somatodendritic region may not be

sufficient to activate NCKX (**Fig. 13C**), and thus I induced higher CaTs by applying HFS at 100 Hz. Despite the higher plateau $[Ca^{2+}]_i$, no difference was found in CaTs between control and KIF21A-depleted groups at somata, dendritic spines and shafts (**Fig. 13D and Table 1**), indicating that shKIF21A has no significant effect on the calcium kinetics in the somatodendritic compartment. Therefore, depletion of KIF21A in dentate GCs altered calcium clearance specifically at the MFBs.

5. Surface expression of NCKX2 is polarized to the axon and its terminals

It has been demonstrated that the Na^+/Ca^{2+} exchange activity in the soma of a dentate GC is independent of intracellular K^+, indicative of little NCKX activity (Lee et al., 2009). Consistently, knockdown of NCKX2 did not affect the calcium dynamics at the somatodendritic region (**Fig. 13C**). I inquired why not only the axon but also the somatodendritic regions are immunoreactive to NCKX2 (**Figs. 5A and 10A**). To address this question, I investigated subcellular distribution of NCKX2 expressed on the plasma membrane (surface NCKX2) in cultured hippocampal neurons using live-cell immunocytochemistry with anti-$NCKX2_{ext}$. In the membrane-permeabilized condition, NCKX2-immunoreactive signals were distributed throughout the cell both in the soma and neurites (**Figs. 10A and 14Aa**). In contrast, the surface NCKX2 signals were co-localized with Tau-1 and a presynaptic protein, synaptophysin (**Fig. 14Ab-d**) but not with MAP2 (**Fig. 14Ae**). To rule out possible effects of endo- and exocytosis, I repeated live-cell immunolabeling at 4˚C. The surface expression pattern of NCKX2 at 4˚C was similar to that at 36˚C (**Fig. 14Af**).

I transfected the NCKX2-GFP construct into cultured hippocampal neurons, and observed protein localization at 3-10 days after transfection. DsRed was co-expressed to

visualize the entire morphology of the neuron. The GFP signal was diffuse throughout the neuron including the axon and dendrites (**Fig. 14Ba**). Live-cell immunostaining with anti-GFP antibody, however, revealed that the immunoreactivity of surface GFP was not co-localized with MAP2, but it was detected on the MAP2-negative neurites (**Fig. 14Bb**). Thus, surface NCKX2-GFP exists along the axon, similar to endogenous NCKX2. These results indicate that surface expression of not only endogenous but also exogenous NCKX2 is highly polarized to the axon and its terminals, and support the results of the functional studies.

6. Endocytosis restricts the surface expression of NCKX2 on the somatodendritic compartment

Under permeabilized conditions, NCKX2-immunoreactivity was positive not only in the axon but also in the somatodendritic compartment where the previous studies could not observe NCKX activity (Kim et al., 2003; Lee et al., 2009). The discrepancy between morphological and functional results could be reconciled by the differential surface expression of NCKX2 between the axonal and somatodendritic compartments (**Fig. 14**). The differential surface and cytosolic distribution of NCKX2 in the dendritic compartment implies that the axonal targeting of NCKX2 is regulated by the selective retention model (Sampo et al., 2003). According to this model, I hypothesized that the cytoplasmic NCKX2 may be transported to the dendrite and then eliminated from the dendritic surface. To test this hypothesis, I investigated whether inhibition of endocytosis has an effect on the somatodendritic surface expression of NCKX2. When the NCKX2-GFP-expressing hippocampal neurons were treated with dynasore (40 μM, for 4 hours), a cell-permeable dynamin inhibitor, they exhibited greatly increased surface expression of NCKX2-GFP in the somatodendritic region, compared to the

neurons treated with vehicle (0.1% DMSO) (**Fig. 15A**). To quantify the polarization of surface expression, I calculated the ADR of surface NCKX2-GFP using the binary mask of MAP2-positive and negative neurites of a cell created from the fluorescence image of NCKX2-GFP (**Fig. 15C**; see Materials and Methods for details). The ADR of surface NCKX2-GFP was significantly lower in the dynasore-treated neurons than in the vehicle-treated control (**Fig. 15D**; control, 3.436 ± 1.120, n = 6; dynasore-treated group, 0.831 ± 0.127, n = 7, $p < 0.05$). Similar to exogenous NCKX2-GFP, the endogenous NCKX2 was notably increased on the somatodendritic surface by dynasore (**Figs. 15E and 15F**; control, 14.62 ± 1.22, n = 7; dynasore, 24.31 ± 3.56, n = 9; $p < 0.01$). As an alternative way to block clathrin-mediated endocytosis, I employed a dominant-negative mutant of dynamin-1, which was created by replacing the lysine residue with alanine at the amino acid position 44 (DYN1-K44A) (Damke et al., 1994). NCKX2-FLAG was co-expressed together with wild-type dynamin-1 (DYN1-WT) or DYN1-K44A. Similar to dynasore, overexpression of DYN1-K44A increased the surface expression level of NCKX2-FLAG in the somatodendritic compartment, whereas DYN1-WT had little effect (**Fig. 15B**). These results demonstrate that preferential endocytosis of NCKX2 from the somatodendritic surface together with KIF21A-mediated axonal transport of NCKX2 underlies the polarized axonal targeting of NCKX2.

7. Inhibition of endocytosis allows the NCKX activity to emerge in the dendritic region of GCs

To confirm the hypothesis that endocytosis suppresses the surface expression of NCKX2 in the somatodendritic region, I tested whether pretreatment of GCs with dynasore enhances the NCKX activity in their proximal dendrites. To estimate Ca^{2+} clearance, I evoked a CaT in a GC with a short depolarizing pulse under eight different

conditions: normal or low extracellular [Na^+] ([Na^+]$_{ext}$); K^+- or TMA^+-based pipette solution (K_i or TMA_i, respectively); pretreatment with dynasore or DMSO as vehicle. Averaged CaTs in each condition are compared in **Fig. 16A**. Pretreatment with dynasore (40 μM, for an hour) accelerated the Ca^{2+} decay rate under normal [Na^+]$_{ext}$ and K_i conditions but not under low [Na^+]$_{ext}$ or TMA_i conditions (**Fig. 16A**). Averaged traces for CaTs in normal and low [Na^+]$_{ext}$ are compared in each panel of **Fig. 16B** under four different conditions as indicated. I fitted a biexponential function to the decay phase of an individual CaT, and regarded the weighted average of rate constants (r_w) of the fitted function as a parameter for Ca^{2+} clearance (Lee et al., 2009). I estimated the NaCaX activity in a GC as a difference between the r_w value measured in the normal [Na^+]$_{ext}$ and that in the low [Na^+]$_{ext}$ (**Fig. 16C**). Consistent with my previous report (Lee et al., 2009), the dendritic NaCaX activity was little altered by TMA^+-based pipette solution, indicating that most NaCaX activity can be attributed to NCX rather than NCKX (**Fig. 16Cc**; K_i, 1.58 ± 0.26/s, n = 7; TMA_i, 1.22 ± 0.16/s, n = 5, $p > 0.1$). In contrast, pretreatment of the GCs with dynasore greatly enhanced the NaCaX activity under the K_i condition (**Fig. 16Cc**; 3.00 ± 0.21/s, n = 5, $p < 0.01$), but not under the TMA_i condition where the NaCaX activity was rather decreased from unknown reasons (**Fig. 16Cc**; 0.78 ± 0.12/s, n = 6, $p < 0.05$). These results indicate that dynasore enhances the dendritic NaCaX activity, and that the effect of dynasore requires intracellular K^+. Therefore, these observations strongly suggest that NCKX rather than NCX is responsible for the NaCaX activity enhanced by dynasore in the proximal dendrite. I conclude that the surface expression of NCKX is restricted by endocytosis in the somatodendritic region.

8. NCKX2 interacts with the μ2 subunit of AP-2

Dynamin-1, one of the key players in clathrin-mediated endocytosis, is involved in the low surface expression of NCKX2 in the somatodendritic region (Lee et al., 2012). Given that clathrin-mediated endocytosis is responsible for the internalization of surface NCKX2, NCKX2 may interact with adaptor protein(s) of clathrin-coated vesicles. Clathrin-mediated endocytosis is initiated by recruitment of AP-2 to a target molecule. The cytosolic loop region of NCKX2 [NCKX2-loop, amino acids (aa) 288-478] has two tyrosine motifs (^{365}YGKL and ^{371}YDTM; **Fig. 17A**), potential recognition sites for the μ2 subunit of AP-2.

To test whether NCKX2-loop interacts with the μ2 subunit, c-myc-tagged NCKX2-loop (myc-NCKX2-loop) and HA-tagged μ2 (HA-μ2) were co-transfected into HEK293 cells. The cell lysate was immunoprecipitated with anti-c-myc IgG-conjugated agarose, and then HA-μ2 was detected by immunoblotting. I found that myc-NCKX2-loop was coimmunoprecipitated with HA-μ2 (**Fig. 17B**).

9. Tyr-365 of NCKX2 is necessary for interaction with μ2

To determine whether either or both of the two tyrosine motifs are important for the interaction, I created mutant constructs of myc-NCKX2-loop, in which the 365th tyrosine (Tyr-365) or the 371st tyrosine residue (Tyr-371) or both of them are mutated to alanine (**Fig. 17A**; denoted as Y365A, Y371A and YYAA, respectively). Using coimmunoprecipitation assay, I examined the interaction of HA- μ2 with each mutant that were expressed in HEK293 cells. Coimmunoprecipitation of HA-μ2 was significantly reduced by mutation of Y365A, but not by Y371A (**Fig. 17B**; WT, 36.91 ± 6.57; Y365A, 9.46 ± 4.73, $p < 0.01$; Y371A, 41.60 ± 11.28, $p = 0.73$, $n = 5$). The

amount of coimmunoprecipitated HA- μ2 was not further reduced by the mutation of YYAA compared with Y365A (**Fig. 17B**; YYAA, 7.92 ± 3.12, n = 5, p = 0.79). These results indicate that Tyr-365, but not Tyr-371, of NCKX2 is necessary for interaction with the μ2 subunit of AP-2. To test whether phosphorylation of Tyr-365 is necessary for the interaction, we replaced Tyr-365 with glutamate (**Fig. 17A**; denoted as Y365E). HA- μ2 was not co-immunoprecipitated with the Y365E mutant, suggesting that μ2 interacts with NCKX2 via dephosphorylated form of ^{365}YGKL (**Fig. 17B**; Y365E, 7.83 ± 4.12, n = 5, p < 0.01).

10. The Y365A mutant of NCKX2 displays higher surface expression in the somatodendritic region than wild-type NCKX2

Given that NCKX2-Y365A is little recognized by μ2, the endocytosis of NCKX2-Y365A might be suppressed in somatodendritic regions of a neuron. To test this prediction, I transfected with FLAG-tagged wild-type or Y365A mutant of NCKX2 (NCKX2-WT or NCKX2-Y365A) in primary cultured rat hippocampal neurons and detected the surface and internalized NCKX2 using anti-FLAG antibody. For immunostaining of surface NCKX2, live cells were incubated with anti-FLAG at 4°C, a temperature prohibiting endocytosis. For immunolabeling of internalized NCKX2, live cells were first incubated with anti-FLAG at 37°C, an endocytosis-permissive temperature, and then surface-bound antibodies were removed by washing with an acidic buffer (pH 2). To visualize the entire morphology of the transfected neuron, a red fluorescent protein, tdTomato, was co-expressed.

Consistent with my previous study (Lee et al., 2012), the surface expression of FLAG-tagged NCKX2-WT was not co-localized with the neurites immunoreactive for

MAP2, a dendritic marker, indicating the polarized distribution of surface NCKX2 to the axonal region. In contrast, surface NCKX2-Y365A was distributed in the somatodendritic as well as the axonal compartment (**Fig. 18A**). On the other hand, the internalized NCKX2-WT was detected in both somatodendritic and axonal regions, whereas little immunoreactivity from internalized NCKX2-Y365A was detected (**Fig. 18A**).

To quantify the polarized expression of wild type or Y365A mutant of NCKX2, I estimated the axon-to-somatodendrite ratio (A/SD ratio; see Materials and Methods). Somatodendritic ROI (SD-ROI) was defined as the overlap between tdTomato- and MAP2-positive regions. The axonal ROI was made by subtracting SD-ROI from the Tomato mask (**Fig. 18B**). I determined an A/SD ratio from the averaged fluorescence intensities of surface or internalized NCKX2 over the axonal- and SD-ROIs.

The A/SD ratio of surface NCKX2-WT (s-WT) was significantly higher than that of tdTomato in the same cell (**Fig. 18C**; s-WT, 0.933 ± 0.056; tdTomato, 0.600 ± 0.037, n = 11, $p < 0.01$). In contrast, the surface expression of Y365A mutant of NCKX2 (s-Y365A) displayed no axonal polarization (**Fig. 18C**; s-Y365A, 0.630 ± 0.038; tdTomato, 0.607 ± 0.020, n = 14, $p = 0.62$). Although tdTomato is assumed to display no polarized distribution in a neuron, the A/SD ratio of tdTomato was smaller than unity, most likely because the larger intracellular volume of the somatodendritic compartment is much larger than that of the axon (Rivera et al., 2003;Lewis et al., 2009). I normalized the A/SD ratio of NCKX2 to that of tdTomato, which was approximately 0.6 (denoted as “normalized A/SD ratio”). The normalized A/SD ratio of s-WT was higher than unity, indicating that s-WT is polarized to the axon (**Fig. 18C**; 1.59 ± 0.10, n = 11). In contrast, the normalized A/SD ratio of s-Y365A was significantly lower than that of s-WT and close to unity (**Fig. 18C**; 1.03 ± 0.04, n = 14, $p < 0.01$), indicating that the surface

expression of NCKX2-Y365A is not polarized.

Next, I estimated the A/SD ratio of the immunofluorescence from internalized NCKX2-WT (i-WT) or NCKX2-Y365A (i-Y365A). Both the somatodendritic region and the axonal region were immunoreactive for i-WT, but immunofluorescence was much higher in the former than in the latter (**Fig. 18A**). Consistently, the A/SD ratio of i-WT was significantly lower than that of tdTomato in the same cell (**Fig. 18D**; i-WT, 0.249 ± 0.052; tdTomato, 0.509 ± 0.026, n = 9, $p < 0.01$), indicating the internalization of NCKX2-WT is much stronger from the somatodendritic surface than the axonal surface. Because the immunoreactivity of i-Y365A was negligible in both axonal and somatodendritic regions (**Fig. 18A**), it is meaningless to estimate the A/SD ratio of i-Y365A. When measured under the same imaging settings, the spatially-averaged immunofluorescence intensity of i-Y365A was significantly lower than that of i-WT in the somatodendritic compartment (**Fig. 18D**; i-WT, 22.3 ± 4.7, n = 9; i-Y365A, 7.6 ± 1.6, n = 7, $p < 0.05$), indicating that the Y365A mutation of NCKX2 prevents its somatodendritic endocytosis. These results strongly suggest that the Tyr-365 of NCKX2 is essential not only for the interaction with the μ2 subunit of AP-2 but also for the endocytosis of NCKX2 from the somatodendritic surface.

11. Knockdown of the μ2 subunit abolishes the endocytosis of NCKX2

To verify the contribution of μ2 to the endocytosis of NCKX2, I studied the effect of shRNA-mediated depletion of μ2 on the NCKX2 trafficking. The knockdown efficiency of μ2-targeting shRNA (shμ2) was tested in HEK293 cells heterologously expressing HA-μ2 together with shμ2 or non-targeting control shRNA (shNT). The shμ2, but not the shNT, completely depleted HA-μ2 (**Fig. 19A**). Next, I tested whether the depletion

of μ2 abolishes the endocytosis of NCKX2. FLAG-tagged NCKX2-WT was cotransfected with shμ2 and tdTomato (as a morphological marker) into DIV8 hippocampal neurons. Five or six days later, surface or internalized NCKX2 was detected by immunolabeling with anti-FLAG antibody. Compared with the neurons expressing shNT, those expressing shμ2 displayed higher surface expression of NCKX2 in the somatodendritic region and a dramatic reduction of internalized NCKX2 (**Fig. 19B-D**). As is evident from the normalized A/SD ratio in **Fig. 19C**, shμ2 abolished axonal polarization of surface NCKX2. These results suggest that the surface expression of NCKX2 is maintained low by μ2-mediated endocytosis in somatodendritic compartments.

12. Src family kinase-mediated Tyr-365 phosphorylation of NCKX2 regulates its surface expression

The inhibitory effect of the phosphomimetic mutation at Tyr-365 (Y365E) on the interaction with μ2 raises a possibility that endocytosis of NCKX2 could be regulated by phosphorylation of Tyr-365 (**Fig. 17B**). Endocytosis of many neuronal membrane proteins, such as the β3 and γ2 subunits of the $GABA_A$ receptor (Jurd et al., 2010; Kittler et al., 2005; Kittler et al., 2008) and the GluN2B subunit of the NMDA receptor (Prybylowski et al., 2005), is regulated by tyrosine phosphorylation of the tyrosine (YxxΦ) motif by a Src family kinase (SFK). In general, phosphorylation of a tyrosine motif by SFK inhibits the interaction of the μ2 subunit and subsequent endocytosis, resulting in the enhancement of surface expression levels. I examined the possibility that phosphorylation of Tyr-365 in the tyrosine motif (YGKL) of NCKX2 by SFK may prevent its endocytosis to increase the surface expression of NCKX2.

First, I tested whether SFK can phosphorylate the tyrosine motif of NCKX2. One of the upstream signaling molecules of SFK is proline-rich tyrosine kinase2 (PYK2), which is activated by intracellular Ca^{2+} elevation or PKC (Lev et al., 1995). Once Ca^{2+} triggers the phosphorylation of PYK2, activation of PYK2 and SFKs is maintained by reciprocal tyrosine phosphorylation (Girault et al., 1999). It is well known that PYK2 and SFK can be activated by carbachol (CCh) in PC-12 cells (Dikic et al., 1996; Lev et al., 1995). I transfected FLAG-tagged NCKX2-WT or NCKX2-Y365A into PC-12 cells, which normally express PYK2 and SFK, and treated the cells with 1 mM CCh for 2 min to activate PYK2 (Lev et al., 1995). To detect phosphorylated NCKX2, NCKX2 was immunoprecipitated with anti-FLAG-conjugated agarose beads, and then immunoblotted with anti-phosphotyrosine (pTyr) IgG. CCh significantly increased the tyrosine-phosphorylation of NCKX2-WT but not of NCKX2-Y365A (**Fig. 20A**), implying that Tyr-365 is the major target residue of the PYK2-SFK signaling cascade. Furthermore, the CCh-induced phosphorylation of Tyr-365 in NCKX2-WT was inhibited by pretreatment with PP2 (10 μM, for 30 min), a selective inhibitor of SFK (**Fig. 20A**), indicating that SFK is involved in the CCh-induced tyrosine-phosphorylation of NCKX2. I confirmed that there was little difference in expression levels of wild-type or Y365A mutant NCKX2 between control and CCh-treated groups by detection of FLAG in the same blot (**Fig. 20A**).

Given that the tyrosine motif of NCKX2 can be phosphorylated by SFK, I next tested whether the surface expression of NCKX2 can be reduced by PP2. I transfected FLAG-tagged NCKX2-WT or NCKX2-Y365A into primary cultured hippocampal neurons at DIV8, and treated the neurons at DIV12 with PP2 (10 μM) or vehicle (0.1% DMSO) for 2 hours. Observing surface NCKX2 by live-cell immunolabeling with anti-FLAG IgG, I found that PP2, but not vehicle, reduced the expression level of NCKX2-

WT both on the axonal and somatodendritic surfaces (**Fig. 20B**). To quantify the surface expression level of NCKX2, spatially-averaged immunofluorescence intensity of NCKX2 was measured in the SD- and axonal ROIs. As described above, SD- or axonal ROIs were defined based on the region immunoreactive for MAP2 and the tdTomato-positive region (**Fig. 218**). The A/SD ratio of surface NCKX2-WT in the vehicle-treated control neurons was not different from that of non-treated controls in **Fig. 18Ca** [0.79 ± 0.12 (n = 8) and 0.93 ± 0.06 (n=11), respectively; p = 0.25]. The inhibition of SFK by PP2 caused a decrease in the immunoreactivity of surface NCKX2 on both the somatodendritic and axonal surfaces [**Fig. 20C**; SD-ROI, 11.41 ± 1.55 (n = 8) vs. 5.92 ± 0.97 (n = 10); Axonal ROI, 8.74 ± 1.43 (n = 8) vs. 1.40 ± 0.42 (n = 10), $p < 0.01$]. These results indicate that Tyr-365 of NCKX2 can be phosphorylated by SFK and that SFK-dependent tyrosine phosphorylation of NCKX2 is essential for the somatodendritic and axonal surface expression. Since the Y365A mutant is not recognized by μ2 (**Fig. 17B**), it is expected that surface expression of the Y365A mutant is not affected by PP2. We found that PP2 did not suppress the surface expression of Y365A mutant on the somatodendritic compartments [**Fig. 20Bb and 20Cb**; SD-ROI, 23.93 ± 2.44 (n = 13) vs. 23.01 ± 2.93 (n = 8), p = 0.81; Axonal ROI, 9.16 ± 1.27 (n = 13) vs. 8.79 ± 1.01 (n = 8), p = 0.84], confirming that the inhibitory effect of PP2 on surface expression of NCKX2 results from inhibition of tyrosine phosphorylation of Tyr-365 residue of NCKX2. Note that neurons were permeabilized to double-immunolabel for MAP2 after live-cell immunolabeling of FLAG. The remaining green immunofluorescence in the somatic region after treatment with PP2 may be caused by nonspecific staining of the nucleus by the secondary antibody, because fluorophore-conjugated secondary antibody stained nuclei without a primary antibody under the permeabilized conditions (**Fig. 20D**). This non-specific immunolabeling may contribute to the higher

immunofluorescence in the SD-ROI than in the axonal ROI in the presence of PP2 (**Fig. 20Ca**).

13. Activation of Src family kinase enhances the NCKX activity in the proximal dendrite

I inquired whether the activation of SFKs can enhance the dendritic NCKX activity. To address this question, I estimated Ca^{2+} clearance in proximal dendrites of hippocampal granule cells (GCs) before and after SFK activation. To activate SFK, I included in the patch pipette a SFK-activating peptide (EPQ(pY)EEIPIA), which disrupts intramolecular interaction between the SH2 domain and phosphorylated tail of SFK (Liu et al., 1993). There was no significant difference in the resting $[Ca^{2+}]_i$ level between eight experimental conditions ($F_{(7,89)} = 0.751$, $p = 0.630$ by one-way ANOVA; **Fig. 21A**). Ca^{2+} clearance was estimated from analysis of the decay phase of Ca^{2+} transients (CaTs) evoked by a short depolarizing pulse (-70 mV to 0 mV) in the GCs loaded with 100 μM fura-4F, a Ca^{2+} indicator dye ($K_D \sim 0.77$ μM), via a whole-cell patch pipette. The pulse duration (50 - 100 ms) was adjusted such that the peak of the CaTs was between 0.8 and 1.2 μM and thus the peak values were not different between eight experimental conditions ($F_{(7,89)} = 1.10$, $p = 0.370$; **Fig. 21B**). I compared Ca^{2+} clearance under eight different conditions: normal or low extracellular $[Na^+]$ ($[Na^+]_{ext}$); K^+- or TMA^+-based pipette solution (denoted as K_i or TMA_i, respectively); with or without 1 mM EPQ(pY)EEIPIA in the pipette solution. Averaged traces of CaTs that were normalized to the peak in each condition are superimposed in **Fig. 21C**. Representative traces of CaTs measured in the same cell under normal and low $[Na^+]_{ext}$ conditions are compared in each panel of **Fig. 21D** under four different conditions.

Intracellular perfusion of EPQ(pY)EEIPIA accelerated the Ca^{2+} decay rate under normal $[Na^+]_{ext}$ and K_i conditions but not under low $[Na^+]_{ext}$ or TMA_i conditions (**Fig. 21C,D**). I fitted a biexponential function to the decay phase of an individual CaT, and regarded the weighted average of rate constants (r_w) of the fitted function as a parameter for Ca^{2+} clearance (Lee et al., 2007b). **Figs. 21Ea and 21Eb** show the summary for Ca^{2+} clearance under four different internal conditions in normal and low $[Na^+]_{ext}$, respectively. Under normal $[Na^+]_{ext}$ conditions, Ca^{2+} clearance estimated as r_w was significantly accelerated by SFK-activating peptide only under K^+-internal conditions [3.26 ± 0.15 (n = 23) vs. 4.76 ± 0.26 (n = 16), $p < 0.01$], and was not different between other three conditions ($F_{(2,46)} = 2.363$, $p = 0.105$; **Fig. 21Ea**). Under low $[Na^+]_{ext}$ conditions, Ca^{2+} clearance was not different between the four experimental conditions ($F_{(3,28)} = 2.422$, $p = 0.087$; **Fig. 21Eb**). I estimated the Na^+/Ca^{2+} exchanger (NaCaX) activity in a GC as a difference between the r_w value measured in the normal $[Na^+]_{ext}$ and that in the low $[Na^+]_{ext}$ (**Fig. 21Ec**). Consistent with previous reports (Lee et al., 2009), the dendritic NaCaX activity was little altered by TMA^+-based pipette solution, indicating that most NaCaX activity can be attributed to NCX rather than NCKX (**Fig. 21Ec**; K_i, 1.44 ± 0.16/s, n = 6; TMA_i, 1.36 ± 0.31/s, n = 8, $p = 0.85$). In contrast, application of EPQ(pY)EEIPIA greatly enhanced the NaCaX activity under the K_i condition but not under the TMA_i condition (**Fig. 21Ec**; K_i, 2.74 ± 0.20/s, n = 7, $p < 0.01$; TMA_i, 0.95 ± 0.21/s, n = 9, $p = 0.28$). These results suggest that NCKX rather than NCX is responsible for the NaCaX activity enhanced by SFK activation in the proximal dendrite. Therefore, I conclude that the surface expression of NCKX is regulated by its endocytosis, and the endocytosis is regulated by SFK-dependent phosphorylation of Tyr-365.

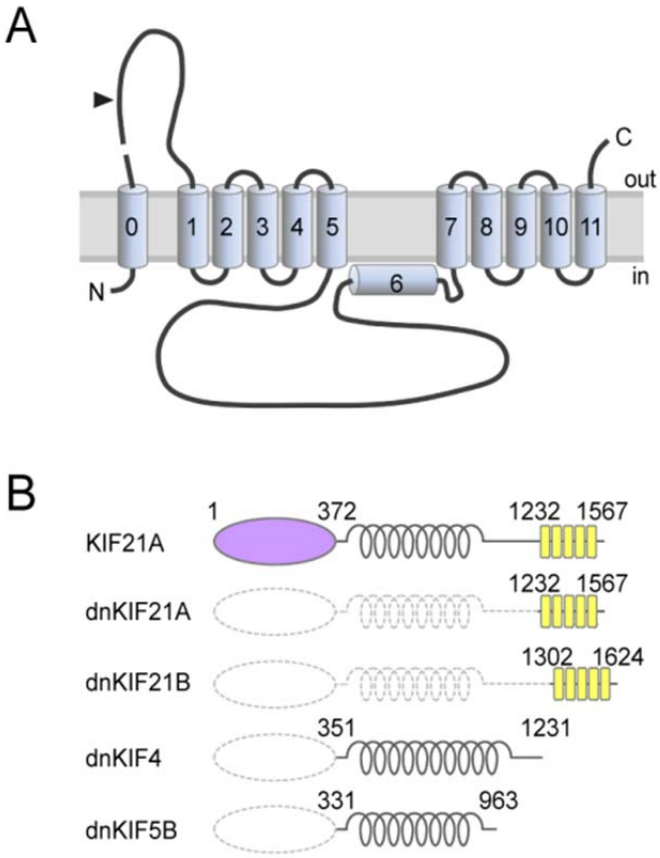

Figure 1. The schematic illustrations of NCKX2 and KIF21A.

(A) A topological model of NCKX2. NCKX2 has a large intracellular loop between the 5th and 6th TMSs. The arrowhead indicates the position where EGFP was inserted to make EGFP-tagged NCKX2 (NCKX2-GFP). **(B)** Schematic illustration of the structure of wild-type KIF21A and dominant negative mutant (dn-) of KIF21A, KIF21B, KIF4 and KIF5B. The kinesin motor heads, coiled-coil stalks and WD-40 repeats are shown by the violet oval, gray-colored coils and yellow boxes, respectively. Deleted regions are indicated by dotted lines. Note that wild-type KIF4 and KIF5B tails have no WD-40 repeats.

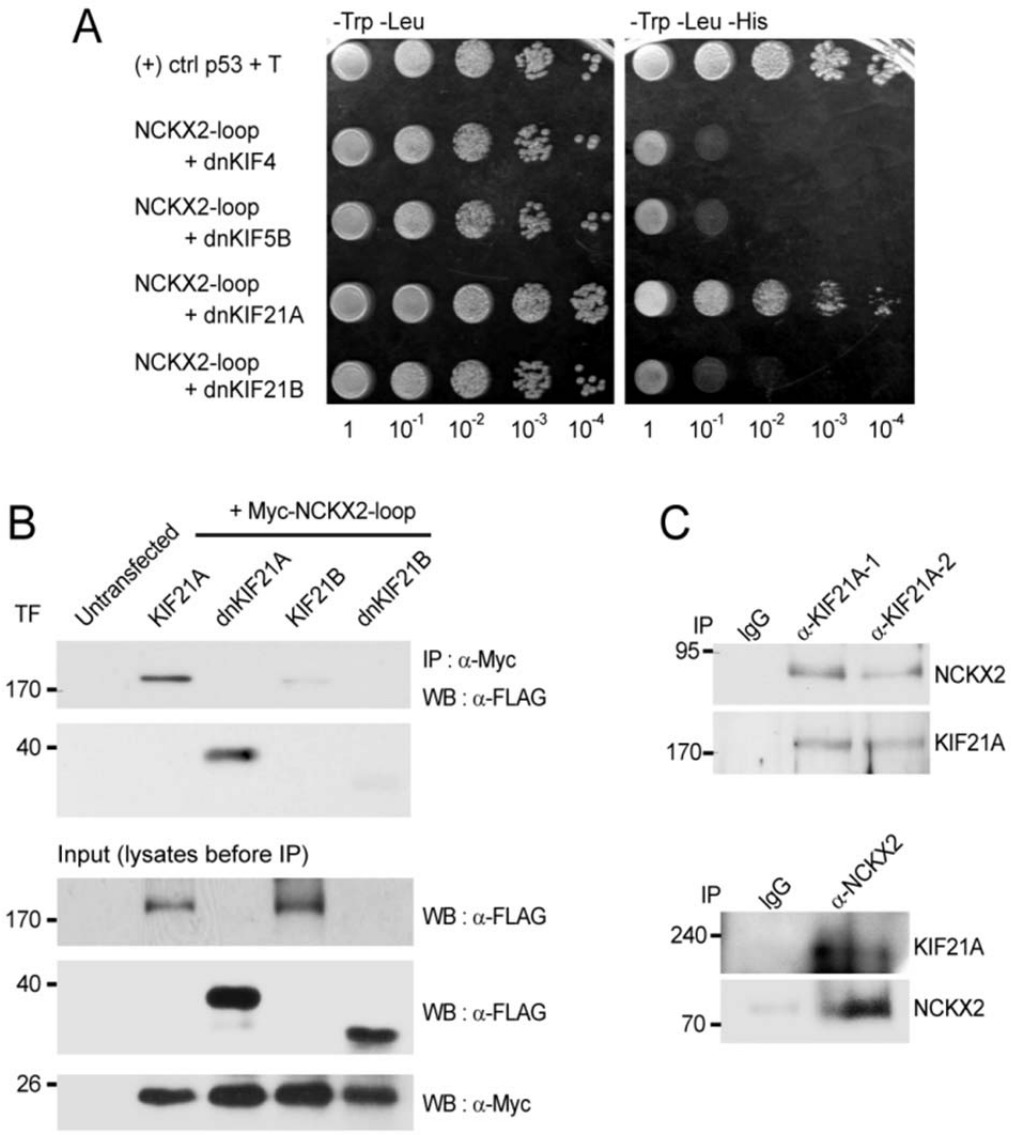

Figure 2. The intracellular loop of NCKX2 (NCKX2-loop) specifically interacts with the WD-40 repeats of KIF21A.

Figure 2. The intracellular loop of NCKX2 (NCKX2-loop) specifically interacts with the WD-40 repeats of KIF21A.

(A) The yeast two-hybrid reporter strain AH109 transformed with the pGBKT7-NCKX2-loop and pGADT7-KIF variants (dnKIF4, dnKIF5B, dnKIF21A or dnKIF21B) was grown overnight in liquid selective synthetic dropout medium (-Trp-Leu) and 10-fold serial dilutions were spotted on the selective synthetic dropout medium -Trp-Leu or -Trp-Leu-His plates. The combination of the T antigen prey and p53 bait was used as a control for positive interaction. **(B)** KIF21A and dnKIF21A but little KIF21B and dnKIF21B were co-immunoprecipitated with myc-NCKX2-loop (upper), when expressed exogenously in HEK293 cells. KIF variants were tagged with FLAG. The loaded amounts of the different FLAG-tagged KIF constructs and myc-NCKX2-loop in each of the transfected cell lysates prior to co-immunoprecipitation are shown in the lower panel. **(C)** Endogenous NCKX2 was co-immunoprecipitated with KIF21A using two different kinds of anti-KIF21A antibodies (upper) and reciprocally endogenous KIF21A was co-immunoprecipitated with NCKX2 (lower) from rat hippocampal neurons (at 14th day *in vitro*, DIV14). Normal rabbit IgG was used as negative control. TF, transfection; IP, immunoprecipitation; WB, western blot.

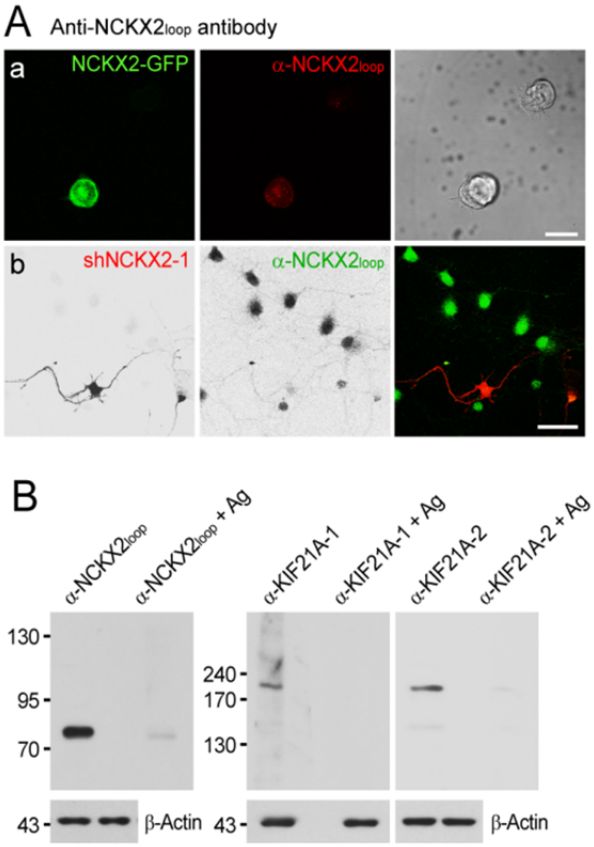

Figure 3. Reliability tests of anti-NCKX2$_{loop}$ and anti-KIF21A antibodies.

(A) Reliability test of NCKX2$_{loop}$ antibody. (Aa) Anti-NCKX2$_{loop}$ antibody (red) specifically immunolabeled the HEK293 cell expressing NCKX2-GFP (green). The untransfected cell is shown in the transmitted image. Scale bar: 20 μm. (Ab) When endogenous NCKX2 was immunolabeled with anti-NCKX2$_{loop}$ (green), The NCKX2-depleted hippocampal neurons using shNCKX2 (See Fig. 11) were not immunostained with anti-NCKX2$_{loop}$. The shNCKX2-transfected cells were identified by co-expressing mRFP fluorescence (red). Scale bar: 50 μm. **(B)** Pre-absorption tests of anti-NCKX2$_{loop}$ (left), anti-KIF21A-1 (middle) and anti-KIF21A-2 (right) antibodies. DIV18 hippocampal neuron lysate was immunoblotted with each antibody that was pre-incubated at RT for 2 h without (left lane of each panel; control) or with (right lane of each panel) an appropriate antigen. β-actin was detected as a loading control (bottom of each panel).

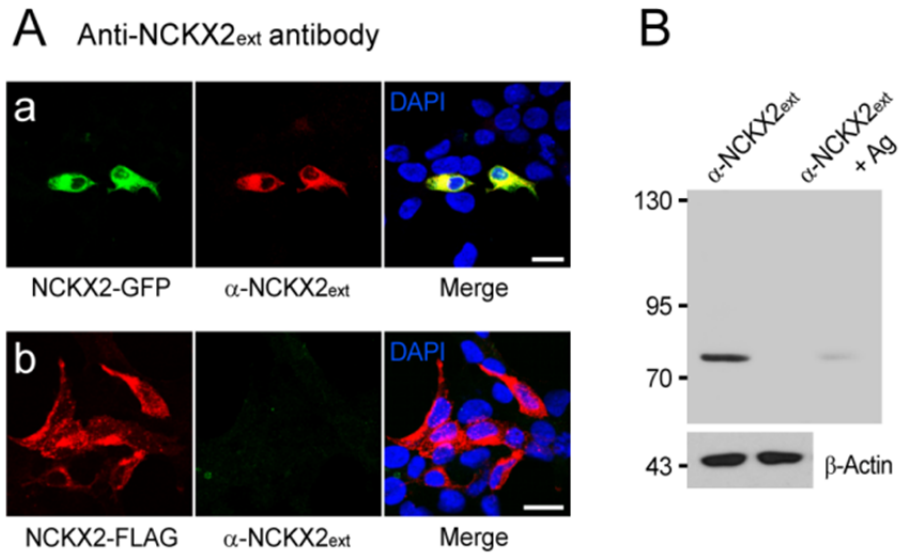

Figure 4. Reliability test of NCKX2$_{ext}$ antibody.

(A) Reliability test of NCKX2$_{ext}$ antibody. (Aa) The HEK293 cells expressing NCKX2-GFP (green) were specifically labeled with anti-NCKX2$_{ext}$ antibody (red). Untransfected cells were visualized by DAPI staining (blue). Scale bar: 20 μm. (Ab) Because the anti-NCKX2$_{ext}$ antibody was raised against a synthetic peptide within the N-terminal extracellular region (residues 90 to 102), HEK293 cells expressing NCKX2-FLAG, in which the FLAG tag (^{90}DYKDDDDK^{97}) replaces the epitope's N-terminal 8 amino acids, were not immunoreactive to the anti-NCKX2$_{ext}$ (green). Expression of NCKX2-FLAG was detected by anti-FLAG (red), and untransfected cells were visualized by DAPI staining (blue). Scale bar: 20 μm. **(B)** Pre-absorption test of anti-NCKX2$_{ext}$ antibody. DIV18 hippocampal neuron lysate was immunoblotted using anti-NCKX2$_{ext}$ antibody without (left lane) or with (right lane) pre-incubation of the antigen peptide. β-actin was detected as a loading control (lower panel).

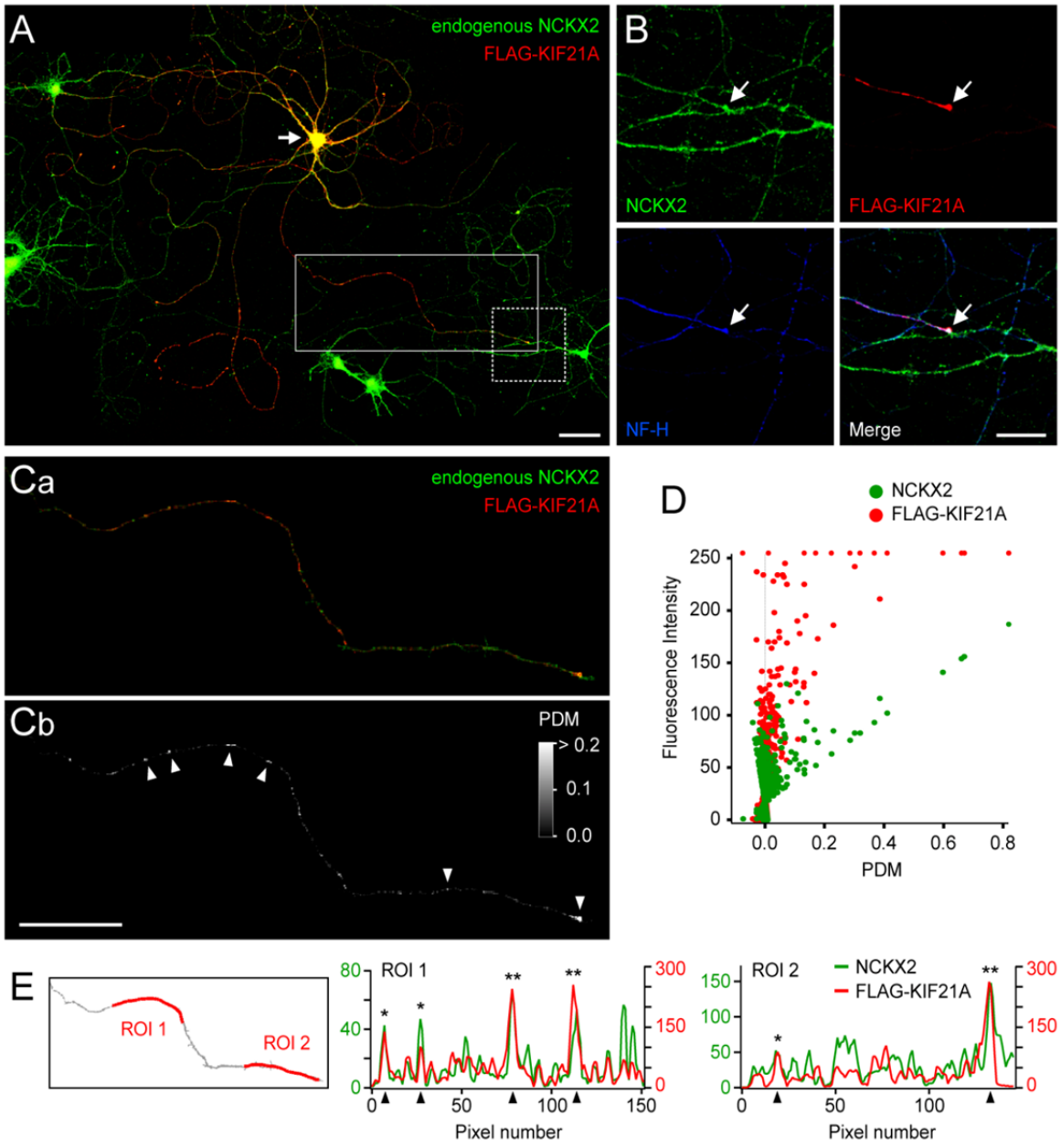

Figure 5. Co-localization of NCKX2 and KIF21A.

Figure 5. Co-localization of NCKX2 and KIF21A.

(A) Endogenous NCKX2 (green) and transfected FLAG-KIF21A (red) were co-localized not only in the somatodendritic region but also in the axon terminals of the cultured hippocampal neuron. Scale bar: 50 μm. **(B)** Higher magnification images of the axonal bouton (dotted box in A), the soma of which was marked by an arrow in C. The axon was identified by NF-H immunofluorescence (blue). Scale bar: 20 μm. **(C-D)** Quantitative analysis of co-localization. (Ca) Higher magnification image of the FLAG-positive axon (boxed region in A). Other FLAG-negative neurites were eliminated using the binary mask made from NF-H fluorescence image. (Cb) The product of difference from the mean (PDM) value was calculated at each pixel and shown as the pixel value at its location. For clarity, the contrast of this PDM image was adjusted where the brightness is saturated at 0.2. Scale bar: 50 μm. (D) A scattered plot of green and red pixel intensities against their PDM value at each paired pixel. **(E)** The line profiles of NCKX2 (green) and FLAG-KIF21A (red) fluorescence intensities along two ROI lines (red lines in the left panel). The locations of arrowheads in the right two panels correspond to puncta indicated by arrowheads in Cb. *, PDM > 0.1; **, PDM > 0.2.

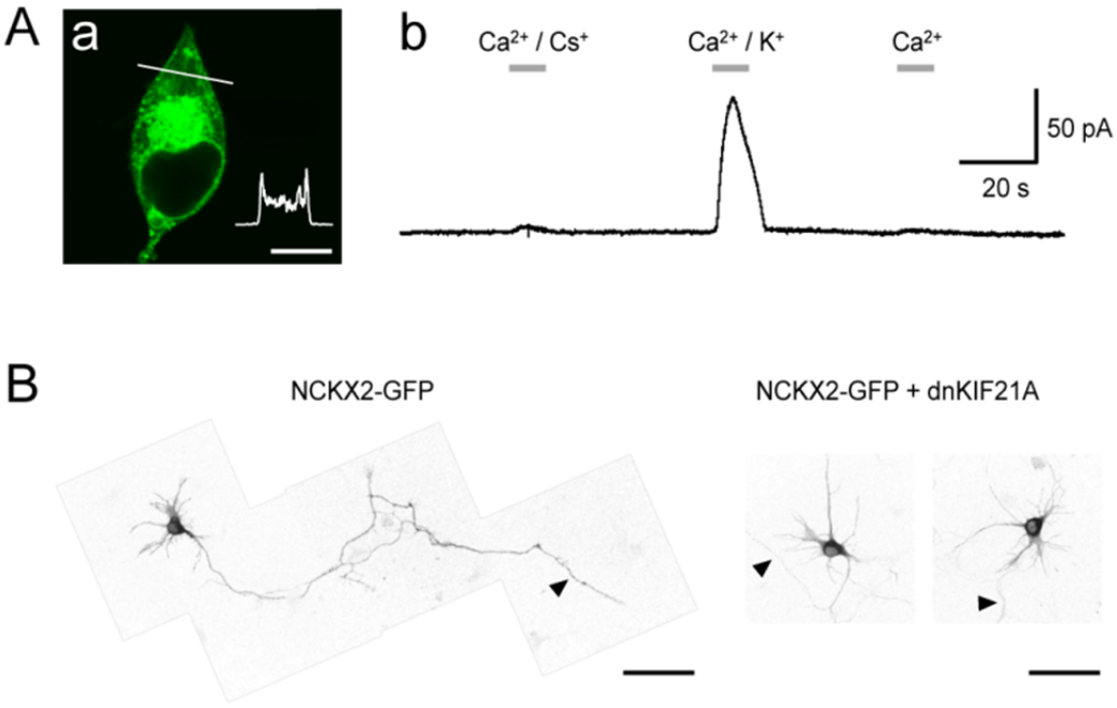

Figure 6. Test for functional competence and overexpression of NCKX2-GFP.

(A) Test for functional competence of NCKX2-GFP. (Aa) Overexpressed NCKX2-GFP was localized both in the cytoplasm and the plasma membrane in the HEK293 cell. A line profile of GFP fluorescence along the white line is shown in the inset of Aa. Scale bar: 10 μm. (Ab) A whole-cell current at the holding potential of 0 mV was recorded from a HEK293 cell expressing NCKX2-GFP using high-Na^+ and high-BAPTA internal pipette solution. Reverse mode NCKX current could be induced by bath application of Ca^{2+} plus K^+, but not by Ca^{2+} plus Cs^+ or Ca^{2+} only. **(B)** Overexpression of NCKX2-GFP alone (left) or co-expression of NCKX2-GFP and dnKIF21A (right) in the hippocampal neurons. GFP fluorescence was inverted into gray color to improve contrast. Scale bar: 100 μm. The longest neurites were indicated by arrowheads.

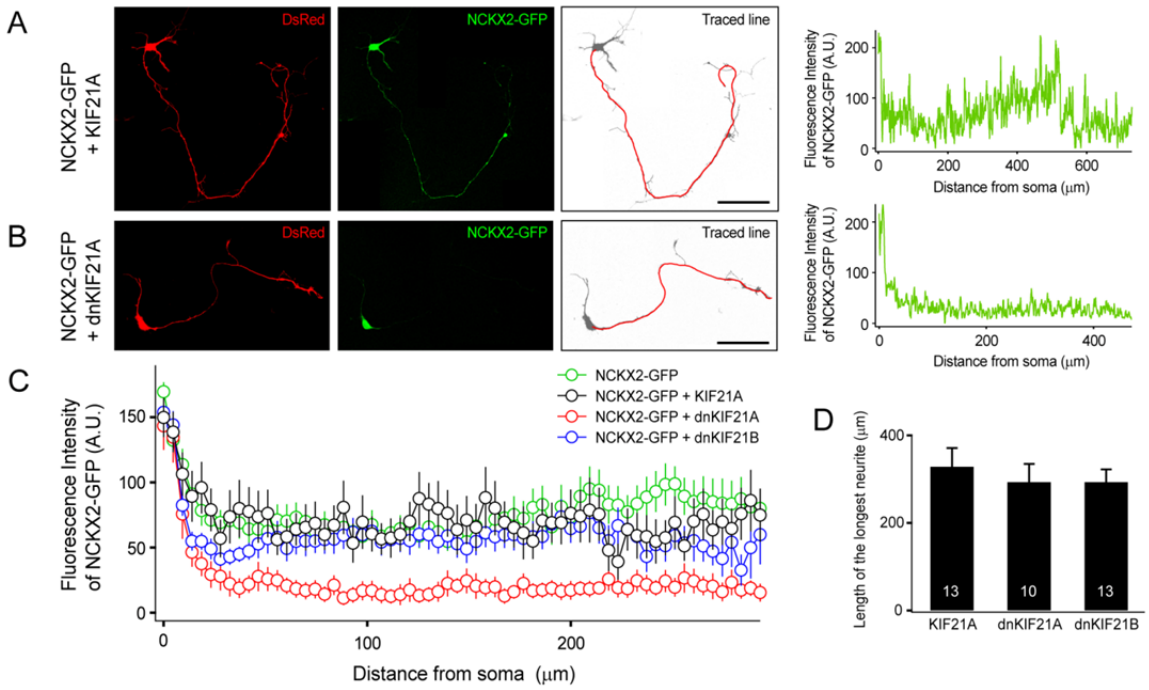

Figure 7. Axonal transport of NCKX2 is inhibited by dnKIF21A.

(A-B) Co-expression of NCKX2-GFP together with KIF21A (A) or dnKIF21A (B) in hippocampal neurons. The longest neurite was traced from DsRed fluorescence using NeuronJ, and then fluorescence intensity of NCKX2-GFP was measured along the traced line (rightmost graphs). The traced line is overlaid as a red line on each DsRed image (gray). Scale bar: 100 μm. **(C)** Mean NCKX2-GFP fluorescence profiles of the longest neurites. Ten points-smoothing was performed with all data. In the range of 50 to 250 μm, intensity values for NCKX2-GFP from neurons expressing dnKIF21A (red, n = 11) were significantly lower than those from three different control groups: 1) neurons expressing NCKX2-GFP alone (green, n = 19) at all 43 points, 2) neurons expressing KIF21A (black, n = 10) at 39 points, and 3) neurons expressing dnKIF21B (blue, n = 20) at 36 points (mean ± SEM, $p < 0.05$). No significantly different point was found between NCKX2-GFP-alone and KIF21A and dnKIF21B groups in the same range ($p > 0.05$). **(D)** Length of the longest neurites was not significantly different among KIF21A-, dnKIF21A- and dnKIF21B-expressing groups ($p > 0.5$).

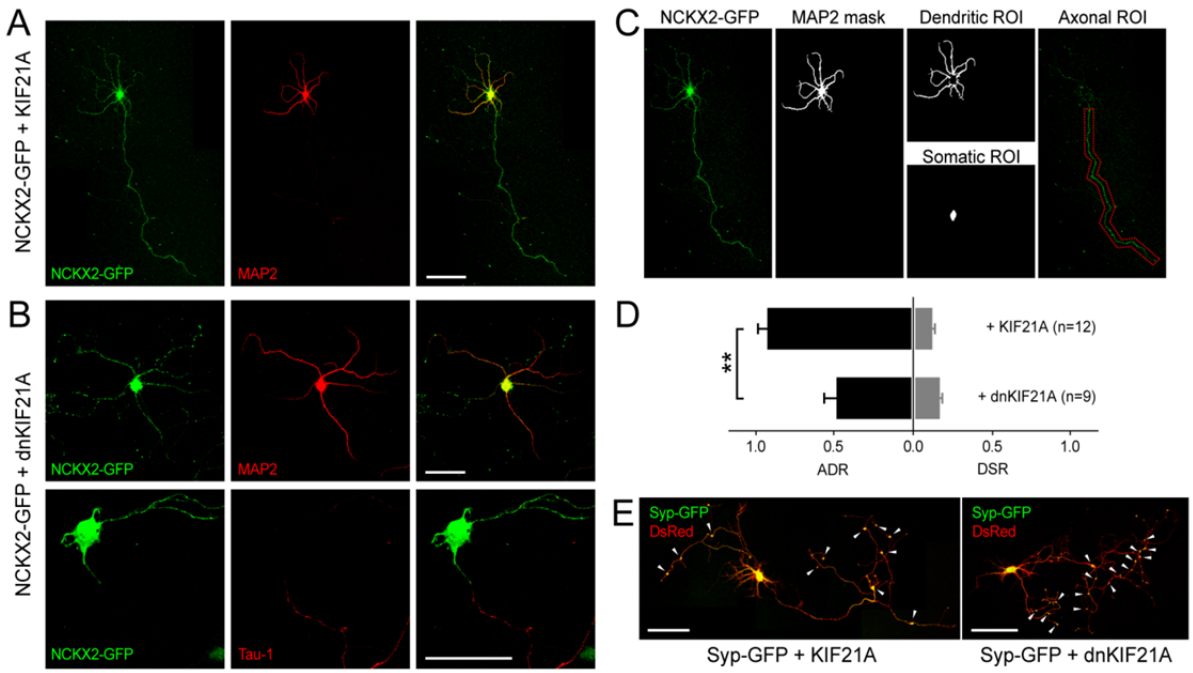

Figure 8. Axonal, but not dendritic transport of NCKX2, is inhibited by dnKIF21A

Figure 8. Axonal, but not dendritic transport of NCKX2, is inhibited by dnKIF21A

(A) Co-expression of NCKX2-GFP and KIF21A. MAP2 was immunolabeled to distinguish dendrites (red). NCKX2-GFP was localized at both axon and dendrites. Scale bar: 100 μm. **(B)** Co-expression of dnKIF21A inhibited the transport of NCKX2-GFP to the axon. Dendrites and axon were distinguished by immunolabeling with anti-MAP2 (red, upper) and anti-Tau-1 (red, lower), respectively. Scale bar: 50 μm. In A and B, merged images are shown in the rightmost panels. **(C)** Analysis of axon-to-dendrite ratio (ADR) of NCKX2-GFP fluorescence. Left two panels show images of NCKX2-GFP fluorescence (the same as A) and the binary mask of MAP2-positive neurites (white). To make the dendritic (somatic) ROIs, the somatic (dendritic) region was erased from the MAP2 mask (two panels in the third column). The axonal ROI was drawn on the NCKX2-GFP image after setting the somatodendritic pixel to zero using the MAP2 mask (red dotted polygon in the right panel). **(D)** The mean ADR (black bars) and dendrite-to-soma ratio (DSR; gray bars) of NCKX2-GFP fluorescence estimated from the neurons co-transfected with KIF21A (n = 12) or with dnKIF21A (n = 9). ADR of NCKX2-GFP in dnKIF21A group is significantly lower than that in KIF21A group. **, $p < 0.01$. **(E)** Axonal transport of synaptophysin-GFP was not inhibited by dnKIF21A. To visualize the distribution of synaptophysin, EGFP was fused to the C-terminus of synaptophysin (Syp-GFP, green). Cell morphology was visualized using DsRed fluorescence (red) in the same way as Fig.7A and B. Syp-GFP was well distributed at putative axon terminals (arrowheads), regardless of co-transfection with KIF21A (left) or dnKIF21A (right). Scale bar: 100 μm.

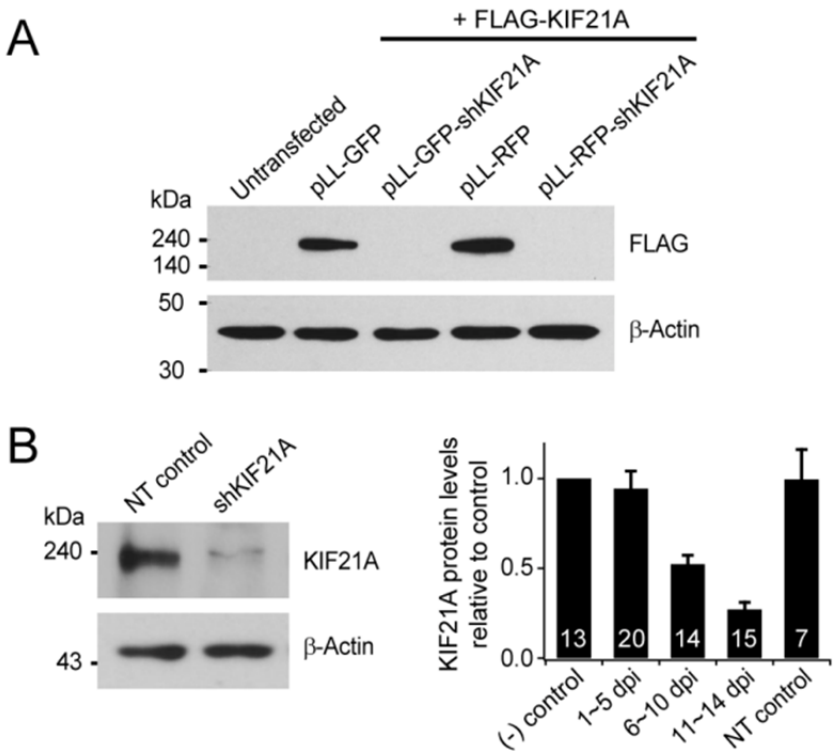

Figure 9. shRNA-mediated depletion of KIF21A.

(A) KIF21A-targeting shRNA (shKIF21A) was expressed by pLentiLox3.7 plasmids (pLL) encoding GFP or mRFP (pLL-GFP-shKIF21A or pLL-RFP-shKIF21A). FLAG-KIF21A was co-transfected with shKIF21A or empty pLL vectors into HEK293 cells. shKIF21A completely depleted FLAG-KIF21A but the empty pLL did not. **(B)** Endogenous KIF21A was remarkably depleted in cultured hippocampal neurons infected with lentivirus encoding shKIF21A but not in those with lentivirus encoding non-targeting shRNA (NT control; left). Time-dependent knockdown of endogenous KIF21A is shown in the right bar graph. The non-infected control is shown in the leftmost bar and the NT control is in the rightmost bar. In A and B, β-actin was detected as a loading control.

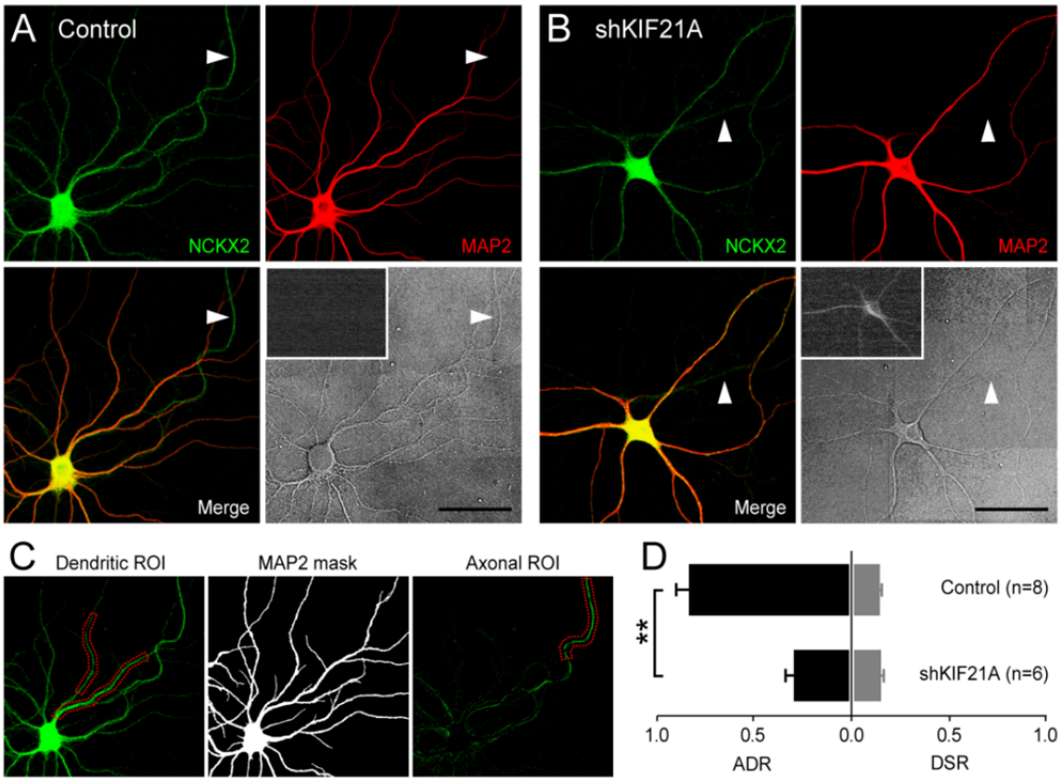

Figure 10. Knockdown of KIF21A inhibits the axonal transport of NCKX2.

(A-B) The axonal transport of endogenous NCKX2 (green) in the shKIF21A-transfected (B) or untransfected control (A) neurons. KIF21A-depleted neuron was identified by red fluorescence of mRFP co-expressed with shRNA (insets on DIC images). Dendrites were identified by MAP2 immunofluorescence (red). Neurites that are MAP2-negative but clearly seen in the DIC images (indicated by arrowheads) were regarded as axons. Scale bar: 50 μm. **(C)** Analysis of ADR of endogenous NCKX2. Dendritic ROIs (left, red dotted polygons) were drawn on the endogenous NCKX2 immunofluorescence image (same as A). After nullifying pixels which overlap the binary mask of MAP2-positive neurites (middle) from the endogenous NCKX2 image, the axonal ROI was set on the NCKX2 image (right, red dotted polygon). **(D)** The mean ADR (black bars) and DSR (gray bars) of endogenous NCKX2 estimated from the untransfected control (n = 8) or KIF21A-depleted neurons (n = 6). ADR of NCKX2 in the KIF21A-depleted group is significantly lower than that in the control group. **, $p < 0.01$.

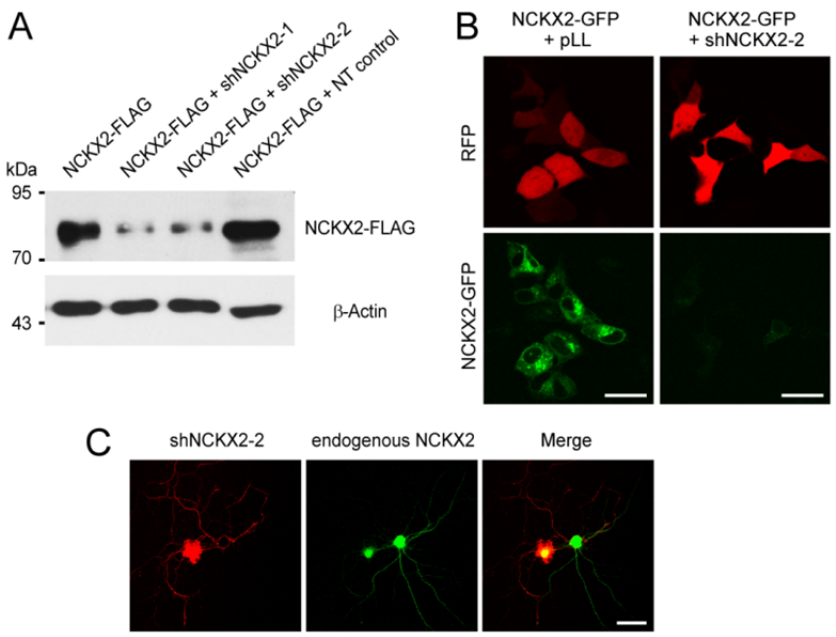

Figure 11. shRNA-mediated depletion of NCKX2.

(A) FLAG-tagged NCKX2 (NCKX2-FLAG) was transfected alone or co-transfected with one of two different types of shRNA targeting NCKX2 mRNA (shNCKX2-1 or shNCKX2-2) or non-targeting shRNA (NT control) to HEK293 cells. Both shNCKX2-1 and shNCKX2-2 efficiently depleted NCKX2-FLAG. **(B)** pLentiLox3.7 plasmids (pLL) encoding RFP alone (red, left) or RFP + shNCKX2-2 (red, right) were co-transfected to HEK293 cells with NCKX2-GFP (green). Fluorescence imaging of the cells confirmed that shNCKX2-2 effectively knocked-down NCKX2-GFP. Scale bar: 30 μm. **(C)** Endogenous NCKX2 was distinctly depleted by shNCKX2-2 on the 15th day after transfection. The hippocampal neuron transfected with shNCKX2-2 was identified by co-expressing mRFP fluorescence (red). Endogenous NCKX2 was immunolabeled with anti-$NCKX2_{ext}$ (green) under the permeabilized condition. The persistent green fluorescence confined in the soma of shNCKX2-2-transfected cell is caused by non-specific staining of nucleus with the secondary antibody because it stained nuclei without a primary antibody under permeabilized conditions (data not shown). Scale bar: 50 μm.

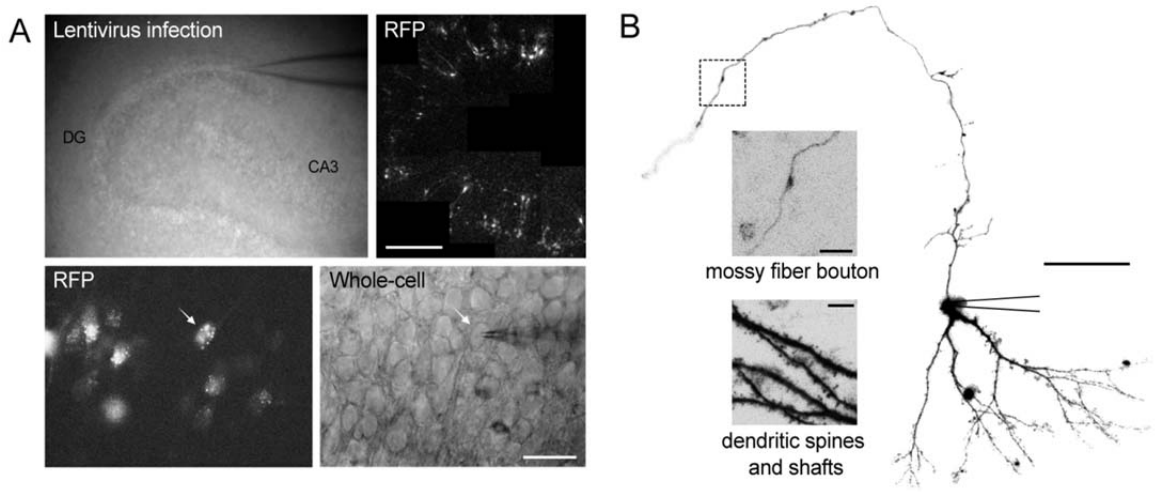

Figure 12. Procedures for viral infection and calcium imaging of hippocampal dentate granule cells (GCs) in the organotypic cultured slice.

(A) Procedures for viral infection and calcium imaging of hippocampal dentate granule cells (GCs) in the organotypic cultured slice. The granule cell layer in dentate gyrus of DIV7-8 cultured hippocampal slice was infected with lentivirus encoding shKIF21A, shNCKX2 or NT control by local injection. Lentivirus-infected cells were identified by mRFP fluorescence. Calcium imaging was performed for the RFP-positive dentate GCs loaded with calcium indicator dye via whole-cell patch pipette. Scale bar: 200 μm (upper), 50 μm (lower). **(B)** A Z-stack projection of laser-scanned images obtained from a dentate GC loaded with 200 μM OGB-5N via a whole-cell patch pipette on the soma. Scale bar: 50 μm. *Insets*, Magnified images of the rectangular region of the axon (upper), and dendrites (from another cell, bottom). Inset scale bar: 5 μm.

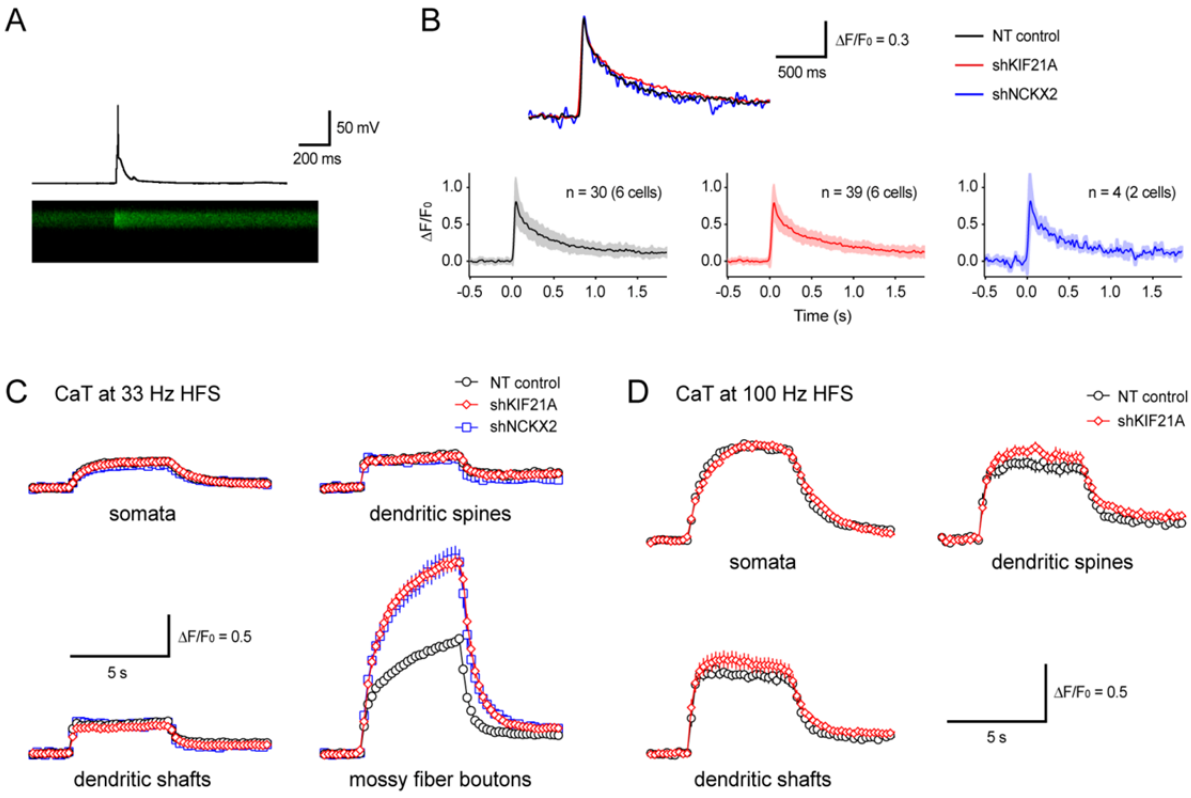

Figure 13. Knockdown of KIF21A did not affect calcium influx evoked by a single action potential (AP) at MFBs.

(A) Single AP evoked by current injection (600 pA, 12 ms) in the soma of a GC (upper). A simultaneous line-scanned image recorded from an axon terminal of the GC loaded with 50 μM OGB-1 is shown on the same time-axis (lower). **(B)** Averaged AP-induced calcium transients (AP-CaTs) at MFBs of GCs infected by lentivirus encoding NT control, shKIF21A or shNCKX2. Traces of AP-CaTs under each condition were smoothed using binomial algorithm (50 passes), and then averaged. The averaged traces are superimposed (upper). The trace for each condition is shown with the range of standard deviation (light colored, lower). **(C)** Averaged CaTs in somata, dendritic spines and shafts and MFBs recorded from GCs infected by lentivirus encoding NT control, shKIF21A and shNCKX2. CaTs were evoked by HFS (33 Hz, 5 s). **(D)** Averaged CaTs recorded under the conditions similar to C except HFS at 100 Hz.

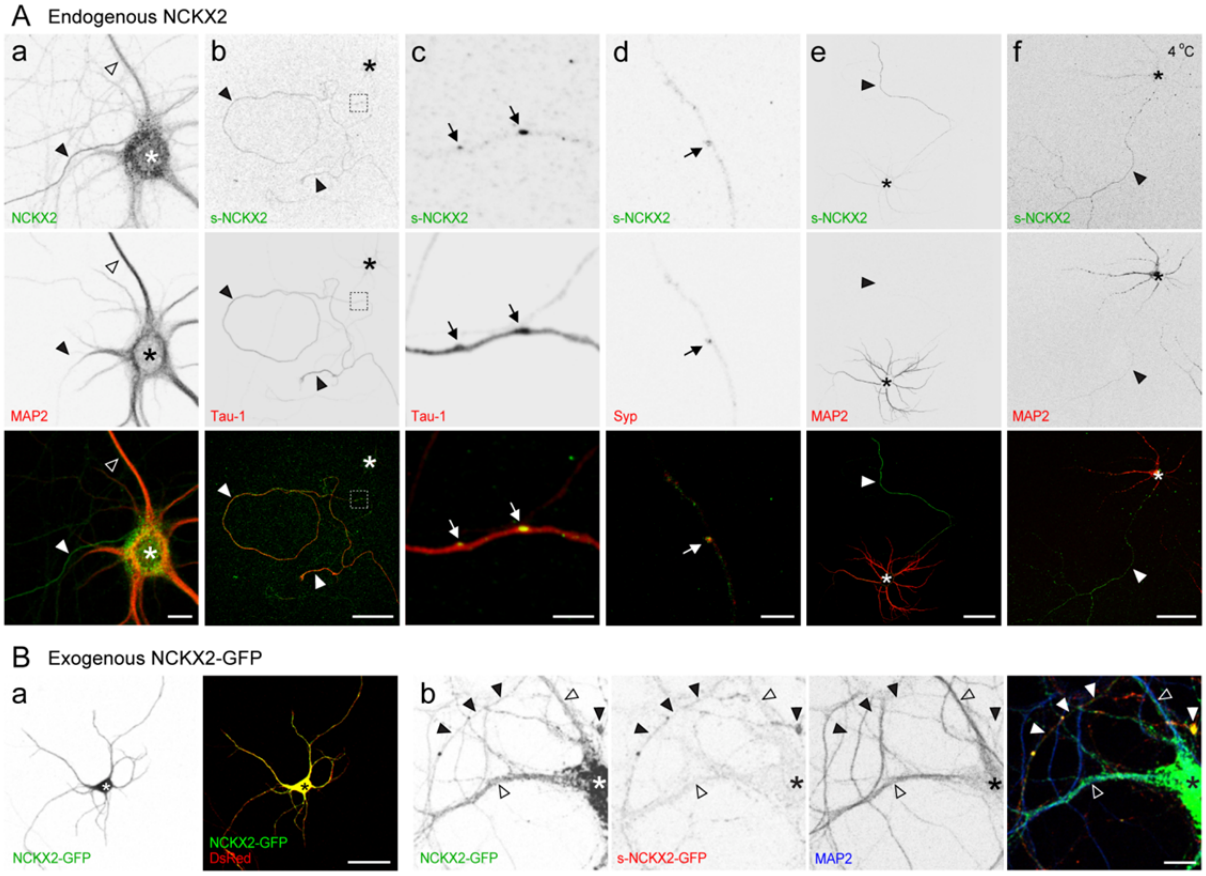

Figure 14. Immunocytochemical localization of endogenous (A) or exogenous (B) NCKX2 in cultured hippocampal neurons.

Figure 14. Immunocytochemical localization of endogenous (A) or exogenous (B) NCKX2 in cultured hippocampal neurons.

(Aa) DIV23 hippocampal neurons were stained for endogenous NCKX2 (green) and dendritic marker MAP2 (red). **(Ab-e)** Surface NCKX2 (s-NCKX2) was immunolabeled by incubating live cells with anti-$NCKX2_{ext}$ (green) at 36 °C, and then cells were fixed, permeabilized and immunostained with antibodies against axonal marker Tau-1 (red, Ab-c) or presynaptic marker synaptophysin (red, Ad) or dendritic maker MAP2 (red, Ae). Higher magnification image of the dashed box in Ab is shown in Ac. The sites where endogenous s-NCKX2 was co-localized with Tau-1 (Ac) or synaptophysin (Ad) are marked with arrows. **(Af)** Endogenous s-NCKX2 (green) was immunolabeled by the same manner as Ae except incubating live cells with anti-$NCKX2_{ext}$ at 4˚C before fixation. Scale bar: 10 μm (Aa), 50 μm (Ab, e, f), 5 μm (Ac, d). **(Ba)** A DIV7 hippocampal neuron transfected with NCKX2-GFP and DsRed. Scale bar: 50 μm. **(Bb)** A DIV13 hippocampal neuron transfected with NCKX2-GFP (green). Surface NCKX2-GFP was visualized by live-cell immunolabeling with antibody against GFP (s-NCKX2-GFP; red) and then stained for MAP2 (blue). Scale bar: 10 μm. Open and solid arrowheads indicate dendrites and axons, respectively. Asterisks show location of somata.

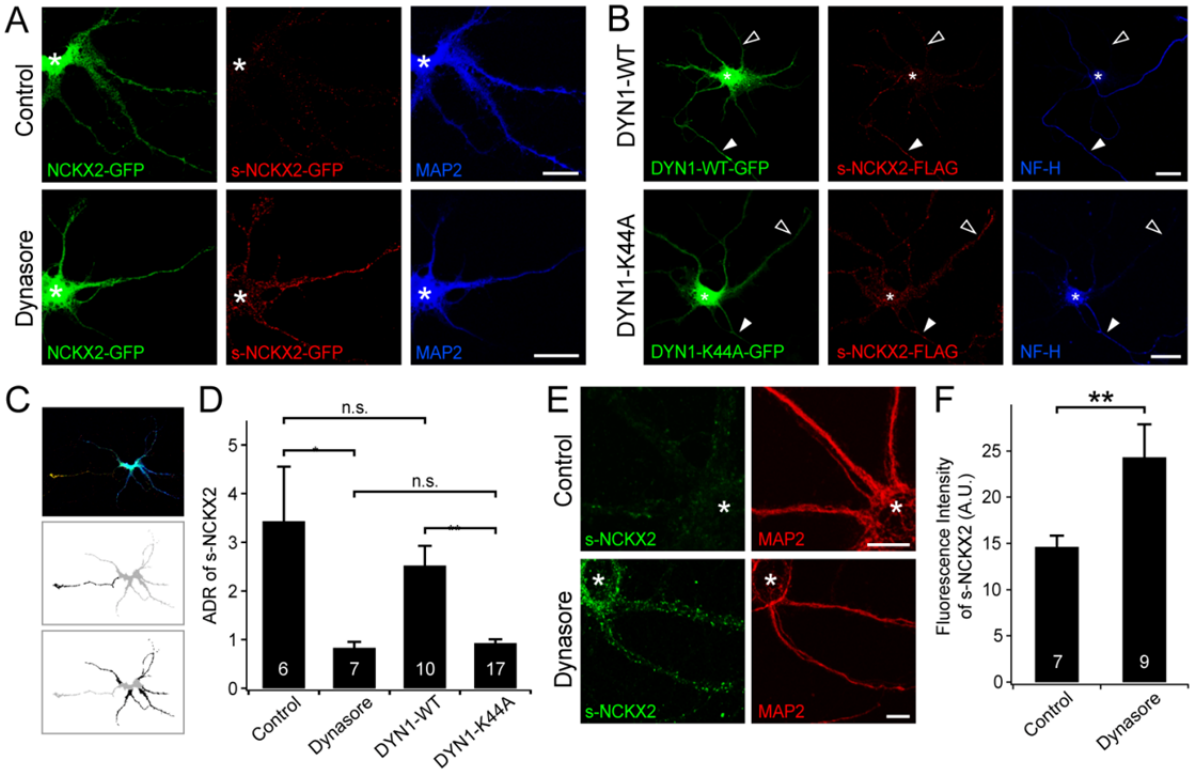

Figure 15. Inhibition of endocytosis enhances the surface expression of NCKX2 in the somatodendritic region.

Figure 15. Inhibition of endocytosis enhances the surface expression of NCKX2 in the somatodendritic region.

(A) Hippocampal neurons expressing NCKX2-GFP were treated with 0.1% DMSO (control; upper) or 40 μM dynasore (lower) for 4 h. Surface NCKX2-GFP (s-NCKX2-GFP) was visualized with anti-GFP (red). Dendrites were immunostained with anti-MAP2 (blue). Scale bar: 20 μm. **(B)** Wild-type dynamin-1 (DYN1-WT) or dominant-negative mutant dynamin-1 (DYN1-K44A) was co-transfected with NCKX2-FLAG to DIV6 hippocampal neurons. Both DYN1-WT and DYN1-K44A were tagged with EGFP on their N-terminals, and transfected cells were identified by green fluorescence (left). Surface NCKX2-FLAG (s-NCKX2-FLAG, red) was detected by anti-FLAG. Axons were immunostained with anti-NF-H (blue). Open and solid arrowheads indicate dendrites and axons, respectively. Scale bar: 20 μm. **(C)** Analysis of the ADR of s-NCKX2-GFP. *Top*, a merged image of three colors from the control neuron shown in A. Note only the axonal compartment exhibits the co-localization (yellow) of s-NCKX2-GFP (red) and NCKX-GFP (green). *Middle and bottom panels*, each panel shows a binary mask image of the same cell created from NCKX2-GFP fluorescence (gray). The MAP2-negative axonal ROI (middle) or MAP2-positive dendritic ROIs (bottom) are overlaid in black. **(D)** Summary for the mean ADR of s-NCKX2-GFP in A or s-NCKX2-FLAG in B. The ADR estimated from the neurons treated with dynasore and those transfected with DYN1-K44A are significantly lower than that from the control neurons. **(E)** Surface expression of endogenous NCKX2 (s-NCKX2) was immunostained with anti-$NCKX2_{ext}$ (green). Dendrites were immunostained with anti-MAP2 (red). Scale bar: 10 μm. **(F)** The mean fluorescence intensity of endogenous s-NCKX2 on MAP2-positive neurites of the control or dynasore-treated groups. Surface NCKX2 (endogenous or EGFP-tagged or FLAG-tagged) was detected by means of live-cell immunolabeling (A, B, E). Asterisks in micrographs indicate the locations of somata. **, $p < 0.01$; *, $p < 0.05$; n.s., not significant.

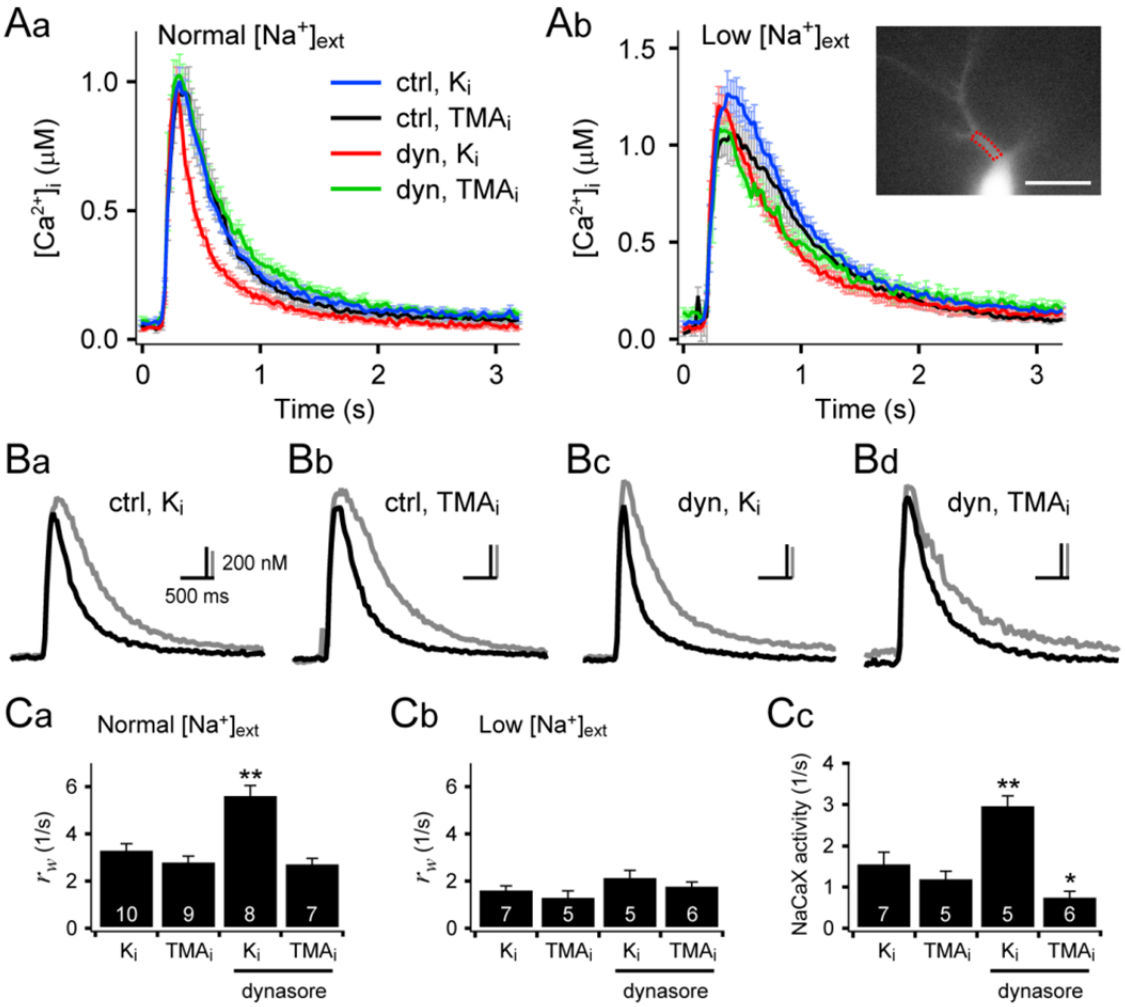

Figure 16. Dynasore enhances the NCKX activity in the proximal dendrite of hippocampal dentate GCs.

Figure 16. Dynasore enhances the NCKX activity in the proximal dendrite of hippocampal dentate GCs.

(A) Averaged traces of CaTs evoked by a short depolarizing pulse (from –70 mV to 0 mV for 50~100 ms) under normal (Aa) or low (Ab) extracelluar $[Na^+]$ ($[Na^+]_{ext}$) conditions. Each panel shows four overlaid averaged traces under different conditions (K_i or TMA_i, K^+- or TMA^+-based pipette solution; ctrl or dyn, pretreatment with vehicle or 40 μM dynasore for 1 h, respectively). Note that pretreatment with dynasore accelerated the Ca^{2+} decay rate only under K^+-based internal and normal $[Na^+]_{ext}$ conditions (red lines). Error bars shown in light colors represent SEM. *Inset*, A fura-4F fluorescence image of a GC. A typical proximal dendritic ROI is shown as a red dotted box. Scale bar: 20 μm. **(B)** Slow-down of Ca^{2+} decay rate in the low $[Na^+]_{ext}$ condition. Each panel shows overlaid averaged CaTs recorded under the same condition except $[Na^+]_{ext}$ (black, normal $[Na^+]_{ext}$; gray, low $[Na^+]_{ext}$). **(C)** Summary for Ca^{2+} clearance and Na^+/Ca^{2+} exchange (NaCaX) activity. Ca^{2+} clearance was quantified as a weighted average of rate constants (r_w) estimated from the biexponential fit to the decay phase of individual CaTs (Ca-b). The difference in the r_w values between normal and low $[Na^+]_{ext}$ conditions in the same cell was regarded as the NaCaX activity (Cc). Mean ± SEM; **, $p < 0.01$; *, $p < 0.05$.

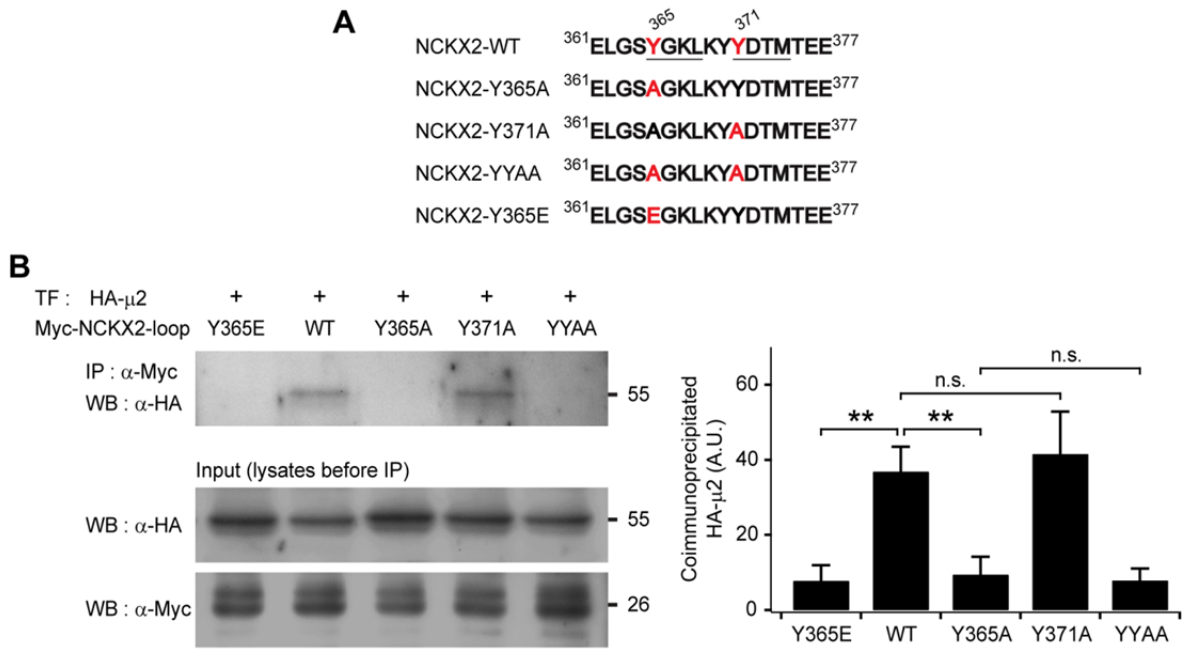

Figure 17. The μ2 subunit of adaptor-binding protein 2 (AP-2) interacts with NCKX2 but not with the Y365A mutant of NCKX2.

(A) The amino acid sequences of a part of cytoplasmic region of NCKX2. Two putative consensus internalization motifs (YxxΦ) that mediates AP-2 binding are underlined (YGKL, aa 365-368; YDTM, aa 371-374). Amino acids (Tyr-365 and Tyr-371) mutated to alanine or glutamate are labeled in red. **(B)** The HA-tagged μ2 subunits of AP-2 were coimmunoprecipitated with the wild-type or Y371A mutant of cytoplasmic loop of NCKX2 (NCKX2-loop), but not with any of the Y365A mutant, double mutant of Y365A and Y371A (YYAA), and the phosphomimetic mutant, Y365E (upper strip), when they were heterologously expressed in HEK293 cells. NCKX2 variants were tagged with c-myc. The loaded amounts of HA-μ2 and the different myc-NCKX2-loop variants in each of the transfected cell lysates before coimmunoprecipitation are shown in lower two strips. The lower bar graph shows the summary for the amount of coimmunoprecipitated HA-μ2 with each of myc-NCKX2-loop variants (n = 5). Mean ± SEM; **, $p < 0.01$; n.s., not significant.

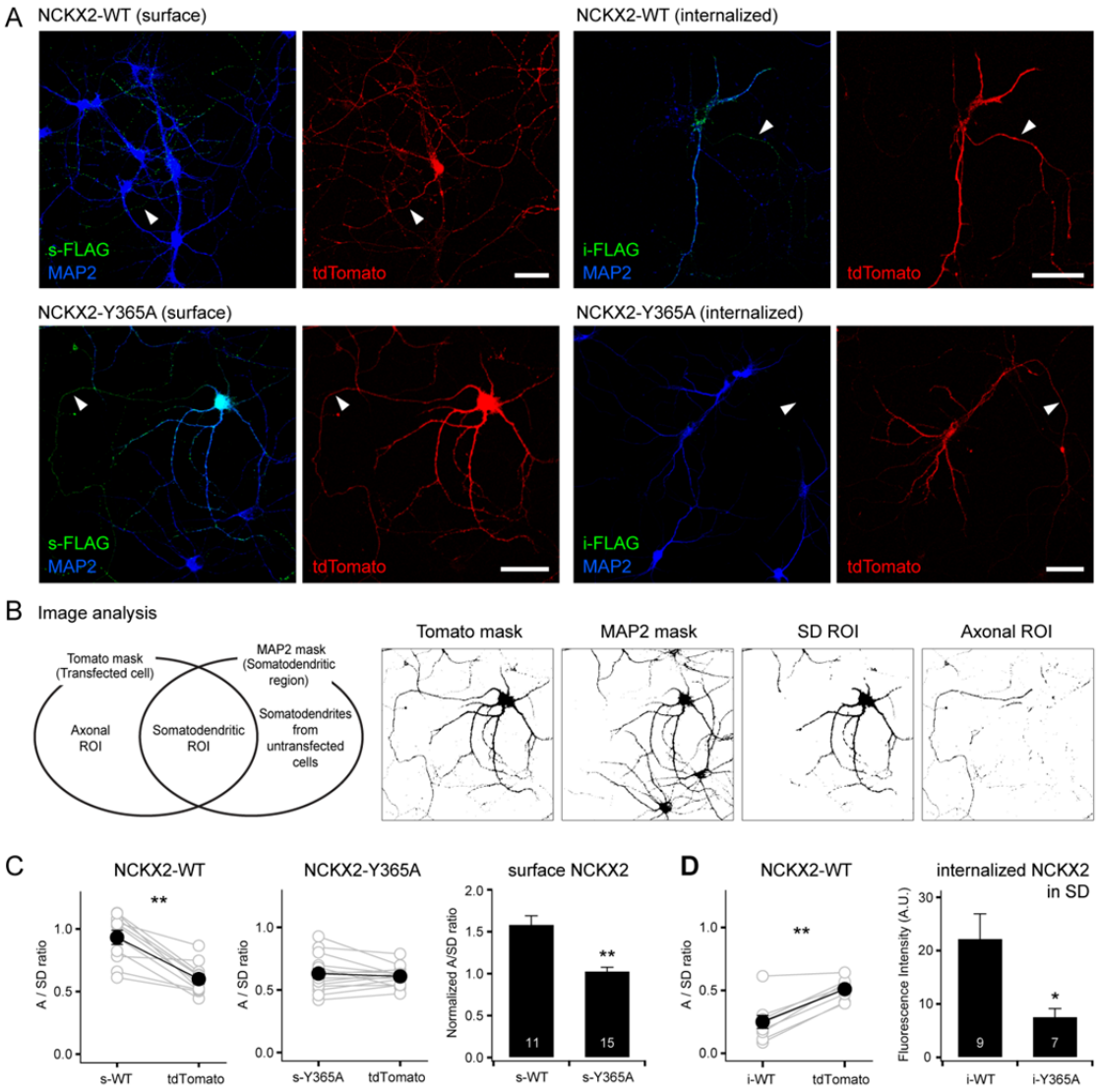

Figure 18. The Y365A mutant of NCKX2 displays higher surface expression in somatodendritic region than wild-type NCKX2.

Figure 18. The Y365A mutant of NCKX2 displays higher surface expression in somatodendritic region than wild-type NCKX2.

(A) Immunocytochemical localization of surface or internalized NCKX2-FLAG in cultured hippocampal neurons. Wild-type or Y365A mutant of NCKX2-FLAG were transfected at DIV7-8. To visualize the entire cell morphology red fluorescence protein tdTomato (red) was cotransfected. At DIV12-14 hippocampal neurons were immunostained for FLAG (green) and dendritic marker MAP2 (blue). For surface immunostaining of NCKX2-FLAG, live cells were incubated with anti-FLAG at 4˚C then fixed. For immunolabeling of the internalized NCKX2-FLAG, live cells were incubated with anti-FLAG for 30 min at 36˚C. After a brief wash with culture medium, cells were washed with acidic medium (pH 2 with HCl) for 2 min to remove surface-bound antibody then fixed. Solid arrowheads indicate axons. **(B)** Analysis of axon-to-somatodendritic ratio (A/SD ratio) of NCKX2-FLAG immunofluorescence. The Venn diagram depicts how the axonal or somatodendritic regions were defined. The representative binary masks were shown on the right (the same cell as A). The overlapping area of tdTomato and MAP2 was defined as the somatodendritic mask (SD mask). Then the axonal mask was obtained by subtracting SD mask from tdTomato mask. Scale bar: 50 μm. **(C-D)** Summary for the mean A/SD ratio of surface NCKX2-FLAG (C) or the internalized NCKX2-FLAG (D) in A. (C) The A/SD ratio estimated from the immunofluorescence of surface NCKX2-WT is significantly higher than that from tdTomato, non-polarized cytoplasmic protein. However, the surface expression of NCKX2-Y365A displays no axonal polarization. (D) The A/SD ratio of the internalized NCKX2-WT is significantly lower than that of tdTomato. The immunoreactivity of the internalized NCKX2-Y365A is significantly reduced in the somatodendritic compartment. Mean ± SEM; **, $p < 0.01$; *, $p < 0.05$.

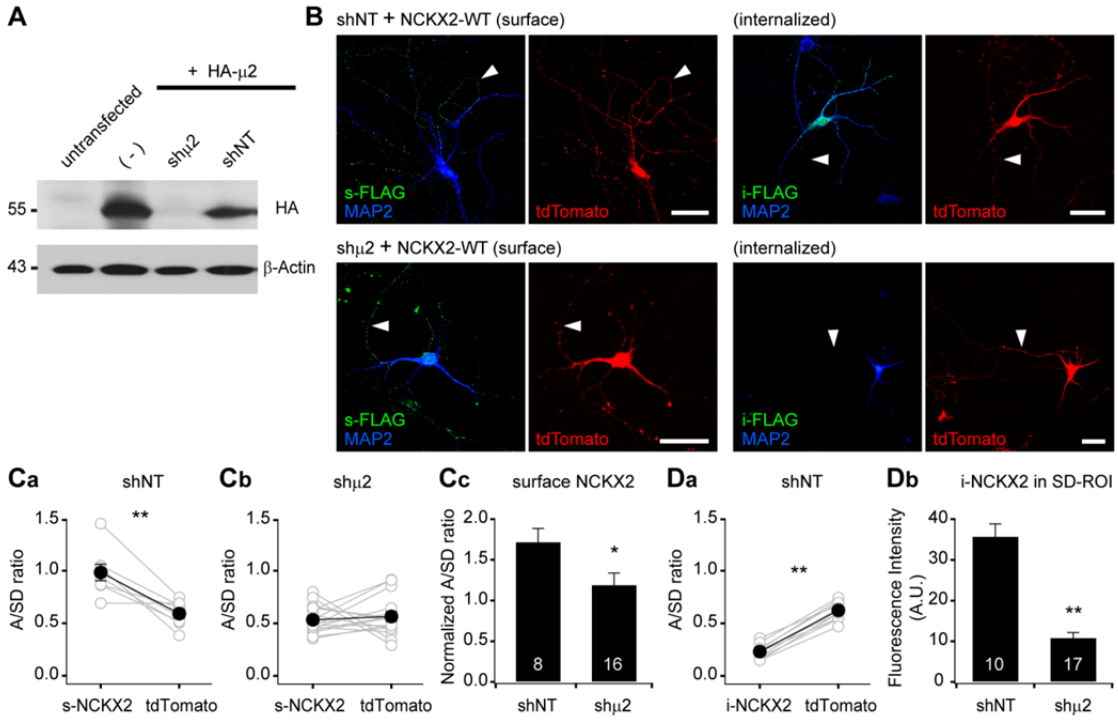

Figure 19. Knockdown of μ2 subunit abolishes the endocytosis of NCKX2.

Figure 19. Knockdown of μ2 subunit abolishes the endocytosis of NCKX2.

(A) shRNA-mediated depletion of μ2. μ2-targeting shRNA (shμ2) was cotransfected with HA-tagged μ2 (HA-μ2) into HEK293 cells. shμ2 completely depleted HA-μ2, but non-targeting shRNA (shNT) did not. β-actin was detected as a loading control. **(B)** FLAG-tagged wild-type NCKX2 (NCKX2-WT) was cotransfected with shμ2 or shNT into DIV8 hippocampal neurons. At DIV13-14, hippocampal neurons were immunostained for FLAG (green). Note that shμ2, but not shNT, caused a dramatic reduction of internalized NCKX2-WT and an increase in the surface expression of NCKX2-WT in the somatodendritic region. Arrowheads indicate axons. Scale bar: 50 μm. **(C-D)** Summary for the mean A/SD ratios of surface or internalized NCKX2-WT. (Ca-b) The A/SD ratio of surface NCKX2-WT was significantly higher than that of tdTomato in the shNT expressing neurons (Ca; s-NCKX2, 0.983 ± 0.007; tdTomato, 0.591 ± 0.042, n = 8, $p < 0.01$), but not different in the μ2-depleted neurons (Cb; s-NCKX2, 0.534 ± 0.033; tdTomato, 0.565 ± 0.047, n = 16, $p = 0.59$). (Cc) The tdTomato-normalized A/SD ratio of surface NCKX2 was significantly lower in the sh μ2 expressing neurons than shNT expressing one (shNT, 1.722 ± 0.163, n = 8; shμ2, 1.195 ± 0.142, n = 16, $p < 0.05$). (Da) The A/SD ratio of the internalized NCKX2-WT was significantly lower than that of tdTomato (i-NCKX2, 0.231 ± 0.022; tdTomato, 0.623 ± 0.028, n = 10, $p < 0.01$). (Db) The spatially averaged immunofluorescence of internalized NCKX2-WT on SD-ROI was significantly reduced in the μ2-depleted neurons (shNT, 35.8 ± 3.0, n = 10; shμ2, 10.9 ± 1.3, n = 17, $p < 0.01$). Mean ± SEM; **, $p < 0.01$; *, $p < 0.05$.

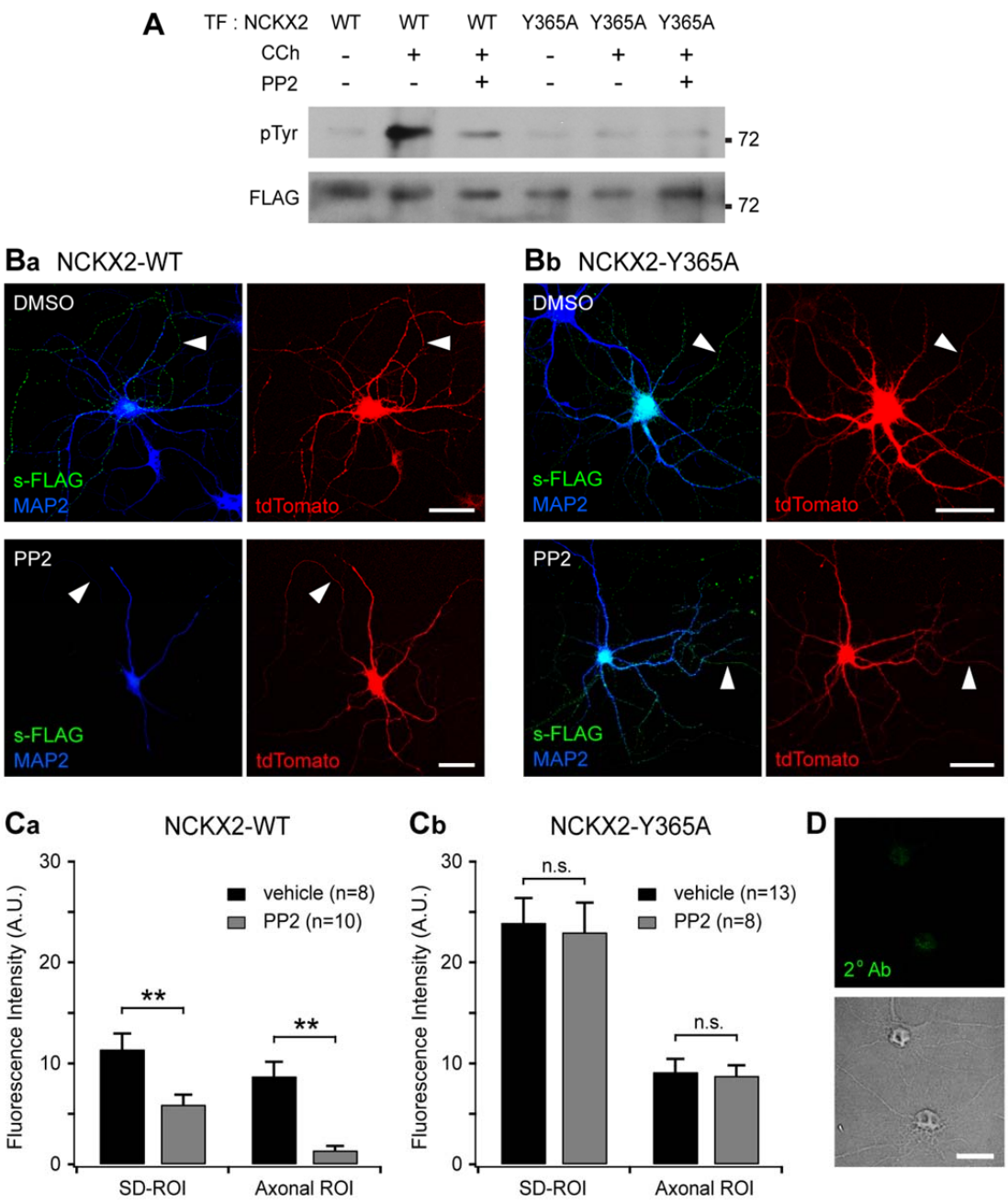

Figure 20. Src family kinase (SFK)-mediated Tyr-365 phosphorylation of NCKX2 regulates its surface expression.

Figure 20. Src family kinase (SFK)-mediated Tyr-365 phosphorylation of NCKX2 regulates its surface expression.

(A) Tyrosine phosphorylation of NCKX2 in response to carbachol (CCh) in PC-12 cells. I transfected FLAG-tagged NCKX2-WT or NCKX2-Y365A into PC-12 cells which normally express PYK2 and SFK, and treated the cells with 1 mM CCh for 2 min. To observe the tyrosine-phosphorylation of NCKX2, NCKX2 was immunoprecipitated with anti-FLAG then immunoblotted with anti-phosphotyrosine (pTyr) IgG. NCKX2-WT, but not NCKX2-Y365A, was strongly phosphorylated by CCh. Pretreatment with 10 μM PP2, a selective inhibitor of SFK, reduced the CCh-induced tyrosine phosphorylation of NCKX2-WT. The FLAG signals on the same blot are shown in the lower image, showing little difference in expression levels of wild-type or Y365A mutant NCKX2 between different conditions. **(B)** Hippocampal neurons expressing FLAG-tagged NCKX2-WT (Ba) or NCKX2-Y365A (Bb) were treated with 0.1% DMSO (control; upper) or 10 μM PP2 (bottom) for 2 h. Wild-type or Y365A mutant of NCKX2 expressed on the surface was visualized with anti-FLAG (s-FLAG; green). Dendrites were immunostained with anti-MAP2 (blue). Arrowheads indicate axons. Scale bar, 50 μm. **(C)** The spatially averaged fluorescence intensity of wild-type (Ca) or Y365A mutant (Cb) of surface NCKX2 on SD- or axonal ROIs of the vehicle (DMSO; black)- or PP2 (gray)-treated neurons under the same imaging settings. **, $p < 0.01$; n.s., not significant. **(D)** DIV8 hippocampal neurons were incubated with the secondary antibody (Alexa Fluor 488-conjugated donkey anti-rabbit IgG) without prior immunolabeling with a primary antibody. In the permeabilized condition the somata (most likely nuclei, shown in the transmitted image) were non-specifically stained. Scale bar: 20 μm.

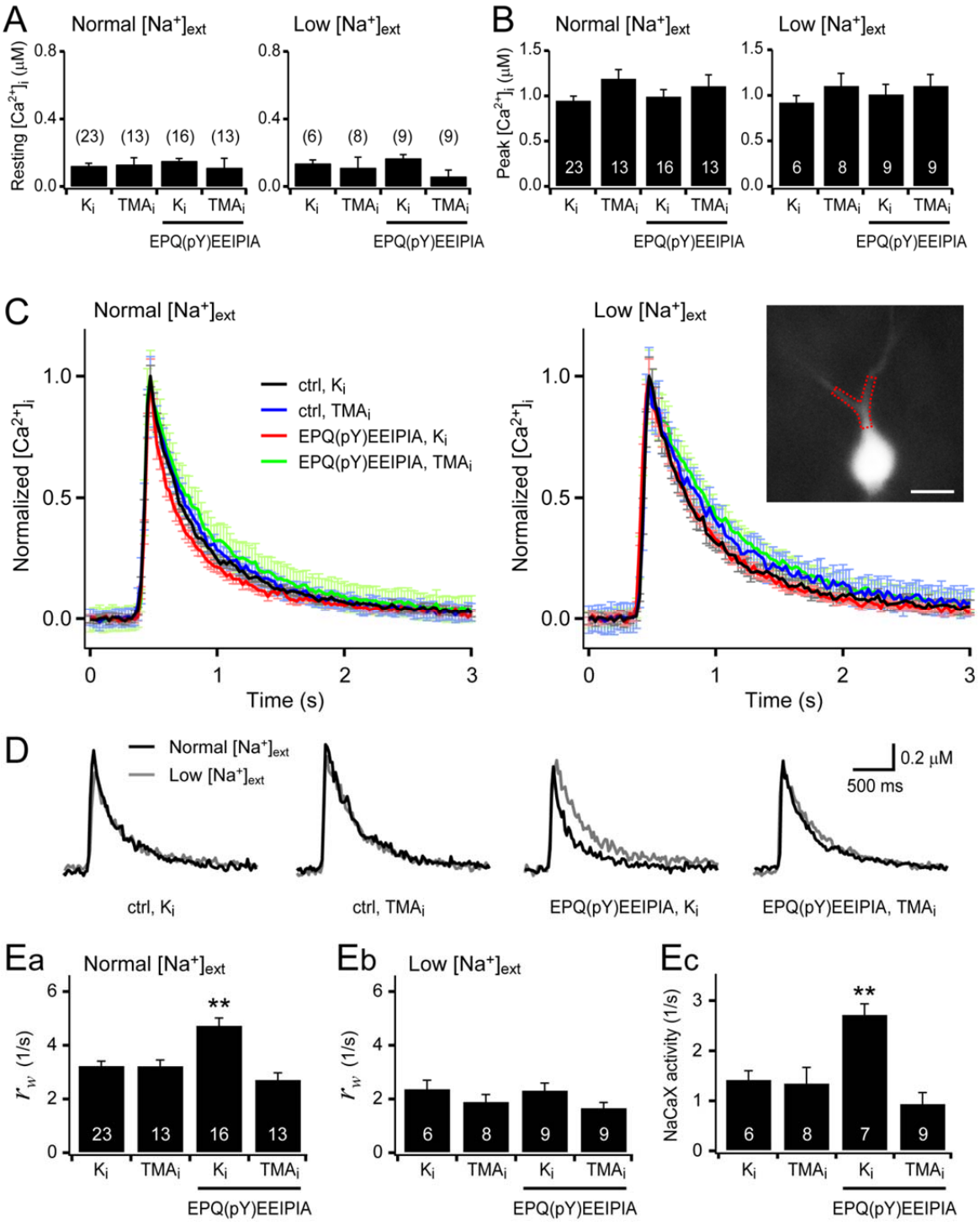

Figure 21. Activation of Src family kinase (SFK) enhances the NCKX activity in the proximal dendrite.

Figure 21. Activation of Src family kinase (SFK) enhances the NCKX activity in the proximal dendrite.

(A-B) In all conditions, the resting $[Ca^{2+}]_i$ level and the peak of CaTs were not significantly different. **(C)** Averaged traces of the normalized CaTs evoked by a short depolarizing pulse under normal $[Na^+]_{ext}$ or low $[Na^+]_{ext}$. Each panel shows four overlaid averaged traces under different conditions (K_i or TMA_i, K^+- or TMA^+-based pipette solution, respectively; ctrl or EPQ(pY)EEIPIA, with or without 1 mM EPQ(pY)EEIPIA, a SFK-activating peptide in the pipette solution, respectively). EPQ(pY)EEIPIA significantly accelerated the Ca^{2+} decay rate only under K^+-based internal and normal $[Na^+]_{ext}$ conditions (red lines). Error bars shown in light colors represent SEM. *Inset*, A fura-4F fluorescence image of a granule cell. A typical proximal dendritic ROI is shown as a red dotted polygon. Scale bar: 20 μm. **(D)** Effects of low $[Na^+]_{ext}$ on the Ca^{2+} decay rate in different conditions. Each panel shows overlaid representative CaTs recorded under the indicated intracelluar condition (black, normal $[Na^+]_{ext}$; gray, low $[Na^+]_{ext}$). **(E)** Summary for Ca^{2+} clearance and Na^+/Ca^{2+} exchange (NaCaX) activity. Ca^{2+} clearance was quantified as a weighted average of rate constants (r_w) estimated from the biexponential fit to the decay phase of individual CaTs (Ea-b). The difference in the r_w values between normal and low $[Na^+]_{ext}$ conditions in the same cell was regarded as the NaCaX activity (Ec). Mean ± SEM; **, $p < 0.01$.

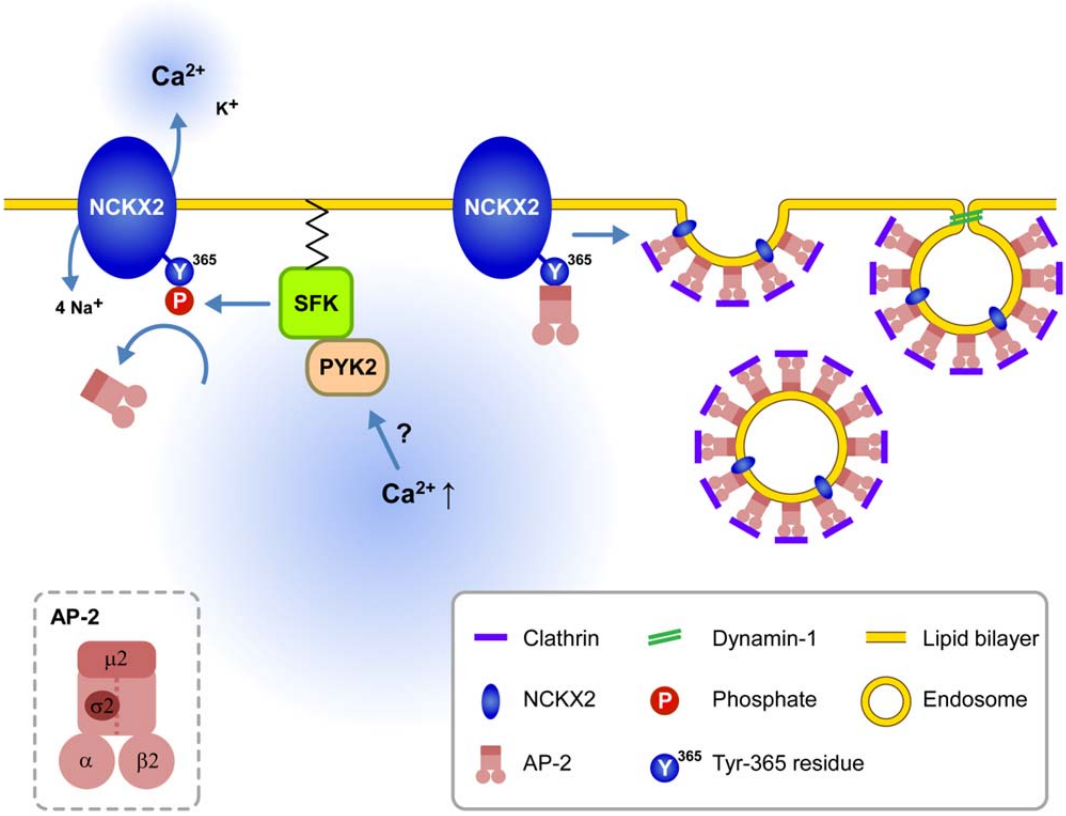

Figure 22. Schematic illustration for the signaling pathways regulating endocytosis of NCKX2 in the somatodendritic compartment.

Under resting conditions, the unphosphorylated or dephosphorylated tyrosine motif of NCKX2 interacts with AP-2 and thereby NCKX2 undergoes endocytosis. When elevation of cytosolic [Ca^{2+}] activates PYK2-SFK signaling pathway, activated SFK phosphorylates Tyr-365 of NCKX2, which in turn prevents interaction of AP-2 with NCKX2. Without interaction with μ2, NCKX2 avoids endocytosis resulting in higher surface expression of NCKX2 and enhanced Ca^{2+} clearance. These processes may contribute to local Ca^{2+} homeostasis. *Inset*, the subunit structure of AP-2.

Table 1. Mean [Ca^{2+}] increments induced by high-frequency stimulation (HFS) of hippocampal dentate granule cells

Cell group	location	n	number of cells	$\Delta F/F_0$
NT control	Somata	18 (6)	18 (6)	0.299 ± 0.015 (0.741 ± 0.021)
	Dendritic spines	34 (11)	14 (4)	0.357 ± 0.022 (0.577 ± 0.046)
	Dendritic shafts	28 (9)	14 (5)	0.368 ± 0.026 (0.603 ± 0.046)
	MFBs	64	12	1.302 ± 0.050
shKIF21A	Somata	19 (5)	19 (5)	0.300 ± 0.018 (0.724 ± 0.043)
	Dendritic spines	45 (11)	13 (5)	0.364 ± 0.029 (0.672 ± 0.047)
	Dendritic shafts	35 (11)	13 (5)	0.306 ± 0.027 (0.673 ± 0.062)
	MFBs	46	15	2.161 ± 0.079**
shNCKX2	Somata	7	7	0.268 ± 0.022
	Dendritic spines	15	4	0.329 ± 0.033
	Dendritic shafts	10	4	0.358 ± 0.037
	MFBs	26	5	2.171 ± 0.148**

[Ca^{2+}] increments presented as $\Delta F/F_0$ of OGB-5N. Ca^{2+} transients were induced by HFS at 33 Hz or 100 Hz (parenthesized numbers). $\Delta F/F_0$ values of a Ca^{2+} transient were read at the end of HFS. NT, non-targeting; MFB, mossy fiber bouton; The statistical values are presented as mean ± SEM. ** Statistical significance compared with control value ($p < 0.01$).

DISCUSSION

1. Previous studies imply that NCKX2 is responsible for the axonal polarization of NCKX activity in a neuron

NCKX activity was first discovered at the retinal photoreceptor, and now it is recognized that isoforms of NCKX are widely distributed in the brain [reviewed in (Lytton, 2007)]. In the brain, NCKX activity was first observed at neurohypophysial axon terminals, although no NCKX activity was observed in the somata of the same neurons, located in the supraoptic nucleus (SON) of the hypothalamus (Kim et al., 2003; Lee et al., 2009; Lee et al., 2002). Several lines of evidence support the idea that NCKX2 is responsible for the NCKX activity at these axon terminals. Firstly, the affinity for intracellular K^+ of the NCKX activity at the neurohypophysial axon terminal was distinctly low and compatible to that of NCKX2 (Lee et al., 2002; Visser et al., 2007). Secondly, transcripts of NCKX2, revealed by *in situ* hybridization analysis, was more prominent than other isoforms in magnocellular neurons of the SON (Lee et al., 2002). Thirdly, the NCKX activity at the glutamatergic presynaptic terminal in medial nucleus of the trapezoid body, a calyx of Held, was enhanced by phorbol ester, an activator of PKC, and NCKX2 is the only isoform modulated by PKC (Kim et al., 2005; Lee et al., 2006). These results imply that NCKX2 is the most plausible isoform responsible for calcium clearance at axon terminals in central neurons.

2. KIF21A may be essential for NCKX2 to pass through the AIS

In the present study, I identified a novel interaction between NCKX2 and KIF21A, and demonstrated that KIF21A is essential for the axonal transport of NCKX2 (**Figs. 7,**

8 and 10). Recently, it has been proposed that the AIS, comprised of F-actin, spectrin and ankyrin-G, functions as a checkpoint to axonal protein transport (Song et al., 2009). The AIS not only initiates action potentials but also functions as a selective filter that regulates axonal transport (Grubb and Burrone, 2010). The AIS is not just a physical barrier that screens a molecule by its size, but a highly flexible structure that is capable of selecting specific molecular components. For example, the axonal entry of 70 kDa dextrans was prevented by AIS (Song et al., 2009), but the large 360 kDa K_v3.1b tetramer which interacts with ankyrin-G could pass through the AIS (Xu et al., 2010). Therefore, axonal transport of a molecule requires not only a molecular motor (kinesin or myosin), but also interaction of motor-cargo complex with AIS components, which allows the complex to pass through the AIS. Recently, it has been reported that the third and fourth coiled-coil domains of the KIF21A stalk can interact with the ankyrin-repeat domain (Kakinuma and Kiyama, 2009), implying that the KIF21A (motor)-NCKX2 (cargo) complex is transported to the axon by interacting with ankyrin-G of AIS.

3. Somatodendritic surface expression of NCKX2

I observed that the surface expression of NCKX2 did not conform to the subcellular distribution of total (surface plus cytosolic) NCKX2 in the neuron (**Fig. 14**). Similar to NCKX2, several axonally targeted proteins such as Na_v1.2 (Garrido et al., 2001), VAMP2 , β1-integrin (Gut et al., 1998) and Caspr2 (Bel et al., 2009) have been found to exhibit differential surface and cytoplasmic distribution. The somatodendritic endocytosis (selective retention mechanism) has been proposed as a mechanism for the axon-specific surface expression of these proteins. In light of my findings that somatodendritic endocytosis of NCKX2 is essential for maintaining the polarized

axonal targeting. I considered that it is one of the potential regulation points for the somatodendritic surface expression of NCKX2. Clathrin-mediated endocytosis is initiated by recruitment of AP-2, an adaptor protein. There are two well-known canonical endocytosis motifs which interact with AP-2. One is a dileucine motif ([D/E]xxxL[L/I]; x = any amino acid) recognized by the μ2 subunit of AP-2 (Rapoport et al., 1998) and the other is a tyrosine motif (YxxΦ, Φ = hydrophobic amino acid) recognized by the μ2 subunit of AP-2 (Ohno et al., 1995). I found that the intracellular loop region of NCKX2 has two tyrosine motifs (^{365}YGKL and ^{371}YDTM), and the former motif interacts with the μ2 subunit of AP-2, and that is essential for endocytic regulation of dendritic NCKX2. Furthermore, I demonstrated that SFK-dependent phosphorylation of the Tyr-365 enhance the surface expression of NCKX2 on dendrites by inhibiting its interaction with μ2.

The low surface expression of NCKX2 in the somatodendritic region indicates that most NCKX2 molecules in this compartment are not tyrosine-phosphorylated in the resting conditions. Under these conditions, surface NCKX2 may be continuously eliminated by the mechanism of endocytosis. My results indicate that NCKX2 may be surface-expressed under conditions in which somatodendritic SFK is activated. PYK2 and PKC have been implicated as upstream signaling molecules of SFK in neurons (Neher and Sakaba, 2008). It is notable that Ca^{2+} increase itself can trigger activation of PYK2 (Kim and Ryan, 2009; Lev et al., 1995), raising a possibility that cytosolic elevation of Ca^{2+} may trigger the surface expression of NCKX2 in the somatodendritic region (**Fig. 22**). The other implication of this study is the role of alternative splicing of NCKX2. The tyrosine motifs of NCKX2 are located in the region that can be removed by alternative splicing (Tsoi et al., 1998). My results imply that such a spliced isoform may be resistant to endocytosis and thus more readily surface-expressed in

somatodendritic regions than the unspliced isoform. Therefore, the somatodendritic expression of NCKX2 may be regulated not only by tyrosine phosphorylation but also by the expression level of spliced NCKX2. Recently, NCKX2 has been implicated to play a protective role in ischemic brain damage (Cuomo et al., 2008). It remains to be elucidated whether brain ischemia and consequent elevation of resting cytosolic [Ca^{2+}] can enhance the surface expression of NCKX2 in the somatodendritic regions of central neurons.

4. Inconsistency between previous studies on the dendritic NCKX activity may result from Ca^{2+}-dependent regulation of dendritic expression of NCKX2

Previous analyses of Ca^{2+} clearance in the somata revealed that the somatic NaCaX activity is independent of intracellular K^+ in the hippocampal GC and the supraoptic magnocellular neuron, indicating lack of NCKX in their surface of somata (Kim et al., 2003; Lee et al., 2009). Nevertheless, NCKX activity in the soma has been reported by other studies in the hippocampal CA1 pyramidal and cortical neurons (Cuomo et al., 2008; Kiedrowski, 2004). The discrepancy can result from different types or developmental ages of the central neurons studied (Lee et al., 2007c). More importantly, it remained to be elucidated whether neurons in the central nervous system are equipped with a mechanism regulating the surface expression of NCKX2 in the somatodendritic compartment.

As aforementioned, when the NCKX activity was estimated from calcium clearance during decay phases of CaTs, NCKX little contributed to calcium clearance in the somatodendritic compartment (Kim et al., 2003; Lee et al., 2009). In contrast, reverse

mode NCKX activity was clearly observed in the soma of forebrain neurons (Cuomo et al., 2008; Kurisu et al., 2010). In the former studies, the somatic NCKX activity may be underestimated because NCKX activity was estimated from the decrease of calcium clearance caused by inhibition of NCKX, which may induce compensatory activation of other CCMs (Kim et al., 2003; Lee et al., 2009). Furthermore, the discrepancy may be caused by unphysiological experimental conditions used for measurement of the reverse mode NCKX activity in the latter studies. The reverse mode NCKX activity causes the cytosolic [Ca^{2+}] to rise to the tens of micromolar range (Kiedrowski, 2004). In light of the present study, such high cytosolic [Ca^{2+}] may enhance the surface expression of NCKX2 in the somatodendritic region through Ca^{2+}-dependent activation of PYK2 and subsequent tyrosine phosphorylation of NCKX2 (**Fig. 22**). Furthermore, the tyrosine motif is located in the alternative splicing region of NCKX2 (aa 361-377) (Tsoi et al., 1998). These endocytosis motifs can be removed by alternative splicing, raising a possibility that such a spliced isoform of NCKX2 may be expressed in the surface of the somatodendritic compartment. Therefore, alternative splicing may be one of potential regulation mechanisms for the polarized targeting of NCKX2. Therefore, the discrepancy on the dendritic NCKX activity might be reconciled not only by different estimation methods for NCKX activity (forward vs. reverse mode) but also by the possible Ca^{2+}-dependent enhancement of dendritic expression ofNCKX2.

5. Role of SFK-dependent regulation of NCKX2 activity in local Ca^{2+}-homeostasis

Calcium homeostasis is crucial not only for the cell survival but also for normal Ca^{2+} signaling. Neurons are multiply compartmentalized, and they display uneven subcellular distribution of neurotransmitter receptors and ion channels that can strongly influence

local Ca^{2+} influx. Local Ca^{2+} homeostasis is a prerequisite for normal Ca^{2+} signaling in a given compartment. Although Ca^{2+} itself can regulate the gene transcription of calcium channels and transporters (Carafoli et al., 1999), the regulation of such gene transcription may not be sufficient for local Ca^{2+} homeostasis. The cellular mechanism by which a neuron balances the local input and output of calcium is little understood. SFKs are implicated in long-term potentiation and associated trafficking of many excitatory neurotransmitter receptors including GluA2, GluN1, GluN2A and GluN2B (Lee et al., 2007b; Ohnishi et al., 2011). SFK-dependent tyrosine phosphorylation enhances the surface expression of these receptors. Given that these receptors mediate depolarization or Ca^{2+} influx, activation of SFK may potentially perturb Ca^{2+} homeostasis without being counter-balanced by a corresponding readjustment of CCMs. The present study shows that the surface expression of NCKX2 is regulated by SFK, which is a downstream effector of a Ca^{2+}-dependent non-receptor tyrosine kinase, PYK2. My results may provide a possible mechanism for local Ca^{2+} homeostasis in a central neuron (**Fig. 22**).

6. Regulation of NCKX2 activity at axon terminals

Previously, Lee et al. (2006) have reported that a PKC activator, phorbol 12, 13-dibutyrate (PDBu), enhances the NCKX activity at the calyx of Held (Lee et al., 2006). This finding was interpreted as PKC-dependent direct phosphorylation of NCKX2, because the activity of NCKX2 heterologously expressed in HEK293 cells was also enhanced by PDBu (Lee et al., 2006). PKC is one of the upstream molecules that activate SFK (Neher and Sakaba, 2008). In light of the present study, the PDBu-induced increase in the NCKX2 activity is necessary to be re-evaluated, as HEK293 cells weakly

express endogenous Src kinases (Holmes et al., 1996). Accordingly, further studies need to test whether activation of SFK is involved in the PDBu-induced increase in the NCKX activity at the calyx of Held. PKC may activate NCKX2 not only directly but also through a PYK2-SFK signaling pathway. The present study provides a possibility that the latter can enhance the NCKX activity by an increase in the surface expression of NCKX2 at the calyx of Held.

The effects of a dynamin mutant (**Fig. 15**) and shμ2 (**Fig. 19**) indicate that endocytosis of NCKX2 occurs more readily in the somatodendritic region than the axonal region under control conditions. As inhibition of SFK using PP2 reduced the surface expression of NCKX2 not only in the soma and dendrites but also in axonal regions (**Fig. 20**), phosphorylation of the tyrosine motif might be a primary determinant for the surface expression of NCKX2 in both compartments. This result together with higher surface expression in the axon implies that axonal NCKX2 may be more tyrosine-phosphorylated than somatodendritic NCKX2. It is little understood, however, whether SFKs are constitutively active in axonal regions. If tyrosine-phosphorylated NCKX2 is polarized to the axon under resting conditions, it needs to be further studied whether it is associated with differences between somatodendritic and axonal regions in SFK activity and/or counteracting molecules such as tyrosine phosphatases.

7. Questions to be resolved: mechanisms underlying dendritic transport of NCKX2

I showed that overexpression of dnKIF21A or depletion of KIF21A did not alter the DSR of NCKX2 (**Figs. 8D and 10D**). These findings, however, cannot be a direct evidence for little role of KIF21A in the dendritic transport of NCKX2, because

NCKX2 molecules in dendritic endoplasmic reticulum may be responsible for the dendritic immunoreactivity. Furthermore, the co-localization of KIF21A with NCKX2 in dendrites implies a possible role of KIF21A in the dendritic transport (**Fig. 5A**). Thus, it remains to be elucidated whether KIF21A plays an essential role in dendritic transport or not.

8. Questions to be resolved: pathogenesis of CFEOM1

The consistent effects of dominant-negative KIF21A and knockdown of KIF21A expression on NCKX2 delivery to the axon indicate that KIF21A mediates the axonal transport of NCKX2 in hippocampal neurons. Mutations in KIF21A cause congenital fibrosis of extraocular muscle type I (CFEOM1), which is a disorder of the superior oculomotor nerve (Yamada et al., 2003). The prevalent hypothesis for the pathogenesis of CFEOM1 is aberrant axonal routing and resultant abnormal development of the oculomotor axis (Engle et al., 1997; Heidary et al., 2008). Given that calcium plays a crucial role in axon guidance (Gomez and Zheng, 2006), a defect in axonal transport of NCKX2 might be the direct cause of CFEOM1. Dr. Lytton (University of Calgary, Calgary, Canada) studied whether functional inactivation of NCKX2 brings about pathological changes similar to CFEOM1 using NCKX2 knockout mice and he found, however, no obvious difference in the morphology of alpha motor neurons in the oculomotor nucleus between wild-type and knockout (data not published; personal communication) (Li et al., 2006), implying that CFEOM1 is not caused directly by a functional defect in NCKX2. Of course one should be cautious in extending the observations from mice to humans, because mice have no subdivision in the oculomotor nucleus observed in the human oculomotor complex.

9. Concluding remarks

Extending the previous view that NCKX plays a pivotal role in calcium clearance in the axon terminal but little contributes to that in the somatodendritic region, I demonstrated that the polarized axonal targeting of NCKX2 arises through the concerted contribution of two mechanisms: KIF21A-mediated axonal transport and preferential somatodendritic endocytosis, and that the latter is mediated by interaction of the tyrosine motif (^{365}YGKL) with the μ2 subunit of AP-2. These findings imply that there is room for diverse subcellular surface expression of NCKX2 depending on the regulation of the two mechanisms. As one of them, I showed that SFK-dependent phosphorylation of the tyrosine motif enhances dendritic surface expression of NCKX2. The regulatory mechanism for the subcellular surface expression of NCKX2 could be essential for understanding the cell-specific role of NCKX2 in Ca^{2+} homeostasis, which is relevant to synaptic plasticity and alleviation of ischemic brain injury (Cuomo et al., 2008; Li et al., 2006).

REFERENCES

Arnold, D.B. 2007. Polarized targeting of ion channels in neurons. *Pflugers Arch*. 453:763-769.

Bel, C., K. Oguievetskaia, C. Pitaval, L. Goutebroze, and C. Faivre-Sarrailh. 2009. Axonal targeting of Caspr2 in hippocampal neurons via selective somatodendritic endocytosis. *J Cell Sci*. 122:3403-3413.

Braam, S.R., C. Denning, E. Matsa, L.E. Young, R. Passier, and C.L. Mummery. 2008. Feeder-free culture of human embryonic stem cells in conditioned medium for efficient genetic modification. *Nat Protoc*. 3:1435-1443.

Cai, X., K. Zhang, and J. Lytton. 2002. A novel topology and redox regulation of the rat brain K^+-dependent Na^+/Ca^{2+} exchanger, NCKX2. *J Biol Chem*. 277:48923-48930.

Carafoli, E., A. Genazzani, and D. Guerini. 1999. Calcium controls the transcription of its own transporters and channels in developing neurons. *Biochem Biophys Res Commun*. 266:624-632.

Cuomo, O., R. Gala, G. Pignataro, F. Boscia, A. Secondo, A. Scorziello, A. Pannaccione, D. Viggiano, A. Adornetto, P. Molinaro, X.-F. Li, J. Lytton, G. Di Renzo, and L. Annunziato. 2008. A critical role for the potassium-dependent sodium-calcium exchanger NCKX2 in protection against focal ischemic brain damage. *J Neurosci*. 28:2053-2063.

Damke, H., T. Baba, D.E. Warnock, and S.L. Schmid. 1994. Induction of mutant dynamin specifically blocks endocytic coated vesicle formation. *J Cell Biol*. 127:915-934.

Davis, H.E., M. Rosinski, J.R. Morgan, and M.L. Yarmush. 2004. Charged polymers

modulate retrovirus transduction via membrane charge neutralization and virus aggregation. *Biophys J*. 86:1234-1242.

De Simoni, A., and L. My Yu. 2006. Preparation of organotypic hippocampal slice cultures: interface method. *Nat Protoc*. 1:1439-1445.

Dikic, I., G. Tokiwa, S. Lev, S.A. Courtneidge, and J. Schlessinger. 1996. A role for Pyk2 and Src in linking G-protein-coupled receptors with MAP kinase activation. *Nature*. 383:547-550.

Dotti, C., C. Sullivan, and G. Banker. 1988. The establishment of polarity by hippocampal neurons in culture. *J Neurosci*. 8:1454-1468.

Engle, E.C., B.C. Goumnerov, C.A. McKeown, M. Schatz, D.R. Johns, J.D. Porter, and A.H. Beggs. 1997. Oculomotor nerve and muscle abnormalities in congenital fibrosis of the extraocular muscles. *Ann Neurol*. 41:314-325.

Garrido, J.J., F. Fernandes, P. Giraud, I. Mouret, E. Pasqualini, M.P. Fache, F. Jullien, and B. Dargent. 2001. Identification of an axonal determinant in the C-terminus of the sodium channel $Na_v1.2$. *EMBO J*. 20:5950-5961.

Girault, J.-A., A. Costa, P. Derkinderen, J.-M. Studler, and M. Toutant. 1999. FAK and PYK2/CAKβ in the nervous system: a link between neuronal activity, plasticity and survival? *Trends Neurosci*. 22:257-263.

Goldberg, J.H., G. Tamas, D. Aronov, and R. Yuste. 2003. Calcium microdomains in aspiny dendrites. *Neuron*. 40:807-821.

Gomez, T.M., and J.Q. Zheng. 2006. The molecular basis for calcium-dependent axon pathfinding. *Nat Rev Neurosci*. 7:115-125.

Grubb, M.S., and J. Burrone. 2010. Building and maintaining the axon initial segment.

Curr Opin Neurobiol. 20:481-488.

Gut, A., M.S. Balda, and K. Matter. 1998. The cytoplasmic domains of a β1 integrin mediate polarization in Madin-Darby canine kidney cells by selective basolateral stabilization. *J Biol Chem*. 273:29381-29388.

Heidary, G., E.C. Engle, and D.G. Hunter. 2008. Congenital fibrosis of the extraocular muscles. *Semin Ophthalmol*. 23:3-8.

Hioki, H., E. Kuramoto, M. Konno, H. Kameda, Y. Takahashi, T. Nakano, K.C. Nakamura, and T. Kaneko. 2009. High-level transgene expression in neurons by lentivirus with Tet-Off system. *Neurosci Res*. 63:149-154.

Hirokawa, N., S. Niwa, and Y. Tanaka. 2010. Molecular motors in neurons: transport mechanisms and roles in brain function, development, and disease. *Neuron*. 68:610-638.

Hirokawa, N., and R. Takemura. 2005. Molecular motors and mechanisms of directional transport in neurons. *Nat Rev Neurosci*. 6:201-214.

Holmes, T., D. Fadool, and I. Levitan. 1996. Tyrosine phosphorylation of the $K_v1.3$ potassium channel. *J Neurosci*. 16:1581-1590.

Hong, Y.H., J.Y. Kim, J.H. Lee, H.G. Chae, S.S. Jang, J.H. Jeon, C.H. Kim, J. Kim, and S.J. Kim. 2009. Agonist-induced internalization of mGluR1α is mediated by caveolin. *J Neurochem*. 111:61-71.

Jeon, D., Y.-M. Yang, M.-J. Jeong, K.D. Philipson, H. Rhim, and H.-S. Shin. 2003. Enhanced learning and memory in mice lacking Na^+/Ca^{2+} exchanger 2. *Neuron*. 38:965-976.

Jurd, R., V. Tretter, J. Walker, N.J. Brandon, and S.J. Moss. 2010. Fyn kinase

contributes to tyrosine phosphorylation of the $GABA_A$ receptor γ2 subunit. *Mol Cell Neurosci*. 44:129-134.

Kaech, S., and G. Banker. 2006. Culturing hippocampal neurons. *Nat Protoc*. 1:2406-2415.

Kakinuma, N., and R. Kiyama. 2009. A major mutation of KIF21A associated with congenital fibrosis of the extraocular muscles type 1 (CFEOM1) enhances translocation of Kank1 to the membrane. *Biochem Biophys Res Commun*. 386:639-644.

Kiedrowski, L. 2004. High activity of K^+-dependent plasmalemmal Na^+/Ca^{2+} exchangers in hippocampal CA1 neurons. *Neuroreport*. 15:2113-2116.

Kim, J., S.-C. Jung, A.M. Clemens, R.S. Petralia, and D.A. Hoffman. 2007. Regulation of dendritic excitability by activity-dependent trafficking of the A-type K^+ channel subunit $K_V4.2$ in hippocampal neurons. *Neuron*. 54:933-947.

Kim, M.H., N. Korogod, R. Schneggenburger, W.K. Ho, and S.H. Lee. 2005. Interplay between Na^+/Ca^{2+} exchangers and mitochondria in Ca^{2+} clearance at the calyx of Held. *J Neurosci*. 25:6057-6065.

Kim, M.H., S.H. Lee, K.H. Park, W.K. Ho, and S.H. Lee. 2003. Distribution of K^+-dependent Na^+/Ca^{2+} exchangers in the rat supraoptic magnocellular neuron is polarized to axon terminals. *J Neurosci*. 23:11673-11680.

Kim, S.H., and T.A. Ryan. 2009. Synaptic vesicle recycling at CNS snapses without AP-2. *J Neurosci*. 29:3865-3874.

Kinjo, T.G., R.T. Szerencsei, R.J. Winkfein, K. Kang, and P.P. Schnetkamp. 2003. Topology of the retinal cone NCKX2 Na/Ca-K exchanger. *Biochemistry*. 42:2485-2491.

Kirchhausen, T. 1999. Adaptors for clathrin-mediated traffic. *Annu Rev Cell Dev Biol*. 15:705-732.

Kittler, J.T., G. Chen, S. Honing, Y. Bogdanov, K. McAinsh, I.L. Arancibia-Carcamo, J.N. Jovanovic, M.N. Pangalos, V. Haucke, Z. Yan, and S.J. Moss. 2005. Phospho-dependent binding of the clathrin AP2 adaptor complex to $GABA_A$ receptors regulates the efficacy of inhibitory synaptic transmission. *Proc Natl Acad Sci U S A*. 102:14871-14876.

Kittler, J.T., G. Chen, V. Kukhtina, A. Vahedi-Faridi, Z. Gu, V. Tretter, K.R. Smith, K. McAinsh, I.L. Arancibia-Carcamo, W. Saenger, V. Haucke, Z. Yan, and S.J. Moss. 2008. Regulation of synaptic inhibition by phospho-dependent binding of the AP2 complex to a YECL motif in the $GABA_A$ receptor γ2 subunit. *Proc Natl Acad Sci U S A*. 105:3616-3621.

Kurisu, J., T. Fukuda, S. Yokoyama, T. Hirano, and M. Kengaku. 2010. Polarized targeting of DNER into dendritic plasma membrane in hippocampal neurons depends on endocytosis. *J Neurochem*. 113:1598-1610.

Lee, D., K.H. Lee, W.K. Ho, and S.H. Lee. 2007a. Target cell-specific involvement of presynaptic mitochondria in post-tetanic potentiation at hippocampal mossy fiber synapses. *J Neurosci*. 27:13603-13613.

Lee, Hye Y., W.-P. Ge, W. Huang, Y. He, Gordon X. Wang, A. Rowson-Baldwin, Stephen J. Smith, Yuh N. Jan, and Lily Y. Jan. 2011. Bidirectional regulation of dendritic voltage-gated potassium channels by the fragile X mental retardation protein. *Neuron*. 72:630-642.

Lee, J.S., M.H. Kim, W.K. Ho, and S.H. Lee. 2008. Presynaptic release probability and readily releasable pool size are regulated by two independent mechanisms during posttetanic potentiation at the calyx of Held synapse. *J Neurosci*. 28:7945-7953.

Lee, J.Y., F. Visser, J.S. Lee, K.H. Lee, J.W. Soh, W.K. Ho, J. Lytton, and S.H. Lee. 2006. Protein kinase C-dependent enhancement of activity of rat brain NCKX2 heterologously expressed in HEK293 cells. *J Biol Chem*. 281:39205-39216.

Lee, K.H., J.S. Lee, D. Lee, D.H. Seog, J. Lytton, W.K. Ho, and S.H. Lee. 2012. KIF21A-mediated axonal transport and selective endocytosis underlie the polarized targeting of NCKX2. *J Neurosci*. 32:4102-4117.

Lee, S.H., W.K. Ho, and S.H. Lee. 2009. Characterization of somatic Ca^{2+} clearance mechanisms in young and mature hippocampal granule cells. *Cell calcium*. 45:465-473.

Lee, S.H., M.H. Kim, J.Y. Lee, S.H. Lee, D. Lee, K.H. Park, and W.K. Ho. 2007b. Na^{+}/Ca^{2+} exchange and Ca^{2+} homeostasis in axon terminals of mammalian central neurons. *Ann N Y Acad Sci*. 1099:396-412.

Lee, S.H., M.H. Kim, K.H. Park, Y.E. Earm, and W.K. Ho. 2002. K^{+}-dependent Na^{+}/Ca^{2+} exchange is a major Ca^{2+} clearance mechanism in axon terminals of rat neurohypophysis. *J Neurosci*. 22:6891-6899.

Lee, S.H., K.H. Park, and W.K. Ho. 2007c. Postnatal developmental changes in Ca^{2+} homeostasis in supraoptic magnocellular neurons. *Cell calcium*. 41:441-450.

Lev, S., H. Moreno, R. Martinez, P. Canoll, E. Peles, J.M. Musacchio, G.D. Plowman, B. Rudy, and J. Schlessinger. 1995. Protein tyrosine kinase PYK2 involved in Ca^{2+}-induced regulation of ion channel and MAP kinase functions. *Nature*. 376:737-745.

Li, Q., A. Lau, T.J. Morris, L. Guo, C.B. Fordyce, and E.F. Stanley. 2004. A syntaxin 1, $G\alpha_o$, and N-type calcium channel complex at a presynaptic nerve terminal: analysis by quantitative immunocolocalization. *J Neurosci*. 24:4070-4081.

Li, X.-F., L. Kiedrowski, F. Tremblay, F.R. Fernandez, M. Perizzolo, R.J. Winkfein, R.W. Turner, J.S. Bains, D.E. Rancourt, and J. Lytton. 2006. Importance of K^+-dependent Na^+/Ca^{2+}-exchanger 2, NCKX2, in motor learning and memory. *J Biol Chem*. 281:6273-6282.

Liu, J., M.C. Liu, and K.K.W. Wang. 2008. Calpain in the CNS: from synaptic function to neurotoxicity. *Sci Signal*. 1:re1-.

Liu, X., S. Brodeur, G. Gish, Z. Songyang, L. Cantley, A. Laudano, and T. Pawson. 1993. Regulation of c-Src tyrosine kinase activity by the Src SH2 domain. *Oncogene*. 8:1119-1126.

Lőrincz, A., B. Rózsa, G. Katona, E.S. Vizi, and G. Tamás. 2007. Differential distribution of NCX1 contributes to spine–dendrite compartmentalization in CA1 pyramidal cells. *Proc Natl Acad Sci U S A*. 104:1033-1038.

Lytton, J. 2007. Na^+/Ca^{2+} exchangers: Three mammalian gene families control Ca^{2+} transport. *Biochem J*. 406:365-382.

Marszalek, J.R., J.A. Weiner, S.J. Farlow, J. Chun, and L.S. Goldstein. 1999. Novel dendritic kinesin sorting identified by different process targeting of two related kinesins: KIF21A and KIF21B. *J Cell Biol*. 145:469-479.

Meijering, E., M. Jacob, J.C.F. Sarria, P. Steiner, H. Hirling, and M. Unser. 2004. Design and validation of a tool for neurite tracing and analysis in fluorescence microscopy images. *Cytometry A*. 58:167-176.

Molinaro, P., D. Viggiano, R. Nisticò, R. Sirabella, A. Secondo, F. Boscia, A. Pannaccione, A. Scorziello, B. Mehdawy, S. Sokolow, A. Herchuelz, G.F. Di Renzo, and L. Annunziato. 2011. Na^+–Ca^{2+} Exchanger (NCX3) knock-out mice display an impairment in hippocampal long-term potentiation and spatial learning and memory. *J Neurosci*. 31:7312-7321.

Neher, E., and T. Sakaba. 2008. Multiple roles of calcium ions in the regulation of neurotransmitter release. *Neuron*. 59:861-872.

Oh, Y.S., K.A. Cho, S.J. Ryu, L.-Y. Khil, H.-S. Jun, J.-W. Yoon, and S.C. Park. 2006. Regulation of insulin response in skeletal muscle cell by caveolin status. *J Cell Biochem*. 99:747-758.

Ohnishi, H., Y. Murata, H. Okazawa, and T. Matozaki. 2011. Src family kinases: modulators of neurotransmitter receptor function and behavior. *Trends Neurosci*. 34:629-637.

Ohno, H., J. Stewart, M.C. Fournier, H. Bosshart, I. Rhee, S. Miyatake, T. Saito, A. Gallusser, T. Kirchhausen, and J.S. Bonifacino. 1995. Interaction of tyrosine-based sorting signals with clathrin-associated proteins. *Science*. 269:1872-1875.

Prybylowski, K., K. Chang, N. Sans, L. Kan, S. Vicini, and R.J. Wenthold. 2005. The synaptic ocalization of NR2B-containing NMDA receptors is controlled by interactions with PDZ proteins and AP-2. *Neuron*. 47:845-857.

Rapoport, I., Y.C. Chen, P. Cupers, S.E. Shoelson, and T. Kirchhausen. 1998. Dileucine-based sorting signals bind to the beta chain of AP-1 at a site distinct and regulated differently from the tyrosine-based motif-binding site. *EMBO J*. 17:2148-2155.

Regehr, W.G., K.R. Delaney, and D.W. Tank. 1994. The role of presynaptic calcium in short-term enhancement at the hippocampal mossy fiber synapse. *J Neurosci*. 14:523-537.

Rubinson, D.A., C.P. Dillon, A.V. Kwiatkowski, C. Sievers, L. Yang, J. Kopinja, D.L. Rooney, M. Zhang, M.M. Ihrig, M.T. McManus, F.B. Gertler, M.L. Scott, and L. Van Parijs. 2003. A lentivirus-based system to functionally silence genes in primary mammalian cells, stem cells and transgenic mice by RNA interference. *Nat Genet*. 33:401-406.

Ryan, X.P., J. Alldritt, P. Svenningsson, P.B. Allen, G.-Y. Wu, A.C. Nairn, and P. Greengard. 2005. The Rho-specific GEF Lfc interacts with neurabin and spinophilin to regulate dendritic spine morphology. *Neuron*. 47:85-100.

Sampo, B., S. Kaech, S. Kunz, and G. Banker. 2003. Two distinct mechanisms target membrane proteins to the axonal surface. *Neuron*. 37:611-624.

Silverman, M., S. Kaech, E. Ramser, X. Lu, M. Lasarev, S. Nagalla, and G. Banker. 2010. Expression of kinesin superfamily genes in cultured hippocampal neurons. *Cytoskeleton*. 67:784-795.

Song, A.H., D. Wang, G. Chen, Y. Li, J. Luo, S. Duan, and M.M. Poo. 2009. A selective filter for cytoplasmic transport at the axon initial segment. *Cell*. 136:1148-1160.

Tsoi, M., K.-H. Rhee, D. Bungard, X.-F. Li, S.-L. Lee, R.N. Auer, and J. Lytton. 1998. Molecular cloning of a novel potassium-dependent sodium-calcium exchanger from rat brain. *J Biol Chem*. 273:4155-4162.

Visser, F., V. Valsecchi, L. Annunziato, and J. Lytton. 2007. Analysis of ion interactions with the K^+-dependent Na^+/Ca^{2+} exchangers NCKX2, NCKX3, and NCKX4: Identification of Thr-551 as a key residue in defining the apparent K^+ affinity of NCKX2. *J Biol Chem*. 282:4453-4462.

Xu, M., Y. Gu, J. Barry, and C. Gu. 2010. Kinesin I transports tetramerized Kv3 channels through the axon initial segment via direct binding. *J Neurosci*. 30:15987-16001.

Yamada, K., C. Andrews, W.-M. Chan, C.A. McKeown, A. Magli, T. de Berardinis, A. Loewenstein, M. Lazar, M. O'Keefe, R. Letson, A. London, M. Ruttum, N. Matsumoto, N. Saito, L. Morris, M.D. Monte, R.H. Johnson, E. Uyama, W.A. Houtman, B. de Vries, T.J. Carlow, B.L. Hart, N. Krawiecki, J. Shoffner, M.C. Vogel, J. Katowitz, S.M. Goldstein, A.V. Levin, E.C. Sener, B.T. Ozturk, A.N. Akarsu, M.C. Brodsky, F. Hanisch, R.P. Cruse, A.A. Zubcov, R.M. Robb, P.

Roggenkäemper, I. Gottlob, L. Kowal, R. Battu, E.I. Traboulsi, P. Franceschini, A. Newlin, J.L. Demer, and E.C. Engle. 2003. Heterozygous mutations of the kinesin KIF21A in congenital fibrosis of the extraocular muscles type 1 (CFEOM1). *Nat Genet*. 35:318-321.

국문 초록

K^+의존적 Na^+/Ca^{2+} exchanger (NCKX)는 중추신경계 축삭 말단에서 중요한 칼슘 제거 기전이지만, 세포체에서는 NCKX의 활성이 거의 없다고 알려져 있다. 본 논문에서는 쥐의 해마 신경 세포에서 NCKX2가 축삭 표면에 특이적으로 분포하는 기전을 연구하였다. 이 연구에서 NCKX2를 kinesin family member 21A (KIF21A)의 신경 세포 특이적 cargo 단백질로서는 처음으로 동정하였고, NCKX2의 세포내측 부위가 KIF21A의 cargo 결합 도메인으로 추측되는 WD-40 repeat과 상호 결합함을 밝혔다. KIF21A의 우성음성 돌연변이체 (dominant-negative)나 RNA 간섭 (RNAi)을 이용한 KIF21A의 결핍은 NCKX2-GFP의 축삭 수송을 억제한다. 또한 KIF21A의 결핍 (knockdown)은 축삭 말단에서의 칼슘 조절 장애를 야기하지만, 세포체나 수상돌기에서의 칼슘 조절에는 영향이 없었다. NCKX 활성이 축삭 특이적으로 나타남에도 불구하고, NCKX2를 면역염색 해보면 세포체/수상돌기 부분과 축삭 모두에 염색이 된다. 하지만 살아있는 세포에 항체를 표지하여 세포막에 발현된 NCKX2만을 관찰해보면, NCKX2의 세포막 발현이 축삭에 치우쳐 분포하고 있음을 알 수 있다. 해마 신경 세포에 dynamin 억제제인 dynasore를 처리하거나 dynamin-1의 K44A 돌연변이체를 과발현시켜서 endocytosis를 막으면, 세포체와 수상돌기 표면에서 NCKX2의 발현이 증가한다. 뿐만 아니라, 해마 치상회절 과립 세포 (dentate granule cell)의 수상돌기에서 dynasore에 의해 NCKX 활성이 증가하였다. AP-2 단백질의 μ2 단위체가 tyrosine motif (YxxΦ)와 결합하면 clathrin-mediated endocytosis가 개시된다는 것이 잘 알려져있다. NCKX2의 세포내측 부위에

는 tyrosine motif로 추정되는 서열이 두 곳 존재한다 (^{365}YGKL, ^{371}YDTM). 먼저 NCKX2가 μ2와 상호작용하는지 알아보기 위하여 면역침전을 수행해본 결과 wild type NCKX2는 μ2와 결합하지만, NCKX2의 Y365A 돌연변이체는 μ2와 상호작용하지 않았다. 반면, Y371A 돌연변이는 NCKX2와 μ2의 상호작용에 거의 영향을 미치지 않았는데, 이는 NCKX2의 ^{365}YGKL motif가 μ2와의 결합에 필요함을 시사한다. 다음으로 ^{365}YGKL motif가 NCKX2의 endocytosis에 필요한지를 알아보았다. 세포막에 발현하는 Wild type NCKX2를 관찰해보면 주로 축삭에 분포하고 있지만, NCKX2의 endocytosis는 축삭 보다는 세포체와 수상돌기 부분에서 더 활발히 일어난다. 하지만 NCKX2의 Y365A 돌연변이체는 endocytosis가 잘 되지 않고 세포막 발현도 축삭 특이적이지 않다. 또한 μ2 단위체가 결핍되면 wild type NCKX2 조차도 endocytosis가 억제되고, 세포막 발현의 축삭 특이성도 감소한다. 본 연구에서는 NCKX2의 ^{365}YGKL motif와 μ2의 결합이 인산화를 통하여 조절될 것이라는 가설을 세우고 다음 실험을 수행하였다. 세포에 carbachol (CCh)을 처리하면 PYK2를 통하여 Src family kinase (SFK)가 활성화된다는 것이 알려져있다. NCKX2의 Tyr-365가 CCh 처리에 의해 인산화되었고, 이러한 CCh에 의해 유발된 NCKX2의 인산화는 SFK 저해제인 PP2에 의해 감소하였다. PP2를 전처리하고 NCKX2를 면역염색 했을 때, 특히 축삭에서 endocytosis가 현저히 증가하였다. SFK 활성화 펩타이드에 의해 해마 치상회절 과립 세포의 수상돌기에서 NCKX 활성이 증가하였다. 이러한 결과들은, KIF21A를 매개한 축삭 수송과 세포체/수상돌기 부분의 선택적 endocytosis가 NCKX2의 세포막 발현을 축삭에 치우치게 하고, 세포

체/수상돌기 부위에서 일어나는 NCKX2의 endocytosis는 SFK 신호 전달 과정과 AP-2를 매개함을 시사한다.

중심 단어 : NCKX2, KIF21A, AP-2, 축삭 수송, clathrin-mediated endocytosis, 칼슘 이미징

학 번 : 2005-22402